

RADON EXHALATION OF BUILDING MATERIALS

FARREL SIDNEY WENTZEL

A thesis submitted in partial fulfilment of the requirements for the degree of Magister Scientiae at the Department of Physics, Faculty of Natural Sciences,



Supervisor: Prof. R. Lindsay

November 2018
KEYWORDS

RADON EXHALATION OF BUILDING MATERIALS

FARREL SIDNEY WENTZEL

Alpha particle
Background radiation
Becquerel
Decay chain
Isotope
Progeny
Radium
Radio nuclides
Radioactive decay
Radioactivity
Radon
Granite counter tops
Building Materials

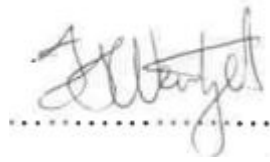


UNIVERSITY *of the*
WESTERN CAPE

DECLARATION

I, the undersigned, declare that the work contained in this thesis, **RADON EXHALATION OF BUILDING MATERIALS**, is my original work and has not previously in its entirety or part been submitted at any university for a degree, and that all the sources I have used or quoted have been indicated and acknowledged by complete references.

Signature:

A handwritten signature in black ink, appearing to read 'J. W. van der Merwe', written over a horizontal dotted line.

Date:.....November 2018.....



UNIVERSITY *of the*
WESTERN CAPE

ABSTRACT

RADON EXHALATION OF BUILDING MATERIALS

FARREL SIDNEY WENTZEL

M.Sc full thesis, Department of Physics,
University of the Western Cape

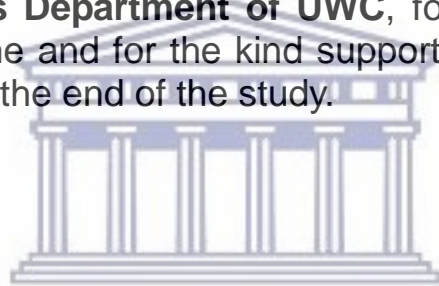
Public concern about all radiation and radon exhalation from building materials has been highlighted recently. The purpose of this study is to address this public concern and to investigate the contribution of building materials to indoor radon levels. As in soil and rocks, radon gas is formed inside the building materials by decay of the parent nuclide ^{226}Ra . It is not possible to determine the radon exhalation rate simply from the activity concentration of ^{226}Ra , instead one must measure radon exhalation rates directly from the surface of the material. ^{222}Rn has been identified as an important factor that could result in a health hazard by studies all around the world.

The exhalation experiments were done at the UWC physics department, in the Nuclear Physics Lab. A RAD7 radon detector was used to measure the radon concentration in an air tight chamber that contained various building material samples. The RAD7 records the number of alpha particles with energy of 6.11 MeV which results from the decay of ^{218}Po , the daughter of ^{222}Rn . The RAD7 detector converts counts into Becquerel's per cubic metre (Bq/m^3). The building materials tested were the raw materials used in construction such as two different types of building sand, building stones, coarse aggregate, floor and roof tiles, various granites from across the world that were sourced locally and uranium bearing sandstone originating from a Beaufort-West prospecting site. Stones from this site were used as filler material in the construction of two farm houses. Most building materials were found to have a very low rate of radon exhalation. The only materials that had any significant radon exhalation were 2 granite samples with a maximum exhalation rate of $1.5 \text{ Bq}\cdot\text{m}^{-2}\cdot\text{h}^{-1}$ and the uranium bearing sandstone. It is safe to say that the overwhelming majority of building materials tested are safe to use but some granites may require further study. The uranium bearing sandstone is a definite radiation protection issue and should not be used in any construction.

November 2018

ACKNOWLEDGEMENTS

I would like to acknowledge with gratitude the following highlighted people and departments for making my studies a real success: **Prof Robbie Lindsay**, my supervisor, for his guidance, his availability in times of need and willingness to help. My **family** for remaining solidly behind me throughout my studies and for their patience and undying support. My **friends** and my **colleagues at Livingstone High School** for their motivation, support and encouragement throughout my studies. The **Physics Department of UWC**, for selecting me to be part of this programme and for the kind support and assistance from the beginning right to the end of the study.



UNIVERSITY *of the*
WESTERN CAPE

TABLE OF CONTENTS

RADON EXHALATION OF BUILDING MATERIALS	I
KEYWORDS	II
DECLARATION.....	III
ABSTRACT	IV
ACKNOWLEDGEMENTS	V
TABLE OF CONTENTS	VI
LIST OF FIGURES	X
LIST OF TABLES	XIII
CHAPTER 1 BACKGROUND AND MOTIVATION	1
1.1. Introduction	1
1.1.1. Motivation for studies	1
1.1.2. Radon in building materials	1
1.2. Thesis Outline	2
1.3. Background to radon	2
1.3.1. Physical and chemical properties of radon	2
1.4. Radiation in general	3
1.4.1. Background to radiation	3
1.4.2. Alpha decay	4
1.4.3. Beta decay	4
1.4.3.1. Beta minus decay	6
1.4.3.2. Beta plus decay	6
1.4.4. Gamma Radiation	6
1.5. The Attenuation of radiation by matter	7
1.6. The radioactive decay laws	9
1.6.1. Deriving the Radioactive decay law.....	9
1.6.2. Deriving the Half-life equation.....	10
CHAPTER 2: THE TRANSPORT AND DANGERS OF RADON	14
2.1. Introduction.....	14
2.2. Radioactive decay processes of uranium-238 (²³⁸ U).....	14

2.3. The different sources of radon in nature.....	14
2.4. How radon enters the human body	15
2.4.1. The radiological effects of radon in the human body.....	16
2.4.2. Health effects of radon progenies and tobacco smoke.....	16
2.5. The presence of radon within rocks.....	17
2.6. The presence of radon within soil	17
2.7. Radon accumulation in houses	17
2.8. Dose rates absorbed by humans	20

**Chapter 3: BUILDING MATERIALS AND THEIR OCCURRENCE
IN SOUTH AFRICA WITH EMPHASIS ON THE WESTERN CAPE 22**

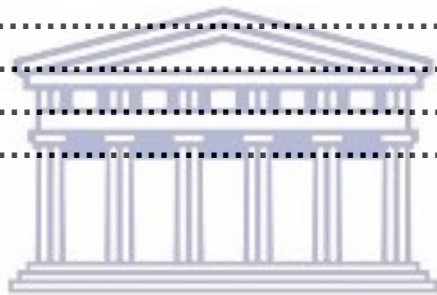
3.1. Introduction	22
3.2. Sand (fine aggregate) used in the construction of dwellings (Building Sand)	22
3.3. Stone aggregate (Coarse aggregate)	22
3.4. Brick clay	23
3.5. Limestone and dolomite.....	23
3.6. Uranium	24
3.6.1. Uranium occurring naturally in nature	25
3.6.2. Uranium mining and locations of uranium deposits in South Africa	25
3.6.2.1 The Karoo Supergroup	26
3.6.3 Uranium mining and its future in Namibia	27
3.6.3.1 Location of uranium mines in Namibia.....	28
3.7 Health Hazards from uranium	28
3.8 Dimension stone: Granite.....	29
3.8.1 Granite in the Springbok flats area.....	29
3.8.2 Namibian granite.....	30

**CHAPTER 4: MEASUREMENT TECHNIQUES AND
EXPERIMENTAL METHODS.. 39**

4.1. RAD7 Specifications.....	39
4.1.1. Setting up the RAD7 detector.....	39
4.1.1.1. Setting up the duration of the experiment.....	40
4.1.1.2. Setting up the Rad7 for radon detection.....	40
4.1.2. RAD7 experimental methods	41
4.1.2.1. Background radiation and noise check	41
4.1.2.2. Initializing the experiment	41
4.2. RAD7 spectrum analysis	44
4.2.1. Window information	44

4.3. Reading and storing of data in the RAD7	46
4.3.1. Starting the test.....	46
4.3.2. The Data command set.....	46
4.3.3. RAD7 test status	46
4.4. RAD7 measurements at Aardoon and Blikkraal	48
4.5. RAD7 measurements in the UWC Nuclear physics lab.....	48
4.6. Hyper-Pure Germanium (HPGe) specifications.....	49
4.6.1. Materials and measurements with the HPGe.....	49
4.7. EPERM electret.....	50
4.7.1. Ion chamber.....	51
4.7.2. Radon ion chamber measurements	51
CHAPTER 5: DISCUSSION OF RESULTS.....	52
5.1. Detectors and Materials Used.....	52
5.2. RAD7 results of diagnostics using a radium source	52
5.3. Background radiation.....	53
5.3.1. Background radiation in Summer	53
5.3.2. Background in Winter.....	54
5.4. Results of RAD7 measuring building materials	55
5.4.1. Philippi Sand.....	55
5.4.2. Malmesbury Sand.....	56
5.4.3. Floor tile.....	58
5.4.4. Roof Tile.....	59
5.4.5. Hornfels Stones.....	60
5.4.6. Tar.....	62
5.5. Uranium bearing sandstone from Beaufort-West.....	62
5.5.1. RAD7 measurement of uranium bearing sandstone.....	63
5.5.2. Measuring the hourly radon levels in the farm house on Aardoon	64
5.5.3 Radon concentration levels in the house on Aardoon	65
5.5.4. L -chamber measurement for Aardoon farmhouse.....	65
5.5.5. Radon concentration of Blikkraal using electrets.....	66
5.6. Using the RAD7 to measure the radon exhalation of granites..	66
5.6.1. Golden Beach	67
5.6.2. Indiana Dakota.....	68
5.6.3. Santa Cecilia.....	69
5.6.4. Namib green	70
5.6.5. Granite African Red.....	71
5.7. Overview of the HPGe readings	72
5.7.1. Uranium Activity of the granite countertops with	

the use of the HPGe.....	73
5.8. Calculations of Radon exhalation from the granite.....	74
5.8.1. Namib Green Radon exhalation calculation.....	74
5.8.2. African Red Radon exhalation calculation.....	74
5.9. Other investigations concerning granite countertops	75
Chapter 6: CONCLUSIONS	76
6.1. General Building materials	76
6.2. Granite Countertops.....	76
6.3. Uranium ore from the Ryst-Kuil farm, Beaufort-West.....	77
6.4. Recommendations	77
REFERENCES.....	78
APPENDICES.....	95
Appendix A.....	95
Appendix B.....	100
Appendix C.....	114
Appendix D.....	115



UNIVERSITY *of the*
WESTERN CAPE

LIST OF FIGURES

Figure 1.1: The complete uranium-238 decay series.....	3
Figure 1.2: Binding energy of different elements, which determines if an element will undergo fission or fusion.....	5
Figure 1.3: The diagram showing penetrating strength of radiation...8	
Figure 1.4: Elements with their isotopes displaying the ‘ Island of stability’, the magic numbers and unstable isotopes.....	13
Figure 2.1: Radon contributions to dwellings.....	18
Figure 2.2: Pathways for radon to enter a house.....	19
Figure 2.3: The uranium decay chain	21
Figure 3.1: Typical building sand	24
Figure 3.2: Tailings at the prospecting site on the farm Ryst Kuil.....	27
Figure 3.3: Map of the mineral potential of the Western Cape province.....	31
Figure 3.4: Uranium deposits in South Africa.....	32
Figure 3.5: Simplified uranium deposits in South Africa , Lesotho and Swaziland.....	33
Figure 3.6: Map of South Africa showing distribution of Karoo basins and major geographical lithostratigraphic units in the main Karoo basin.....	34
Figure 3.7: Uranium deposits of Namibia.....	35
Figure 3.8: Part of the Central Zone of the Damara Belt showing domes and the location of the known uranium deposits.....	36
Figure 3.9: Alaskite hosted uranium province.....	37
Figure 3.10: Damara belt Tectonic map of the Damara Orogen Namibia.	38
Figure 4.1: The RAD7 inside its carrying case.....	40
Figure 4.2: RAD7 setup for measurement.....	42
Figure 4.3: The desiccant with the plastic pipe end caps for Storage.....	43
Figure 4.4: Purging taking place to reduce the relative humidity of the RAD7.....	44
Figure 4.5: HPGe detector at iThemba Labs... ..	49
Figure 4.6: The S-Chamber Electret ion chamber.....	50
Figure 4.7: The L-chamber Electret ion chamber.....	50

Figure 5.1: RAD7 measurement of the radium source.....	52
Figure 5.2: Background radiation of radon during summer.....	53
Figure 5.3: Background radiation of radon during winter.....	54
Figure 5.4: Radon exhalation of Philippi sand.....	55
Figure 5.5: Philippi sand placed in a pan before it was placed in the RAD7 to measure the radon exhalation.....	56
Figure 5.6: Radon exhalation of Malmesbury sand.....	56
Figure 5.7: Malmesbury sand placed in a pan before it was placed in the RAD7 to measure the radon exhalation.....	57
Figure 5.8: Radon exhalation of a Floor tile.....	58
Figure 5.9: The floor tile that was placed in the RAD7 to measure the radon exhalation.....	58
Figure 5.10: Radon exhalation of Roof tile.....	59
Figure 5.11: The roof tile was placed in the RAD7 to measure the radon exhalation.....	59
Figure 5.12: Radon exhalation of Hornfel stones.....	60
Figure 5.13: The Hornfel stones that were placed in the RAD7 to measure radon exhalation.....	60
Figure 5.14: Radon exhalation of tar.....	61
Figure 5.15: The tar piece that was placed in the RAD7 to measure the radon exhalation.....	61
Figure 5.16: Radon exhalation from Beaufort-West uranium ore....	62
Figure 5.17: The uranium ore was placed in the RAD7 to measure the radon exhalation.....	63
Figure 5.18: A 24 hour measurement of TV room within Aardorn	64
Figure 5.19: Golden beach RAD7 measurement.....	67
Figure 5.20: The Golden beach granite used for measurements using the RAD7 and HPGe.....	67
Figure 5.21: Indiana Dakota RAD7 measurement.....	68
Figure 5.22: The Indiana Dakota granite used for measurements using the RAD7 and HPGe.....	68
Figure 5.23: Santa Cecilia RAD7 measurement.....	69
Figure 5.24: The Santa Cecilia granite used for measurements using the RAD7 and HPGe.....	69
Figure 5.25: Namib Green RAD7 measurement.....	70
Figure 5.26: The Namib Green granite used for measurements using the RAD7 and HPGe.....	71
Figure 5.27: African Red RAD7 measurement.....	71

Figure 5.28: The African Red granite used for measurements using the RAD7 and HPGe.....72

Figure 5.29: The granite countertops used for measurements in the RAD7 and HPGe.....73



UNIVERSITY *of the*
WESTERN CAPE

LIST OF TABLES

Table 1.1: Tabulated data on radiation characteristics.....	9
Table 5.1: Radon measurement of Aardorn using S chamber - electret.....	65
Table 5.2: L-Chamber Measurements of Aardorn.....	65
Table 5.3: L-Chamber Measurements of Blikkraal.....	66
Table 5.4: Dimensions (cm), Volume (cm ³), Mass (kg) and Density (g/cm ³) for different granite samples.....	66
Table 5.5: Overview of the general HPGe readings.....	72

APPENDIX

Table 1: RAD7 measurement of Radium	95
Table 2: RAD7 measurement of Background Radiation (Summer)...	95
Table 3: RAD7 measurement of Background Radiation (Winter)...	97
Table 4: RAD7 measurement of Phillipi sand.....	100
Table 5: RAD7 measurement of Malmesbury sand.....	101
Table 6: RAD7 measurement of a floor tile.....	102
Table 7: RAD7 measurement of a roof tile	104
Table 8: RAD7 measurement of Hornfel Stones.....	107
Table 9: RAD7 measurement of Tar.....	108
Table 10: RAD7 measurement of Beaufort-West uranium ore.....	110
Table 11: RAD7 measurement of Background Radiation of Aardorn.....	114
Table 12: RAD7 measurement of the granite Golden Beach	115
Table 13: RAD7 measurement of the granite Indiana Dakota.....	116
Table 14: RAD7 measurement of the granite Santa Cecilia.....	119
Table 15: RAD7 measurement of the granite Namib Green.....	120
Table 16: RAD7 measurement of the granite African Red	123

Chapter 1: Background and Motivation.

1.1 Introduction

1.1.1 Motivation for studies

There is considerable public concern about radon exhalation from building materials (Abu-Jarad, Fremlin and Bull, 1980; Chen et al., 2010; Khan et al., 1992). The purpose of this study is to address this public concern and to estimate the contribution of building materials to indoor radon levels in South Africa. All soil contains naturally occurring primordial radio nuclides such as ^{238}U , ^{232}Th and ^{40}K . These radio nuclides have long half-lives and were present from the time the earth was formed. Radioactivity was always part of life (Åkerblom and Mellander, 1997). The radio nuclides that were formed pose a radiological health hazard externally due to their gamma-ray emissions from progeny and internally due to alpha radiation emissions from radon and its progenies (Al-Hamarneh and Awadallah, 2009). These radioactive particles enter the food chain, ending up in fruits, within fish and animals. In order to survive human beings, have to consume these organisms, thus it is unavoidable for radon not to enter the human body (Beir, 1999). The decay products of radon have the ability to attach to the surface of aerosols, dust and smoke particles which may be inhaled and become deeply trapped in the lungs (Lubin et al., 1995). Radon is carcinogenic and since the particles become deeply trapped in the lungs, studies have found that when people are exposed to an elevated level of radon, it increases the risk of developing lung cancer even though the person is a non-smoker (Beir, 1999).

1.1.2 Radon in Building materials.

The earth's crust contains small amounts uranium-238 (^{238}U) and it decays through a chain of radioactive nuclides until it produces the stable isotope of Lead-206 (^{206}Pb) (Vogiannis and Nikolopoulos, 2014). The concentration of uranium in soil varies geographically, but it on average normally contains about 3 parts per million (ppm), or about 0.074Bq/g. (Crawford-Brown and Cothern, 1987). Uranium is generally found as oxides and soil contains primarily (80-90%) of uranyl cation (UO_2^{2+}) (Ebbs and Kochian, 1998; www.atsdr.cdc.gov). Naturally occurring isotopes of uranium include ^{234}U , ^{235}U , and ^{238}U (Beir, 1999). The ^{238}U isotope is the most abundant isotope (99.28%) followed by ^{235}U (0.72%) and ^{234}U (0.0055%). Uranium is mobilized from rock by the weathering of uraninite (UO_2). Surface water and groundwater causes oxidative dissolution of uraninite to the soluble uranyl ion (UO_2^{2+}). Worldwide from 27 000 to 32 000 tonnes uranium are released from igneous, shale, sandstone, and limestone rocks annually by weathering and natural erosion (minerals.usgs.gov). Uranium is present in all rocks and soils and since it undergoes radioactive decay, it can be expected that radon and radium will be present too. Radon and radium are daughter products of the radioactive decay chain of ^{238}U (Bossew, 2003). The most important materials needed for building material are soil and rocks (Åkerblom, 1997), hence building materials are a radon source (Elzain, 2014). (There are many ways how radon enters a house, but it is mainly due to the soil and rock upon which it is built by means of diffusion) Exhalation from various building materials can be another

potential source of radon in the indoor environment (Cothorn and Smith, 1987; UNSCEAR, 1982). This makes radon a source of radiological health risks to humankind received by both ingestion and inhalation. The death of underground miners from lung cancer led to the identification of radon as a health hazard (Těšínská, 2009; Wilson et al., 2014). Radium alpha decays by ejecting two neutrons and two protons from its nucleus (Bossew, 2003) and thus an alpha particle is ejected. Radon, an atom formed by the alpha decay of radium, recoils in the opposite direction (Markkanen, 1992).

1.2 Thesis Outline

The remaining parts of this thesis are as follows:

Chapter 1 describes and illustrates the interaction of radiation with matter, basic theories, and formulas in radiation. The chapter also describes the types of radiation and the radioactive decay laws. The chemical properties of radon and research on radon radioactivity are also described. Chapter 2 describes the radiological risk associated with radon and also tobacco smoke. The origin of radon in uranium-238 decay chain are described in detail, as well as how radon enters the body through the food chain and inhalation; how radon enters a house. Chapter 3 describes the origins of the building materials used. It describes how the materials are mined. It also describes the uranium industry and its reserves. Chapter 4 describes the experimental set-ups, methods and measurement instruments of the study. Chapter 5 displays the results of the experiments. Chapter 6 describes the overall outcomes of the study and the general discussion of the experiment.

1.3. Background to radon

1.3.1 Physical and Chemical Properties of radon

Radon has a chemical symbol of Rn; it is a noble gas with no colour and taste. Since radon is a noble gas, the electrons completely fill the outer shell of radon, which means that there will be no free electrons. Noble gases are monatomic, which is contrary to most gasses which are diatomic. They have stable electron configurations and under normal conditions they do not react with other elements. Radon has a half-life of 3.82 days and decays by alpha emission with energy of 5.5 MeV. It has a melting point of -71°C and the boiling point is -62.7°C . Radon has 86 protons and thus an atomic number of 86 (Jones and Childers, 1990). Radon is a gaseous descendant of radioactive ^{238}U that undergoes a series of decay steps before it ultimately reaches the stable ^{206}Pb , which is the final product. Figure 1.1 and figure 2.3 shows the complete decay chain of ^{238}U . There exist isotopes of radon besides ^{222}Rn ; the most notable ones are thoron (^{220}Rn) and actinon (^{219}Rn) (Jones and Childers, 1990). Thoron, with a half-life 55.6 seconds, is a product of the thorium-232 (^{232}Th) decay series wherein radium-224 (^{224}Ra) decays to form ^{220}Rn . Actinon with a half-life of about 3.96 seconds is a product of the ^{235}U decay series when Radium-223 (^{223}Ra) decays to actinon (www.chemcool.com). Radon is the highest contributor of natural background radiation and it contributes about 55% of the background radiation (Table 1.1) dose to which an average person is exposed in their lifetime (Jones and Childers, 1990). Other sources of

background radiation come from synthetic radiation, such as nuclear medicines and x-rays in hospitals and household products like smoke detectors (Cancio, D et al., 1994).

Nuclide	Half-Life	Major Radiations
Uranium-238	4.47 billion years	alpha, x-rays
Thorium-234	24.1 days	beta, gamma, x-rays
Protactinium-234m	1.17 minutes	beta, gamma
Uranium-234	245,000 years	alpha, x-rays
Thorium-230	77,000 years	alpha, x-rays
Radium-226	1600 years	alpha, gamma
Radon-222	3.83 days	alpha
Polonium-218	3.05 minutes	alpha
Lead-214	26.8 minutes	beta, gamma, x-rays
Bismuth-214	19.7 minutes	beta, gamma
Polonium-214	164 microseconds	alpha
Lead-210	22.3 years	beta, gamma, x-rays
Bismuth-210	5.01 days	beta
Polonium-210	138 days	alpha
Lead-206	stable	

Figure 1.1: The complete uranium-238 decay series. (Isite.lps.org, 2015)

1.4 Radiation in general

1.4.1 Background to Radiation

Background radiation is unavoidable and it shall always affect any radiation reading because it is present everywhere due to the different sources of radiation. Radiation can be placed in two categories, natural and synthetic radiation. There are three types of Background radiation that can occur. These are Cosmic, terrestrial and internal radiation (www.nrc.gov,a).

Cosmic radiation occurs when the earth is bombarded by radiation, originating from outer space. The main source of cosmic radiation on earth is the sun since it is the nearest star to the earth. The sun undergoes fusion and due to that process it is the primary source of cosmic radiation (www.ems.psu.edu). The charged particles from the sun and to a lesser extent the stars, interact with the atmosphere which generates a shower of radiation by also interacting with the earth's magnetic field (Gaisser and Stanev, 2000).

Terrestrial radiation was present since the earth's formation. Radioactivity is common throughout nature which can be found in soils, rocks, water, and vegetation. The most common natural radioactive nuclides are ^{238}U , ^{232}Th , potassium-40 (^{40}K) and their progenies. The amount of terrestrial radiation differs globally due to the different concentration of uranium and thorium, with their progenies respectively, in soil (Chang *et al.*, 2008). Likewise the exposure of radon differs depending on the uranium concentration (Smethurst *et al.*, 2008).

Synthetic radiation is caused by human activities and the concentration differs immensely. Sources of synthetic radiation that occur in normal circumstances mostly have elevated levels of radiation but in selected cases extremely high concentrations of radiation (Whicker and Schultz, 1982). The first example of synthetic radiation is granite countertops, which are usually placed in kitchens or the patio around a dwelling. The second example is radiation sources which are used in experiments and the amount of exposure depends on the type of source and its strength. Radiation sources are also used in the medical field to prepare Nuclear medicine for patients (de González et al., 2009). The third example is Nuclear power and since nuclear power stations are quite shielded from radiation from the core and the effects would be minimal to anyone outside of the power station (www.mirion.com,a).

Internal radiation is the radiation that originates from within the human body. There are different causes to internal radiation such as cosmic, terrestrial and synthetic radiation. Chapter 2.4 and its subsections discuss in detail how uranium and the progenies enter the human body. It also discusses the adverse effects it has on the human body (Weinstein and Sandman, 1992; Carvalho, 1995).

1.4.2 Alpha Decay

The decay of heavy nuclei, due to alpha radiation, is a natural occurrence in a radioactive series. Alpha decay occurs when unstable, heavy radio-nuclei discharge an alpha particle which causes a new element to form. The alpha particle is also known as a ${}^4\text{He}$ nucleus (Hosny, Al-Anezi and Khalil, 2017). The alpha emission takes place because the nucleus gains binding energy from a decrease in the mass of the system (Blatt and Weisskopf, 2012). The alpha particle is a very stable and tightly bound nucleus, with the mass being relatively small compared to the remaining parts of the nucleus. In unstable nuclei, this reaction of alpha decay is favoured with an alpha particle being spontaneously emitted from the system with the release of kinetic energy (Povh, Rith and Zetsche, 1995).



When the two protons and neutrons leave the nucleus together, they form the positively charged alpha particle. The RAD7, the continuous radon monitor used in this study, measures the energy of the emitted alpha (see eq. 1.1) from ${}^{218}\text{Po}$ (DurrIDGE Co, USA, 2000).

1.4.3 Beta Decay

There are about 270 stable isotopes of elements in nature and its stability is dictated by the configuration of their protons and neutrons. (See figure 1.4 for more details). In a nucleus there are certain number of nucleons (Protons or Neutrons), known as magic numbers that have a higher binding energy per nucleon. The magic numbers are 2, 8, 20, 28, 50, 82 and 126. If a proton and a neutron in the same element have a magic number in its configuration, then it is called a double magic nucleus. These are very stable against decay and

examples are ^4He , ^{16}O , ^{40}Ca , ^{208}Pb etc. The stable isotopes on figure 1.4 are concentrated around the line of stability and it is collectively known as the island of stability, which is surrounded by the sea of instability. The figure 1.4 shows the plot of atomic numbers versus neutron numbers. Iron is the most stable nucleus (See figure 1.2 for more details). Elements with smaller atomic numbers than ^{56}Fe often have a (N/Z) ratio of 1 neutron per proton. Elements with protons more than ^{56}Fe have a (N/Z) ratio of up to 1.6 neutrons per proton. Beta decay occurs when the unstable radio nuclide attains its stability by either changing a neutron to a proton or vice versa. There are two types of beta decay, beta plus and beta minus decay. All isotopes with a proton number higher than 83 will be radioactive in nature. Likewise, neutron numbers higher than 126 are radioactive in nature (Fermi et al., 1934). During beta decay, the nucleus gives off either an electron with a corresponding anti-neutrino or positron with a corresponding neutrino. A positron is the antimatter counterpart of the electron. It has the same mass and spin of the electron but the electric charge is +1 (Morison, 2013). The neutrino and anti-neutrino have many similarities. Both particles have a velocity which is close to the speed of light, are electrically neutral, have negligible mass and the particles penetrate through the earth without any interaction with matter. The neutrino has three leptonic flavours which are electron neutrinos, muon neutrinos and tau neutrinos (Rajasekaran, 2016). The only instance where the lepton number for neutrino and anti-neutrino are different is the electron neutrino, which has two possible lepton numbers, +1 and -1. For neutrinos it is +1 and anti-neutrinos it is -1. If a radionuclide is neutron deficient then positron emission occurs, whereas if it is neutron rich, then electron emission occurs (Lilley, 2001).

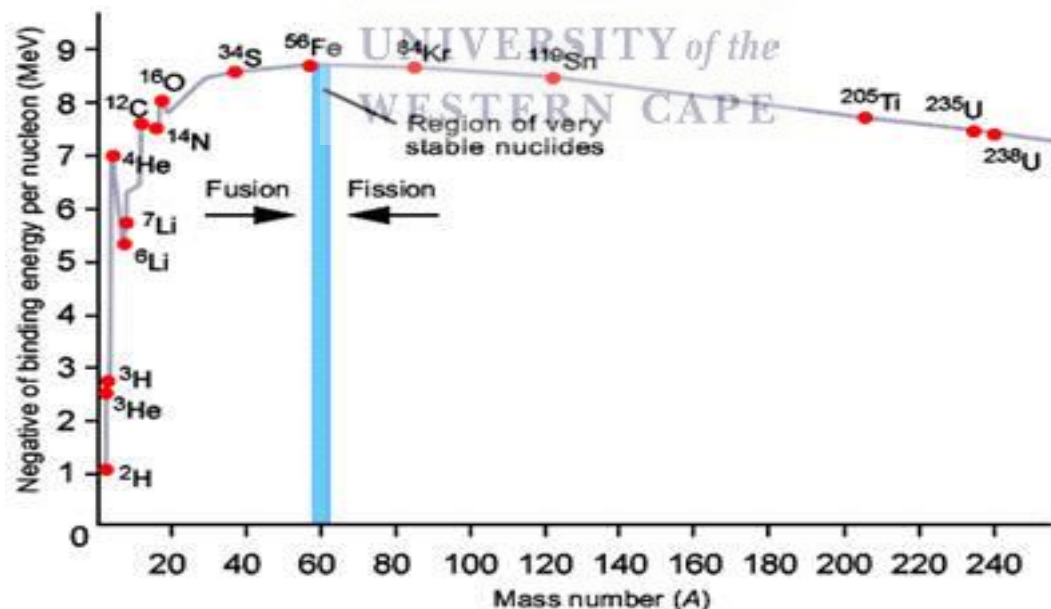


Figure 1.2 Binding energy of different elements which determines if an element will undergo fission or fusion (www.daviddarling.info).

1.4.3.1. Beta minus decay

Beta minus decay occurs when a neutron (n) is converted to a proton (p) via the weak nuclear force. The result is an electron (e^-) also known as a Beta minus particle and an anti-neutrino. The anti-neutrino is symbolized by the Greek letter nu, with a circumflex accent, ($\bar{\nu}$). The anti-neutrino usually penetrates through the earth without any interaction. After Beta minus decay takes place, the atomic number of the daughter nucleus increases by a unit. Beta minus decay occurs if there is an excess of neutrons in the nucleus. There are more Beta minus decay reactions than Beta plus decay reactions in nature (Knoll, 2010).

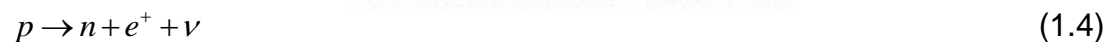


The neutron converts into a proton and an electron. As an electron cannot exist inside the nucleus, it is ejected. For instance, bismuth-214 (^{214}Bi) transforms into polonium-214 (^{214}Po) in the following way:



1.4.3.2. Beta plus decay

Beta plus decay occurs when a proton (p) is converted to a neutron (n) via the weak nuclear force. The outcomes are a positron (e^+) also known as a Beta plus particle and a neutrino. The neutrino is symbolized by the Greek letter nu (ν). Beta plus decay is favoured if there is an excess of protons in the nucleus. The neutrino usually penetrates through the earth without any interaction. After Beta plus decay takes place in nature, the atomic number of the daughter nucleus decreases by a unit (Knoll, 2010).



A proton converts into a neutron and a positively charged electron, the positron, is emitted. Radium-228 (^{228}Ra) decays to actinium-228 (^{228}Ac) by emission of a positron in the following way:



1.4.4. Gamma Radiation

Gamma radiation is the third type of natural radioactivity that occurs in nature and is a product of excited nuclei. Gamma rays are the most energetic form of electromagnetic radiation. Gamma radiation is caused by the emission of high-energy electromagnetic waves from a radionuclide. The wavelengths of gamma rays are typically less than a nanometer (Bushberg and Boone, 2011).

Gamma radiation is also produced when an annihilation reaction occurs. An annihilation reaction is when a particle and an anti-particle, electron and positron, collides with each other and produces energy in the form of two gamma ray photons (Bushberg and Boone, 2011).



Gamma rays often accompany the emission of particulate radiation. They are also produced in annihilation reactions. They internally and externally present radiation hazard to the entire body. Protactinium-234 (^{234}Pa) decays by alpha emission as given in eq. (1.7). Protactinium is formed in an excited state that then decays by gamma emission giving off a gamma ray with energy about 258 keV:



The asterisk (*) in Equation 1.7 indicates that the radionuclide is in an excited state and the atom is very unstable. The excited state is denoted by an m to distinguish the natural state. ${}^{234}\text{Pa}^m$ (meta state) has a relatively short half-life of 1.2 minutes, compared to the 6.1 hours of ${}^{234}\text{Pa}$. A gamma particle (γ) indicates that an amount of energy was released in the form of electromagnetic radiation. This was done by the nucleus to ensure that the element achieves stability, after the gamma particle was ejected.

1.5 The Attenuation of matter by radiation

Charged particles do not penetrate far in matter, because energy is lost by interacting with the electrical interaction. This interaction is induced by electrons in atoms of the matter. Ionization of atoms requires energy and all three types of radiation lose energy as they pass through matter. Any of the three types of radiation can be blocked or absorbed completely (Peterson, 2015).

The intensity of radiation decreases exponentially with distance as it passes through matter. The intensity of radiation decreases because the incident radiation interacts with the particles making up the matter and loses energy. The exponential decrease can be described by:

$$I(x) = I_0 e^{-\mu x} \quad (1.8)$$

I_0 is the incident radiation beam, while $I(x)$ is the attenuated radiation beam. μ (μ) is the mass absorption or attenuation coefficient in per meter (m^{-1}) and x is thickness of the absorber in meters (m). The information of attenuation of radiation is important since it is crucial when setting up shielding of radiation sources, X-rays and tumour irradiation (Podgorsak, 2005).

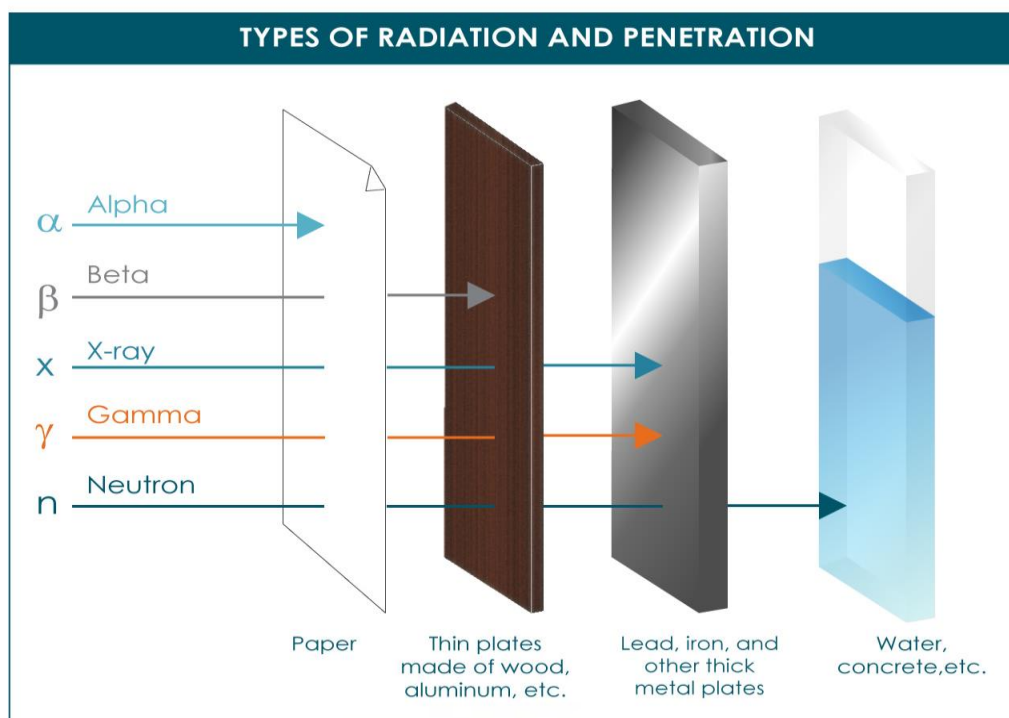


Figure 1.3 The diagram showing penetrating strength of radiation (www.mirion.com, b)

Neutrons form part of the nucleus and it is also a by-product of fission. A neutron is extremely hazardous to the human body. Free neutrons are unstable and decay to a proton, electron and an anti-neutrino. (See equation 1.2) The neutron cannot penetrate concrete and water very deeply. The neutrino and anti-neutrino are by products of Beta decay and these particles can penetrate through the earth. These particles hardly react with anything and are quite safe (Rajasekaran, 2016).

Alpha particles create the greatest ionization density per path length of the three types of radiation. The alpha particles are absorbed by paper and it cannot penetrate the human body (Carroll and Finlay, 2010). Beta Particles can penetrate skin but cannot penetrate a thin piece of aluminium (See Figure 1.3). Beta particles are used in radiation therapy to treat cancer cells. Beta particles can cause cancer when absorbed into living matter (O'donoghue, Bardies and Wheldon, 1995). There are three different processes that can attenuate gamma radiation through matter namely the photoelectric effect, Compton scattering and pair production. Each single process dominates at different energy levels. Different processes occur between levels of energies. For energies less than 0.1 MeV mostly the photoelectric effect occurs. If the energy levels are between 0.1 and 1 MeV then the Compton Effect mostly takes place. At any energy above 1.022 MeV pair production takes place as well (Knoll, 2000). Gamma rays can attenuate through almost all matter and are absorbed by a thick wall of concrete or a few centimetres of lead. Gamma rays can pass completely through the human body, but it has a high possibility to be absorbed by tissue inside the human body, which can be a radiation hazard. For people working with gamma rays, it is recommended to make use of lead shields to lower the chance of radiation (O'donoghue, Bardies and

Wheldon, 1995). Since lead is a common element with high atomic number, it is commonly used as a shielding material. The thicker the lead shield the better the attenuation (Nelson and Reilly, 1991). Table 1.1 summarises the above information.

The characteristics of radiation				
Characteristics	Alpha Particle	Beta Particle	Neutrons	Gamma ray
Symbol	${}^4_2\text{He}$ or α	β^+ or β^-	n^0	γ
Mass (a m u)	4	0.0005	1	0
Charge	+2	± 1	0	0
Speed	Fast	Very Fast	Fast	Speed of light
Ionizing ability	High	Medium	Low or Zero	Low
Penetrating Power	Low	Medium	Very High	High
Radiation type	Particulate	Particulate	Particulate	Photon
Shielding	Paper/Hand	Aluminium	Concrete/H ₂ O	Lead

Table 1.1: Tabulated data on radiation characteristics (Knoll, 2000).

1.6 The Radioactive decay laws

1.6.1 Deriving the Radioactive decay law

The radioactive decay laws are universal and each isotope has a distinct decay constant, lambda (λ). The activity A of a sample of N nuclei decays proportionally to the decay constant and N.

$$A = \lambda N \quad (1.9)$$

dN/dt signifies the change of number of the amount of nuclei of a time period. This change is directly proportional (\propto) to the amount of nuclei present.

$$\frac{dN}{dt} \propto N \quad (1.10)$$

$$\frac{dN}{dt} = -\lambda N \quad (1.11)$$

The negative sign indicates that a decay or a decreasing function is in place, rather than an increasing function. λ is the constant of proportionality and is called the decay constant. The differential equation 1.11 is first order and also separable. To integrate we divide by N ($N \neq 0$, otherwise the function is going to be invalid).

$$\frac{1}{N} \frac{dN}{dt} = -\lambda \quad (1.12)$$

The dt variable is placed on the right side and it represents a small interval in time. This equation can now be integrated.

$$\int \frac{dN}{N} = \int -\lambda dt \quad (1.13)$$

Before integration takes place the constants are moved in front of the integration sign since it will have no effect on the integration operation. The constant in this case is $-\lambda$.

$$\int \frac{dN}{N} = -\lambda \int dt \quad (1.14)$$

When we perform the integral we produce the following equation:

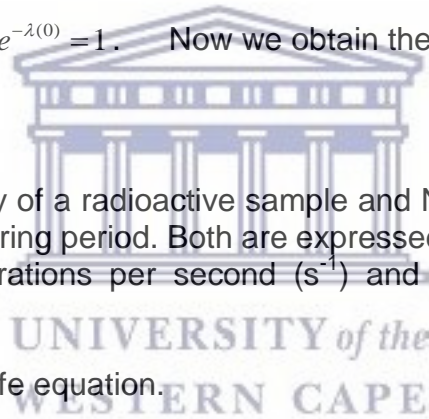
$$\ln(N) = -\lambda t + C; \quad C \in \mathfrak{R} \quad (1.15)$$

$$N(t) = Ae^{-\lambda t} \quad (1.16)$$

At $t = 0$, $A = N_0$ since $e^{-\lambda(0)} = 1$. Now we obtain the radioactive decay law.

$$N(t) = N_0 e^{-\lambda t} \quad (1.17)$$

Where $N(t)$ is the activity of a radioactive sample and N_0 is the original activity at the start of the measuring period. Both are expressed in Becquerel (Bq). λ is the number of disintegrations per second (s^{-1}) and time t is measured in seconds (s).



1.6.2 Deriving the Half-life equation.

We use the radioactive decay law (Equation 1.18) in order to find the half-life equation.

$$\frac{N(t)}{N_0} = e^{-\lambda t} \quad (1.18)$$

Since half-life is the time ($t_{\frac{1}{2}}$) when half of the radionuclides have decayed,

$$\frac{1}{2} N_0 = N_0 e^{-\lambda t} \quad (1.19)$$

$$\frac{1}{2} = e^{-\lambda t_{\frac{1}{2}}} \quad \text{and} \quad \lambda t_{\frac{1}{2}} = \ln 2 \quad (1.20)$$

$$t_{\frac{1}{2}} = \frac{\ln(2)}{\lambda} \quad (1.21)$$

$$t_{\frac{1}{2}} = \frac{\ln 2}{\lambda} \quad (1.22)$$

λ is the decay constant and t is the time. The decay λ is related to the half-life and it is unique for each element and isotope:

$$t_{\frac{1}{2}} = \frac{0.693}{\lambda} \quad (1.23)$$

In this thesis we will measure the radon in a chamber where the building material acts as a source of radon. The radon measurement using this set up can be modelled as followed. Assume that the building is acting like a source of radon of strength S expressed in radon atoms released into the volume of the chamber per second. The change in the radon atoms in the volume can then be expressed as

$$\Delta N = S\Delta t - \lambda N\Delta t \quad (1.24)$$

If we also include the usual decay term where λ is the decay constant of radon, this leads to:

$$\frac{dN}{dt} = S - \lambda N \quad (1.25)$$

$$\int_0^N \frac{dN}{S - \lambda N} = \int_0^t dt \quad (1.26)$$

$$-\frac{1}{\lambda} \ln(S - \lambda N) = t + c \quad (1.27)$$

The equation can be solved to give:

$$N = \frac{S}{\lambda} (1 + e^{-\lambda t}) \quad (1.28)$$

For the concentration of Radon

$$C_{Rn} = \frac{N}{V} = \frac{S}{\lambda V} (1 - e^{-\lambda t}) \quad (1.29)$$

Finding the concentration activity, we use the following:

$$C_{ac} = \frac{A}{V} = \frac{\lambda N}{V} = \frac{S}{V} (1 - e^{-\lambda t}) \quad (1.30)$$

This leads to the formula for modeling of the concentration activity at time t where C_0 = the concentration at $t = 0$:

$$C_{ac} = C_0 e^{-\lambda t} + \left(\frac{S}{V}\right) (1 - e^{-\lambda t}) \quad (1.31)$$



Equation 1.30 shows that after a long period (compared to its half-life of 3.8 days) the activity of the system will be $C_{ac} \sim \frac{S}{V}$ (1.32)

So the “effective” strength of the sample measured $S \approx V \times C_{MAX}$

For the first few hours (under 50 hours and if the original concentration is low) we can approximate

$$C_{ac} = \frac{S}{V} (1 - e^{-\lambda t})$$

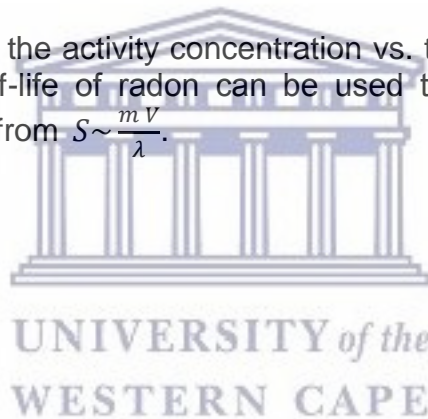
$$C_{ac} \sim \frac{S}{V} (1 - (1 - \lambda t)) \quad (\lambda t < 1)$$

$$C_{ac} \sim \frac{\lambda S t}{V}$$

Hence the activity concentration vs. the time for the first hours is given by

$$C_{ac} \sim \frac{\lambda S}{V} t = mt \quad (1.33)$$

Hence, the slope (m) of the activity concentration vs. the time graph for times much less than the half-life of radon can be used to extract the “effective strength” of the sample from $S \sim \frac{m V}{\lambda}$.



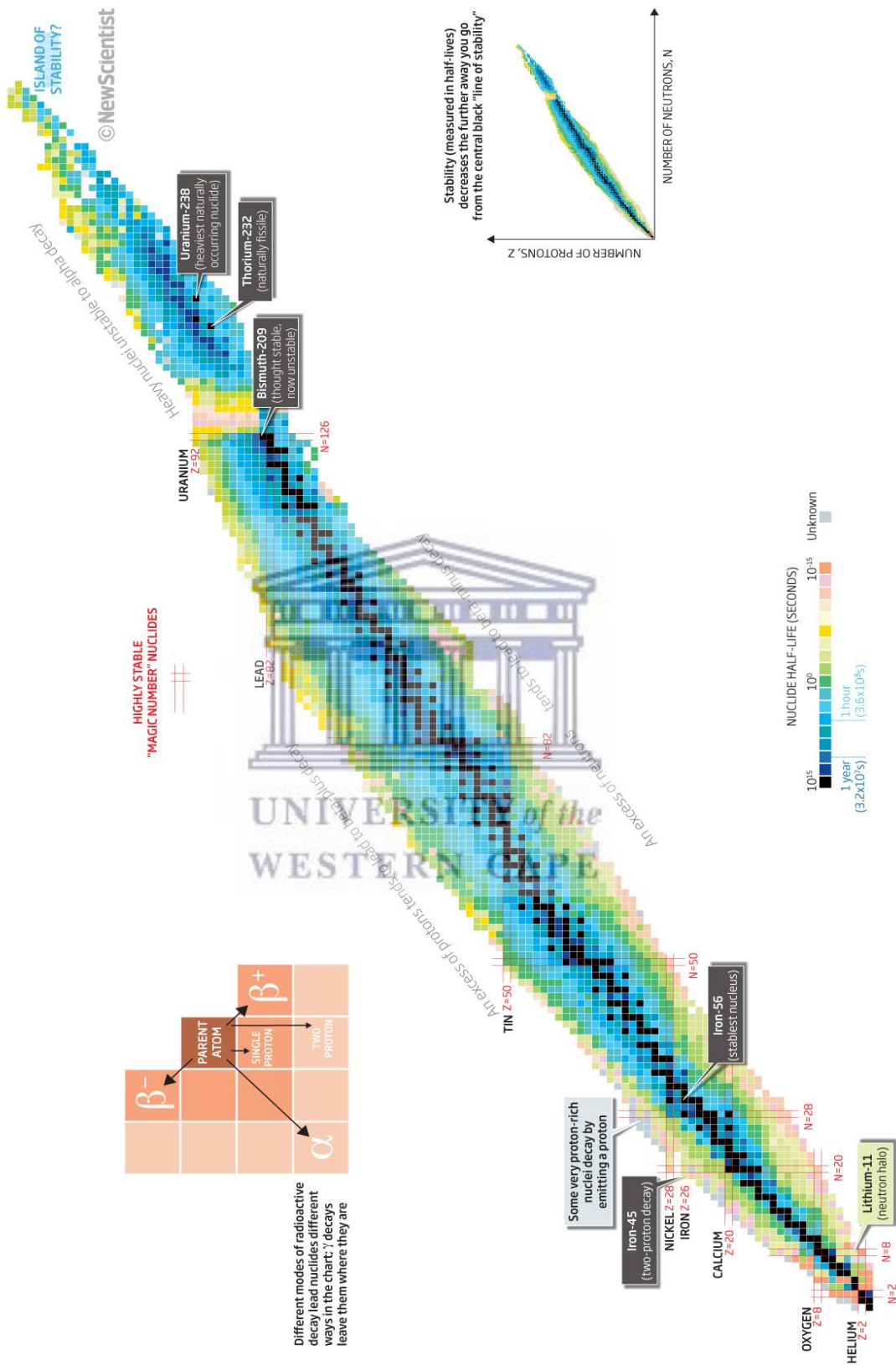


Figure 1.4 Elements with their isotopes displaying the 'Island of stability', the magic numbers and unstable isotopes. (<https://www.nuclear-power.net>)

Chapter 2: The Transport and Dangers of Radon

2.1 Introduction

Radon (^{222}Rn) gas is a noble gas (See 1.3.1 for more details.) and it does not interact with matter around it (Stieglitz, 2005). Radon is found throughout the earth and small concentrations of radon do not pose a danger to anyone. A high radon concentration can have dire consequences to plants, animals and humans, because radon is carcinogenic (Lubin et al., 1995). Radon has been identified as the largest source of exposure to naturally occurring radiation for humans (Těšínská, 2009). The International Agency for Research on Cancer classified radon as a human carcinogen (Cogliano et al., 2011).

2.2 Radioactive decay processes of uranium-238 (^{238}U)

All isotopes that are not stable (infinite half-life), will undergo decay. There are two major isotopes of uranium that are found in nature. The most common isotope is ^{238}U which make up 99.274% of the uranium present in the earth's crust. The second most common isotope is uranium-235 (^{235}U) which makes up 0.7205%. The decay chain starts with ^{238}U which undergoes a series of 14 decays where 8 are alpha decays and 6 are beta decays. ^{238}U will decay until it reaches the stable element of Lead-206 (^{206}Pb). (Figure 2.3) There are three types of decay that can occur. These are alpha, beta or gamma decay (Hosny, Al-Anezi and Khalil, 2017; Lilley, 2001; Bushberg and Boone, 2011). In chapter 1.4 the alpha, beta and gamma decay were discussed in detail. ^{238}U is a heavy nucleus, those alpha decays to start the decay chain (Masterson, 2017). A decay chain is a series of radioactive decays of different radioactive decay products as a sequential series of transformations (Birky, 2014). The Rad7 continuous radon monitor that is used in this work, measures the radon concentration of various materials and each result will be shown in Chapter 5. The Rad7 measures the average concentrations of two decays within the ^{238}U decay chain. When the Rad7 is in sniff mode, it measures the alpha decay of polonium-218 (^{218}Po), which produces a 6 MeV alpha. When the normal function of the Rad7 is activated after three hours of measuring, the Rad7 measures the alpha decay of both ^{218}Po and polonium-214 (^{214}Po) and table the average concentration.

2.3 The different sources of radon in nature

In the ^{238}U decay chain, radon is the only element in the decay chain that is in the gas phase. Radon-222 (^{222}Rn) has a relatively short half-life of 3.8 days. A half-life ($T_{1/2}$) is the time taken for an isotope to decay to half its original value (Boyes, 2003). Radon has two other prominent isotopes, (Vogiannis and Nikolopoulos, 2014) ^{220}Rn also known as Thoron and ^{219}Rn also known as Actinon. Thoron has a half-life of 56 seconds and Actinon has a half-life of 4 seconds. Radon follows all the gas laws concerning temperature and pressure (Surbeck, 2007). Naturally occurring radon, originates mainly from the proximal distances beneath the ground. A Proximal distance is the area which is located close to a centre of a geological process such as sedimentation or volcanism (Babonneau et al., 2013). The primary sources of radon can be

found in soils on the ground, rocks in the earth's crust and natural gas. The rocks located in the earth's crust breaks into soil during weathering. Soil formation occurs due to the weathering of rocks and since all rocks contain various levels of uranium, which means that all soils would also have various levels of uranium (Lyle, 2007). ^{238}U has a 4.6-billion-year half-life (Lang, 2006). The rocks that contained uranium will eventually become soil due to weathering. It also ensures that the uranium that was originally was in the rock will be in the soil too (Rosner, 2007). In the ^{238}U decay chain, radon is an immediate daughter of the radium-226 (^{226}Ra) isotope (Figure 2.1) in the earth crust (Chang *et al.*, 2008). Radium is commonly found in water (Kappke *et al.*, 2011) and leads to significant quantities of radon prevalent in groundwaters. Aquifers and rocks with a high level of uranium, can lead to high concentration of radium and radon within its groundwaters. An aquifer is a body of permeable rock which either contains or transmits groundwater (Geddes and Campbell, 2015). Radon is also moderately soluble in cold water, which means that radon dissolves in ground water and can be present in drinking water (Mechenich and Shaw, 1996). Radon is also readily soluble in organic solvents, such as toluene and xylene, which means that it can lead to higher concentrations of radon in hydrocarbon contaminants (Field, 1999). Radon is eight times heavier than air; it travels low to the ground and deposits its daughters in the form of radioactive particles or fallout. The radioactive particles are deposited on the vegetation, soil and water in nature (Bleise, Danesi and Burkart, 2003).

2.4 How radon enters the human body

Radon gas is the highest contributor to background radiation in humans (Shahbazi-Gahrouei, Gholami and Setayandeh, 2013). Radon enters the food chain in various forms because radioactive particles were deposited on vegetation, soil and water. Also eating animals that consumed plants with elevated radiation levels or using their products, such as milk, can also cause an increase in internal radiation (Dlamini, 2014). Water with a high concentration of radon or its progenies when consumed, will raise the internal radiation of humans and animals. Plants need water in order to survive and if the water source has a high level of radiation, then plants will have a high level of radiation too when it absorbs water through its roots. Soil contains naturally occurring primordial radio-nuclides such as uranium-238 (^{238}U), thorium-232 (^{232}Th) and potassium-40 (^{40}K) and they will eventually decay into different often radioactive progenies (Hamed, 2016). Plants obtain uranium and radium in the form of minerals and it is absorbed from the soil through its roots. These plants will have a high concentration of uranium if the soil has a high concentration of uranium. Tobacco leaves trap the radon and its progenies while the plant grows (Lauria *et al.*, 2009; Prueitt *et al.*, 2009). It will also raise the internal radiation within humans and animals when plants are consumed (Papastefanou *et al.*, 2009). Radon and its progenies can attach to the surface of aerosols, dust and smoke particles. This can lead to radon gas being inhaled by humans. The radon progeny can be attached to the different aerosols, dust and smoke and also enter the lungs. After being inhaled, radon and its daughters can become deeply trapped in the lungs (Al-Hamarneh and Awadallah, 2009).

2.4.1 The radiological effects of radon in the human body

Since radon and its daughters become deeply trapped in the lungs, the exposure to high concentrations of radon and its daughters for a long period can lead to respiratory functional changes and the occurrence of lung cancer (Vogiannis and Nikolopoulos, 2014). Radon and its daughters have a carcinogenic effect and it was attributing to lung cancer in non-smokers (Choi and Mazzone, 2014). There were also studies of miners that were smokers and a correlation with some of them developing cancer. The cancer study done on miners, found that those who also smoke find a higher risk in contracting cancer, especially lung cancer. This can be due to the synergistic effect of alpha radiation of radon and its progenies (Archer, 1988). The synergistic effect occurs when two or more processes in this case alpha radiation with radon and its progenies produce a combined effect, which is greater than the sum of their separate effects. Uranium occurs in every natural and edible material (Beir, 1999) and since humans need sustenance in the form of plants and animals in order to survive, ingesting radon is unavoidable (Anderson, 1996).

2.4.2 Health effects of radon progenies and tobacco smoke

Radon is the second highest cause of lung cancer within humans, while cigarette smoking is the biggest cause of lung cancer for humans (Archer, 1988). The high concentration of radon in indoor air increases the risks of developing lung cancer and the risk increases by up to ten times for smokers (Chang *et al.*, 2008). As discussed earlier, radon progenies and tobacco smoke enter the lungs attached to aerosol particles. These particles deposit on the walls of alveolar parenchyma inside the lungs (Prueitt *et al.*, 2009). Tobacco smoke and radon cause damage to the epithelium similar to how it damages lungs (Alavanja, 2002). The epithelium is the wall linings inside the organs and veins. When a cigarette burns between 500°C and 800°C, it causes lead-210 (^{210}Pb) and polonium-210 (^{210}Po) to become volatile. ^{210}Pb ($T_{1/2} = 22$ years) and ^{210}Po ($T_{1/2} = 138$ days) are radioactive metals in the vapour phase, which get inhaled due to smoke; it lodges itself into the lungs which causes the internal radiation to increase within humans (Savidou *et al.*, 2006). This increases the probability of developing lung cancer (Carvalho *et al.*, 1995). ^{210}Pb and ^{210}Po effects are not only localized within lungs because ^{210}Pb deposits on the surfaces of bones while ^{210}Po deposits in the liver, kidney, and spleen. Phosphate fertilizers enhance radiation in tobacco and the naturally occurring radiation material (NORM) enhances the level of the radionuclides accumulating in leaves of the tobacco plant while the plant grows (Prueitt *et al.*, 2009). Tobacco smoke and radon increases the chances of inducing lung cancer due to the synergistic effect of the two. The risk of contracting cancer is much higher with smoking, than radon (Savidou *et al.*, 2006). A 20 cigarette a day smoker inhales about 50 times more ^{210}Po than a non-smoker whom only receives ^{210}Po from air (Yngveson *et al.*, 1999).

2.5 The presence of radon within rocks

Since radon is an inert noble gas, it freely moves between particles of building materials to the soil surface. Building materials are usually made up of soil, rock and sand (Nielson et al. 1996; Bossew, 2003). Rocks are the ingredient that occurs in many building materials such as building bricks, concrete and it can be used as filler material. In Beaufort-West some residents used mine tailings containing uranium bearing sandstone as filler material for their dwellings. In some occurrences, the radon concentrations were at a very high level (See 5.5.1 for more details). Uranium is a by-product from gold and copper mining in South Africa (Toth, 2011). Rocks containing these minerals are crushed and treated with chemicals like cyanide. This is to extract the minerals such as gold, copper or any other mineral that is mined within the rock. After the process, the residue or mine tailings is left to dry out in huge constructed dams. The mine tailings may contain the radioactive element uranium and other trace elements but at higher activity concentrations (de Meijer et al., 2001). The mine tailings can also contain other radioactive elements such as ^{232}Th , ^{40}K and ^{238}U and ^{235}U . The ^{238}U will eventually decay to ^{222}Rn (See 2.2 for more details). Radon might escape the soil particle by recoil and then by the processes of diffusion and advection. Advection occurs when heat (or matter) moves due to temperature (or pressure) differences (Ganguly, 2008).

2.6 The presence of radon within soil

All soils contain the primordial radionuclides ^{238}U , ^{232}Th and ^{40}K (Åkerblom and Mellander, 1997). The focus will be on ^{238}U , since radon follows on the uranium decay chain. (See 2.2 for more details) Since ^{238}U is in the earth's crust, it is present in all soils, building materials, groundwater and natural gas, which means that radon will emerge since ^{238}U eventually decays into radon. Soils with high uranium content will yield a high radon concentration too (Markkanen and Arvela, 1992; Åkerblom and Mellander, 1997). In soil, uranium occurs in the form of a uranyl cation (UO_2^{2+}) (Ebbs and Kochian, 1998). (See 3.6.3 for more details). Radon might escape the soil particle by recoil and then by the processes of diffusion and advection (Ganguly, 2008). Nevertheless, the ground is the major radon source. Certain rocks and soil, such as some granites and shales, contain more uranium than others.

2.7 Radon accumulation in houses

Radon concentration is measured in Bq.m^{-3} (Becquerels per cubic metre), which is also the unit that the RAD7 uses. All the measurements in Chapter 5 were measured in Bq.m^{-3} . The United States Environmental Protection Agency (EPA) has different levels of recommendations for different concentrations within the house. Anything lower than 200 Bq.m^{-3} requires no action while 100 Bq.m^{-3} is considered as the target level. The target level is the international reference proposed by the World Health Organization (WHO) to minimize the health hazards due to indoor radon exposure. This varies from country to country and WHO allow a concentration as high as 300 Bq.m^{-3} (Ting, 2010) The National Radiological Protection Board (NRPB) proposed

that the action level for dwellings (domestic properties) is 200 Bq.m^{-3} and 400 Bq.m^{-3} in the work place (Amin and Eissa, 2008). Concentrations between $200 - 750 \text{ Bq.m}^{-3}$ requires action within a few years, although a measurement over 300 Bq.m^{-3} can be hazardous to one's health in the long run. The $750 - 7500 \text{ Bq.m}^{-3}$, action required within months. Anything higher than 7500 Bq.m^{-3} requires immediate action. There were instances where the concentration of radon in the air was measured to be approximately 2000 Bq.m^{-3} in some homes (Guimond, 1988). According to Figure 2.1, soil is the largest contributor of radon, followed by groundwater (which is grouped as well water since the source is the same) (nationalradondense.com). Radon enters through cracks in foundations and construction joints through various processors such as the water supply and molecular diffusion. This happens at a microscopic level and it is impossible for a foundation to be free of cracks and thus radon will always seep into the dwelling (Nazaroff *et al.*, 1987; Vinson *et al.*, 2008). In houses with air conditioning windows are sealed for various reasons and it also causes that the dwelling will have a higher concentration of radon (Urosevic *et al.*, 2008). A house that is well ventilated will normally have a lower level of radon concentration than a poorly ventilated house.



Figure 2.1 Radon contributions to dwellings. (www.nationalradondense.com)

The two dwellings that were studied in chapter 5 were Aardoon and Blikkraal. The Rad7 could not measure the dwelling at Blikkraal because it was well ventilated (See 5.5.5 for more details). The other dwelling Aardoon (See 5.5.2 for more details) showed a significant rise of radon concentration during the evening in one test due to poor ventilation. Air pressure in most cases is lower inside the dwelling than in the soil and the foundation of the dwelling. The dwelling acts like a vacuum and traps radon inside due to the pressure gradient (Mohamed *et al.*, 2008). Cold radon-containing air from the ground replaces the warm air inside the house and it causes the radon to seep into the dwelling (Zhuo *et al.*, 2008). Environmental factors such as temperature of the soil, atmospheric temperature and pressure affects the radon flux. Increased temperature, pressure and lower wind speeds increases radon flux. Radon flux is the activity of radon that passes through an area per unit time expressed in Becquerel ($\text{Bq.m}^{-2}.\text{s}^{-1}$) (Eff-Darwich *et al.*, 2008). Houses that use ground water for water supply for household activities can have a higher level of radon within the house (Singh *et al.*, 2008).

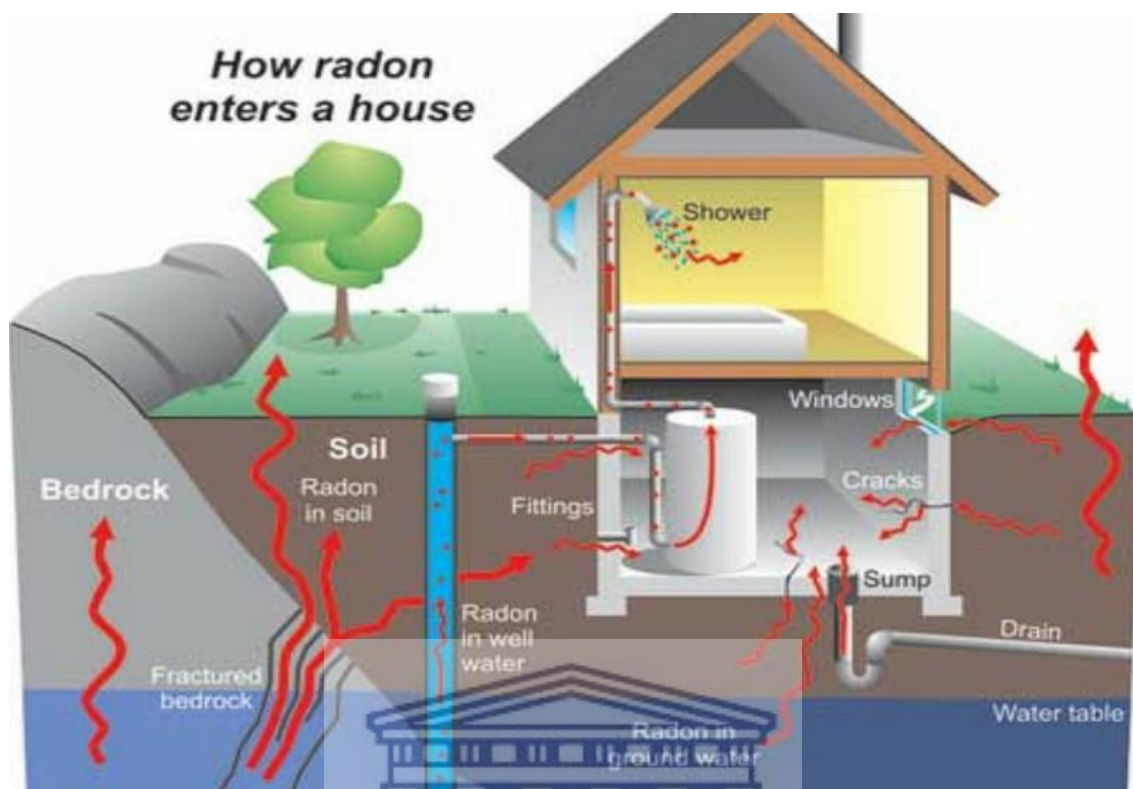


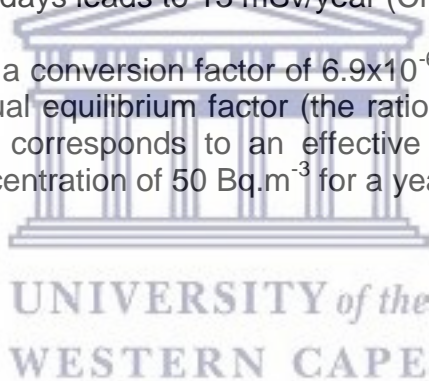
Figure 2.2 Pathways for radon to enter a house. (www.remtekenvironmental.com)

Radon comes into the house in various ways and means. The first is the air which naturally comes in the house and this was discussed in detail (See Figure 2.2). Soil with moderate contents of uranium and/or radium can also give high indoor radon concentrations (Kreuzer and McLaughlin, 2010). Air from the soil and groundwater are sources of radon and it seeps through the foundation to come in the house (Vinson *et al.*, 2008). Building materials can also be a source of radon due to various factors which will be discussed in Chapter 3 in detail (Faheema *et al.*, 2008). Ventilation plays an important role in the radon level of a dwelling since a well-ventilated house keeps the radon level low due to fresh air coming into the dwelling and flushing the radon out of the dwelling. A poorly ventilated house will build up radon inside the dwelling if it has a poor air exchange rate (Loureiro *et al.*, 1990). Groundwater usually has a higher level of radon than surface water. Radon from water and ingestion from dissolved radon which poses a radiological risk that affects the stomach and lungs (Marques *et al.*, 2004). When measuring radon exposure in a dwelling it is important to evaluate the radon concentration in water and air. The transfer velocity coefficient of radon from water to air should be known determine the values of the corrections can be made to remedy the high level of radon (Loureiro *et al.*, 1990; Faheema *et al.*, 2008).

2.8 Dose rates absorbed by humans

The SI unit for dose is measured in Sieverts, which measures the health effect of ionizing radiation on the human body (Liptak and Venczel, 2016). The measurement period varies on the specific experiments. The most common measurement periods are hour, day, month or year. The period in use will be per year (annum). Dose rate indicates the amount of radioactive dose of a person over a specified period of time (Liptak and Venczel, 2016). The unit in use will be millisieverts per year (mSv/a). Background radiation due to terrestrial and cosmic radiation has the following readings. Cosmic radiation contributes about 0.6 mSv/year at sea level, while at high altitude (1500 m above sea level) it contributes 0.47 mSv/year (Karam and Leslie, 1999). In nuclear power stations, the radiation workers have a limit of 20 mSv/year on average over a five-year period. During a flight the dose rate is about 0.005 mSv/hour due to cosmic radiation (Cho et al. 2017). Synthetic radiation increases the dose rate, mostly due to medical treatments. Medical treatments will be measured in dose per treatment, since the time period varies. A mammogram is about 0.30 mSv, a brain CT scan between 0.8–5 mSv, a chest CT scan is between 6 to 18 mSv and a Chest x-ray equals 0.1 mSv. Internal radiation on average contributes roughly 0.40 mSv/year. Smoking 30 cigarettes a day for 300 days leads to 13 mSv/year (Cho et al. 2017).

The ICRP recommends a conversion factor of 6.9×10^{-6} mSv per $\text{Bq} \cdot \text{h}^{-1} \cdot \text{m}^{-3}$ for radon assuming the usual equilibrium factor (the ratio between radon and its progeny) of 0.4. This corresponds to an effective dose of 3 mSv when breathing air with a concentration of $50 \text{ Bq} \cdot \text{m}^{-3}$ for a year (www.icrpaedia.org).



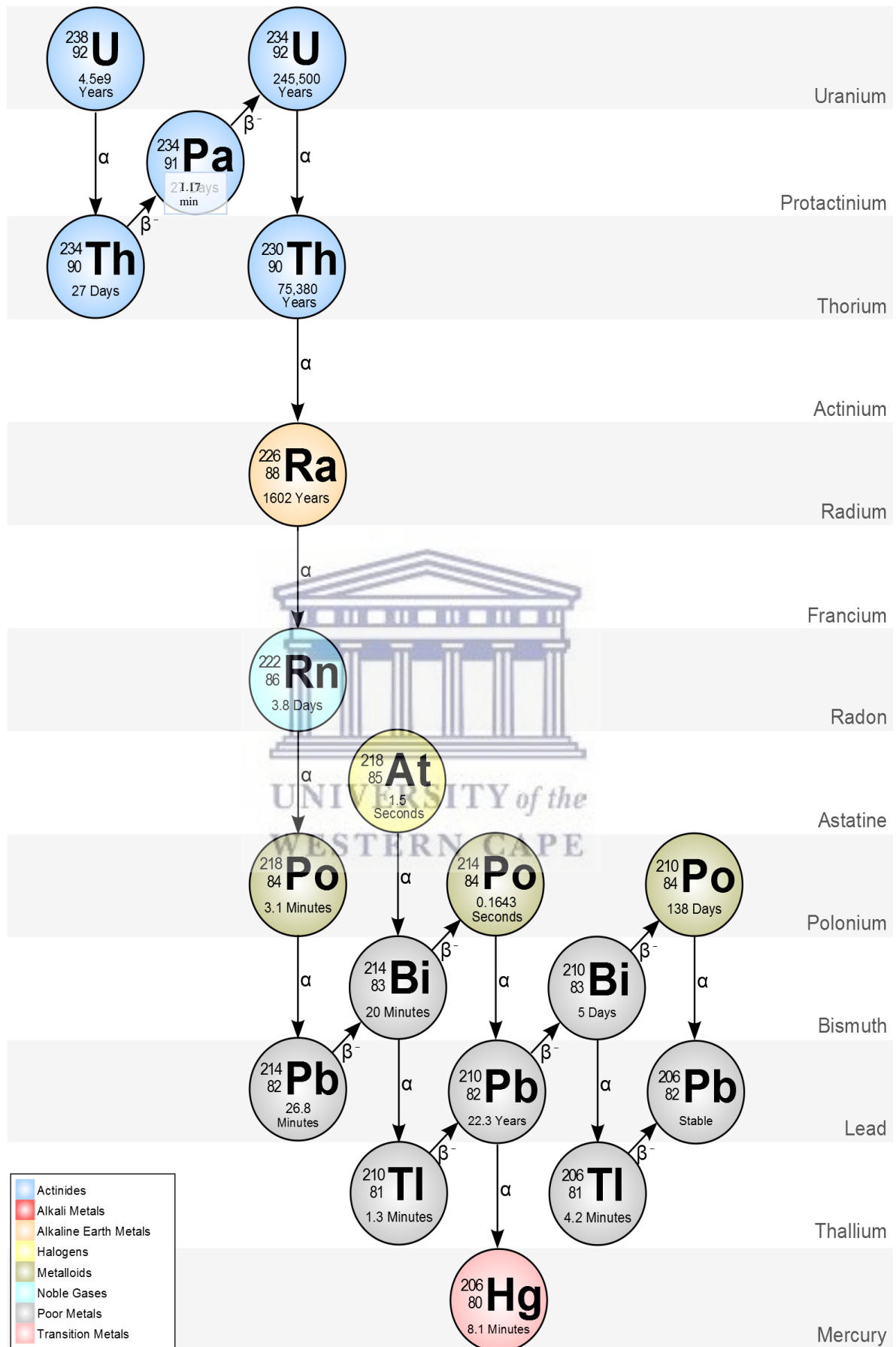


Figure 2.3 The uranium decay chain (metadata.berkeley.edu).

Chapter 3: Building Materials and their occurrence in South Africa with emphasis on the Western Cape.

3.1 Introduction

Most building materials in South Africa are sourced close to the construction site due to the expensive cost of transporting building materials (Ngcofe and Cole, 2014). With the exception of granite, (See 5.3.1 to 5.3.7 for more details.) most building materials are sourced relatively close to the dwelling or construction site. Decorative materials used for dwellings will also (in this study) be considered as Building materials. This will place them in the same category as construction materials. Uranium is present in all types of soil with varying levels of concentration. A high concentration of uranium will usually yield a high concentration of radon in the environment, since radon is in the uranium decay chain. (Figure 1.1 and Figure 2.3)

3.2 Sand (Fine aggregate) used in the construction of dwellings (Building Sand)

Building sand is distributed over most of the Western Cape Province but is generally absent in areas underlain by Karoo Super Group which includes Beaufort-West. In these areas building sand has to be transported from other areas (Ngcofe and Cole, 2014). Building sand is an integral part of construction and it is commonly used in the concrete mortar and plaster manufacturing. It is expensive to transport building sand more than 80km (Roberts et al., 1998). Philippi sand and Malmesbury sand (Figure 3.1) are the most common types of sand that builders use in the Greater Cape Town area and the West Coast. Philippi sand can be identified by its light brown to beige colour and it is situated amongst dune sands, in the Philippi Horticultural Area (Cole, 2011), Macassar and the region situated to the West (Figure 3.3). It consists of very fine to coarse grained quartz sand with comminuted shell fragments. The mining area is close to the sea. Malmesbury sand is mainly used in manufacturing the sands of concrete, plaster and mortar. All three of these components are crucial in the building industry. (Cole and Viljoen, 2001).



Figure 3.1 Typical Building sand

3.3 Stone aggregate (Course aggregate)

Stone aggregate is crushed rock that has a diameter of more than 6.7mm. It is used in the construction of roads and pavements. Rocks from the quartzitic sandstone are mined in the quarries that are located in the Table Mountain Group which is situated in the greater Cape Town area (Cole, 2003; Roux, 1998). Stone aggregates in the Malmesbury Group are sourced by three mines in the area and these aggregates are mainly used for concrete and road-construction material (South African Bureau of Standards, 1994). The largest source of stone aggregate in the greater Cape Town area is a quarry located in the Tygerberg Hills area which is close to the suburb of Durbanville. The other significant quarry is Peak Quarry which is located near Eerste River (Motsoenyane, 2010) with smaller disused quarries located near the areas of Blouberg, Philadelphia, Blackheath and the region South East of Somerset West. The Peak Quarry contains hornfels which are used for concrete aggregate and road construction (Hill et al., 1992; Cole, 2003). Hornfels are metamorphic rock which was formed by the contact of shale or any clay rich rock that come in contact with a hot igneous rock. Metamorphic rock is a type of rock which was changed by extreme heat and pressure. An igneous rock is formed through the cooling and solidification of magma or lava (www.uotechnology.edu.iq). Stone aggregate based in the Table Mountain Group sandstone can be found North East, East and South East of Somerset West. The main source of the Stone Aggregate in the Southern Cape is in the Bredasdorp, George and Knysna regions (Roberts et al. 2008; Motsoenyane, 2010). These are present in the Peninsula and Skurweberg Formations which contains quartzitic sandstones and it is a good source for high quality concrete aggregate. One of the most prominent active mines is Palmiet, a quarry located near Cape Town is the town of Grabouw. The quarry located close to a farm called Elgin forest, which is located between the N2 and Peninsula Dam (Motsoenyane, 2010). The Grabouw area contains ample resources of Sandstone (Gresse and Theron, 1992). Near the West Coast Town of Mamre, stone aggregate from granite contains coarse-grained, porphyritic granites (Minerals Bureau, 1987). Coarse-grained porphyritic granites as well as sheared granites are found in Klipheuwel, Kuilsriver and Somerset West (Theron et al., 1992; Cole, 2003) but are excluded from the potential sources of stone aggregate because they are located too close to houses. Sources of granite suitable for stone aggregate are also located at the Rheeboek quarry North of Malmesbury (Cole, 2003; Motsoenyane, 2010). This is stone aggregate granite that is crushed into small pieces for use in concrete etc. The Malmesbury Group does not contain granite. The rocks of the Malmesbury Group contain shale, hornfels, sandstone which had been intruded by granite.

3.4 Brick clay

The Western Cape's supply of wood and natural building stone is not sufficient for building materials, which leads to the use of brick clay as an important component for building materials. Brick clay is the most popular building material in South Africa. The largest resource in the Greater Cape Town area for Brick clay mining is located between Stellenbosch and Klipheuwel with 12

mines (of which most are currently closed). The Malmesbury Group contains various mines located South and South East of Atlantis (Cole, 2003; Heckroodt, 1980). The minerals illite, kaolinite and quartz must be present to ensure that the quality of the brick clay is sufficient to use in construction of low rise dwellings such as houses, flats and office blocks (Horn, 1998), (Heckroodt 1991). Kaoline has good sintering characteristics which are compacted and forming a solid mass of materials without melting it. Quartz acts as a stabilizer and illite produces the plasticity of the plastic bricks (Van Strijp, 1998).

3.5 Limestone and dolomite

Pure limestone is a sedimentary rock which contains mainly minerals out of calcium carbonate (CaCO_3) namely calcite and aragonite. Most limestones are composed of skeletal fragments of marine organisms such as coral, forams and molluscs. Both limestone and dolomite were formed in similar geological environments and both have similar uses, but since limestone is the purer substance, it is more valuable. Dolomite is CaMgCO_3 (Cole and Ngofe, 2013) and it is mostly found in the Malmesbury Group (Martini, 1987). The high-grade limestone also occurs in the Cango Group North of Oudtshoorn. Low-grade limestone occurs in the Bredasdorp and Strandveld Group. Dolomite is found mostly in the Malmesbury Group and it occurs in small quantities across the Western Cape (Martini, 1987). Limestone has several applications such as cement manufacturing, purification of metals and water, steel production, and it neutralizes acidic soils (Martini and Wilson, 1998). Limestone and Dolomite can be found in different areas such as Vredendal, Velddrif, Piketberg, and Saldanha on the West coast. The only areas in the Western Cape with inland mines are located near Robertson (Cole, Gcofe and Halenyane, 2013).

3.6 Uranium

Uranium is the parent of the radon hence the occurrence and mining of uranium is important indication of radon sources. This section will discuss uranium and uranium mining in some detail. Uranium is the heaviest element that occurs in nature and has an atomic number of 90. Uranium has an average concentration of 0.0003% (3 parts per million or 3 mg/kg) in the earth's crust (Cinelli et al., 2017). Uranium has three naturally occurring isotopes namely ^{234}U , ^{235}U , and ^{238}U ; since each natural isotope is radioactive. The natural occurring isotopes have a Natural Abundance of 99.28% for ^{238}U , 0.72% for ^{235}U and 0.0055% for ^{234}U (Beir, 1999). These three isotopes are each radioactive and it decays into more stable atoms with the use of alpha-, beta- and gamma decay.

3.6.1 Uranium occurring naturally in nature

The natural occurrence of uranium could give an indication if building materials may contain high concentrations of radium, the parent of radon. Like many elements, uranium is found in a variety of chemical forms in nature. These compounds are found in soils, oceans, food, and drinking water (Bleise, Danesi and Burkart, 2003). In soil, uranium occurs in the form of a uranyl cation (UO_2^{2+}) (Ebbs and Kochian, 1998). Granite weathers to soil, so if the granite contains Uranium it can occur in the soil after the weathering of granite. One can safely assume that there will be uranium content inside any building material (NCRP, 1984). The uranyl ion (UO_2^{2+}) is soluble and formed by the oxidative dissolution of uraninite (UO_2). The uranyl ion (UO_2^{2+}) occurs in various concentrations in surface waters and groundwater. In soils, uranium is soluble due to the uranyl ion (UO_2^{2+}) which was caused by the oxidation of uranium. This makes for easy mobilization during surficial processes. In contrast, thorium is relatively insoluble, and is adsorbed onto clay minerals and residual minerals, whilst uranium is distributed in groundwaters (Pertlik et al, 1978). Uranium in rocky areas is mostly found in granites and mineral deposits. Rocks contains uraninite (UO_2) is a source major of uranium. Uranium content in igneous rocks has a great variation in uranium content which is due to the petrological subgroups. Petrological subgroups are the classification of the different types of rocks. Rocks are classified in different sections with origin, structure, composition and distribution (Hunter-Smith, 2012).

3.6.2 Uranium mining and locations of uranium deposits in South Africa

In South Africa, most uranium is extracted as a by-product of gold, silver and copper mining. South Africa produces about 0.89% of all uranium globally (www.world-nuclear.org a). Between 2004 and 2008, uranium prices experienced a sudden surge in price and prospecting for new mines across the world. This affected the demand in uranium and also prospecting for new mines, especially in the Beaufort-West area. After the price implosion of 2009, many projects were abandoned for a later time (www.karooinvest.co.za). Uranium is found in different areas and in different types of soils throughout South Africa. Figure 3.3 shows the spread of the uranium mines and reserves across South Africa.

The Witwatersrand Supergroup contains uranium in the form of uraninite(U_3O_8). This is the largest source of uraninite(U_3O_8) in South Africa (Frimmel et al. 2014). The main source of uranium is the Black Reef Formation which contains many gold mines in the area. (Fuchs, Williams-Jones and Przybylowicz, 2016) The Phalaborwa Complex has uranium that occurs within carbonatite (Heinrich, 1970). In the Glenover Complex contains low grades of uranium. Uranium is found in the Waterberg Group and Pilansberg Alkaline Complex where uranium occurs in green foyaite (Fourie, Henry and Maré, 2009).

The Cape Granite Suite consist only of Sandstone and Shale, while the Cape Granite suite contains uranium (Ngcofe and Cole, 2014).

The Verena Porphyritic Granite and Klipkloof Granite which are located in the vicinity of Bronkhorstspuit. The other significant location is in the granite suite of the George Pluton which contains uranium (Ngcofe and Cole, 2014).

The Griekwaland West Supergroup contains different types of uranium in various areas. The Namaqualand Metamorphic Complex contains many different suites that contain uranium. Roodewal Suite contains uranium is located in granite gneiss. Spektakel Suite located in central Namaqualand contains a high concentration of uranium due to the granite gneiss present in the region (Haddon, and McCarthy, 2005).

3.6.2.1 The Karoo Supergroup

The Karoo Supergroup contains many different uranium sources. The two groups that will be discussed in detail is the Adelaide subgroup and the Springbok flats area which is situated in the Irrigasie Formation. The Adelaide subgroup contains uranium which is sandstone hosted. The uranium in the Adelaide subgroup spans between Beaufort-West going East towards Cradock and North towards Bloemfontein (Cole, 2009).

The Irrigasie Formation encompasses the entire Springbok flats within the Karoo Supergroup (Nel, 2012). The Springbok flats are located around the town of Rustenburg which contains many coal mines (None of them are active at the moment). Uranium is a byproduct of coal mining and thus it is said to be coal hosted. In the Bushveld complex the uranium was probably derived from granite, which is locally in contact with the coal zone on the flank and shoulders of the palaeo valleys. This rock type from the Bushveld complex contains relatively high uranium values, around 20 – 40 ppm uranium (Kruger, 1981). The Springbok flats are located in the province of Gauteng with the Northern border moving slightly into the Limpopo province and the Western border into the North West province.

The Molteno Formation is overlaid by the Elliot, Clarens and Letaba Formations. The Elliot Formation contains red mudstone which contains uranium (Roberts et al., 1998).

Beaufort-West has a huge reserve of uranium and mining will only occur when there is a bigger demand for uranium (See Chapter 3.6.1 and 3.6.2 for more details) (Ngcofe and Cole, 2014). Some of the prospective pits are located on farms and some farmers used the mine tailings created by prospectors. The mine tailings were used as filler material, when maintenance works on some of the dwellings (See Chapter 5.5 for more details.) (Masia, 2010). The filler material was collected around the Beaufort-West area. Since it is not economically viable to transport sand and other building materials over vast distances, some farmers decided to use the rubble on the farms to minimize cost in erecting a dwelling (Ngcofe and Cole, 2014). During 2009, two farms Blikkraal and Aardoorn were found to have elevated levels of radon inside their dwellings probably due to stones from a prospecting site that was used during construction (Masia, 2010). There were three types of measurements done on

the Aardoorn farm. The first test was a RAD7 test in the dwelling for 24 hours to measure the radon levels (See section 5.5.2 for the results of the experiment.). The second test was an S-Chamber test of different rooms within the Aardoorn dwelling (See Chapter 5.5.3 for the results of the experiment) and the third test was an L-Chamber measurement of the same room. The radon level of Blikkraal was measured using L-chamber electret. (See section 5.5.5 for the results of the experiment.) Since Beaufort-West has a massive uranium reserve, it can be expected that the soils will have elevated levels of uranium. Since radon is on the uranium chain, the soils will have elevated levels of radon. The sample was mined at a farm called Ryst Kuil and the tailings (see Figure 3.2) were used by the surrounding farms. (Heritage Western Cape, 2015) A sample of uranium bearing sandstone that originated from the mine tailings was measured by the RAD7 as part of this thesis (See 5.5.1 for the results of the experiment.).



Figure 3.2: Tailings at the prospecting site on the farm Ryst Kuil.

3.6.3 Uranium mining and its future in Namibia

According to a 2014 survey, Namibia is the 5th largest producer of uranium and contributes up to 6% of the annual world demand (Figure 3.1). Japan the largest importer of Namibian uranium. Namibia exports to other areas such as North America, Europe and various countries within Asia. Since uranium exports are classified information, further information is not available. In 2016 mining contributed 11% to the GDP and 50% of the foreign exchange earnings of Namibia (www.thevillager.com). All Namibian uranium deposits are mined in open pits, as this practice is the most cost effective way to mine. (Hore-Lacy, 2016) It is more cost effective than underground mining. The danger of open pit mining is that it poses a higher health risk than underground mining due to the dust residues created by the mining. The uranium residue decays and it eventually forms radon which could be hazardous to one's health when inhaled. Most uranium resources contain only a fraction of uranium and 1 metric tonne of ore leads to about 500 grams of usable uranium (www.world-nuclear.org e). The mined uranium bearing sandstone is crushed and then leached to dissolve the uranium, which is then separated and precipitated as a concentrate containing 90% or more uranium oxide (U_3O_8). This granular concentrate is generally referred to as yellow cake. The remains called tailings are still radioactive and are usually disposed into the pits. It is

expected that uranium mining will surpass Diamond mining in earnings around 2020 to 2022 (www.ijg-research.net). The future of uranium mining in Namibia depends on many factors such as the spot price of uranium and further demand for building nuclear reactors in the near to medium future.

3.6.3.1 Location of uranium mines in Namibia

According to Figure 3.7, the overwhelming majority of the uranium mines and deposits are located between the central shoreline between the cities of Walvis Bay and Swakopmund on the Western region of Namibia and the central region of Namibia near the city of Usakos. The most Northern located mine in the cluster, is a mine called Lofdal, which is located near the city of Khorixas. (Figure 3.7) The mine produces various rare earth materials (www.mindat.org a). It also has a sizeable amount of uranium reserves (www.namibiarareearths.com). The mine located in the North Western region of Namibia near the Northern shoreline and the Angolan border is called the Sarusa mine, near the city of Uropembe in the Kunene region. Sarusa is located outside the area where the bulk of mines are situated and according to the Ministry of Mines and Energy of Namibia (Mining Directorate, Ministry of Mines and Energy, 1995), the mine contains sand stone hosted uranium, but no information on the uranium reserves of this mine is available, since the mine is not in use. Information on uranium mining is only available on active mines. Currently, Sarusa is an abandoned marble mine which also yields Carnelian, a type of quartz (www.mindat.org b). The bulk of the mines are situated within the 400 to 500 km-wide Upper Damara orogenic belt. According to Figure 3.8, 11 major mines and advanced projects are located within this area. The mining activity of these mines is dependent on the uranium price and water availability (Hawkesworth, Menzies and van Calsteren, 1986; Gray et al., 2008). There are about 6 mines or advanced mining projects that are located roughly in the alaskite hosted uranium province (Figure 3.9). An alaskite or leucogranite is a light coloured granitic igneous rock with almost no dark minerals. A uranium province can be defined as a large geologically and tectonically distinct region where substantial uranium is concentrated into clusters. The uranium is recovered either economically or as the sole commodity or as a by-product from another commodity such as gold, copper and phosphate. (Finch, 1996) The largest mine in Namibia is the Rössing mine which is also the 4th largest uranium mine in the world and its location is 65 km NE of Swakopmund (Conde and Kallis, 2012). The Rössing mine is also located in the middle of the alaskite uranium province.

3.7 Health Hazards from uranium

Uranyl (UO_2^{2+}) is highly soluble in water, which in turn enters the human body due to surface and ground waters. Uranyl (UO_2^{2+}) is more readily absorbed into the human body than other forms of uranium which have significantly lower forms of solubility in water (Zavodskaya et al., 2008). Although ingesting of water with an elevated level of uranium is not recommended, it can be assured that more than 95% of the uranium that enters the body will be eliminated due to the excretion of faeces. Uranium can be absorbed in the blood and 67% of that uranium will be filtered by the kidneys through urinating within 24 hours. Up to 2% of uranium in food and water is absorbed by the gastrointestinal

tract. Minute traceable quantities of uranium are found in the liver and studies found it does not have any adverse effects on the organ (Jakhu, Mehra and Mittal, 2016). The 5% of uranium that are absorbed can be quite hazardous to the human body because it can cause adverse effects such as an increasing risk of contracting cancer (Berlin and Rudell, 1986). Uranium affects the functions of the kidneys and causes serious problems with the osseous matter. Osseous matter is the building material that makes up the bones and cartilage of the human body. Uranyl ions (UO_2^{2+}) that accumulate in the bones replace the calcium of bone crystals in the hydroxyapatite complex (Moss, 1985) and cartilage (Hunter, 1987). Hydroxyapatite is a mineral that is present within bones and teeth in the human body. Hydroxyapatite is a major ingredient of normal bone and teeth which gives bones and teeth their rigidity; It also makes up 50% of the volume and 70% of the weight of a human bone. (Fuller, et al., 2002) The effect that uranium has on bones and teeth can be extremely devastating. Uranyl ions (UO_2^{2+}) that accumulate in the kidneys run a high risk in contracting nephritis. There are other ways how uranium can indirectly affect humans due to the major anthropogenic activities that release uranium into the soil. These activities include uranium mining and milling, uranium processing, phosphate mining, heavy metal mining, coal use, and inappropriate waste disposal (www.atsdr.cdc.gov).

3.8 Dimension stone: Granite

Granite in general exhales more radon than any other types of construction material due to the possible presence of a relatively high uranium content, in its natural formation (Bertrand et al 1994; Cole, 2013). Dimension stone is a term used to include various natural stones used for decorating of buildings and stone structures. The Western Cape has three major types of dimension stone, which are granite, marble and sandstone. The two are types of granite that are currently mined in the Western Cape; they are Paarl Grey and Green Granite (Durrani and Ilic, 1997). There are pink granite outcrops that are located in Saldanha which is located in the Saldanha Strandveld Biozone which is located in a critical biodiversity area. These areas are also earmarked for oil and gas storage, which makes the mining of the pink granite quite minimal (Rossouw, 2014). The granite named Paarl Grey is only mined in the Paarl area and it consist of 5 varieties, all of which are mined in the Paarl mountain area. (Figure 3.3) The quarry mining the Paarl grey is located close to the slopes of Paarl Mountain called De Hoop quarry which mines Laborie granite, otherwise known as Paarl green. The other major variety is known as Bretange which is similar to the Paarl grey granite. Green granite mines are found near the towns of Bitterfontein, Vredenberg, Vanrhynsdorp (Figure 3.3).

3.8.1 Granite in the Springbok flats area

The Springbok flats have a lot of different type of granites and there is a variety of colours such as Red, Black, Brown, Lilac, Pink, Grey, Green and Blue. The Granite African Red which is mined in the Springbok flats showed elevated levels of radon. Granite in general exhales more radon than other types of construction material due to the fact that granite can act as a radon trap

(Wagner, 1994). Generally, granite contains minerals that is radio-active zircon, monosite etc. Granite samples from the Springbok Flats area are expected to have a higher radon count due to high concentration of uranium in the area (www.infomine.com). It is known that granite in general exhale more radon than other types of construction material due to the presence of relatively high uranium content in its natural formation (www.largeigneousprovinces.org; Bertrand et al, 1994; Cole, 2013).

3.8.2 Namibian granite

The upper Damara belt (See Figure 3.8 and Figure 3.10), which includes alaskite hosted uranium province which is about 100 kilometres long and 50 kilometres wide, host the bulk of active mines and major projects. (See section 3.6.1 for more details.) The alaskite hosted uranium province (Figure 3.10) has two major types of deposits; they are located mineralization associated with intrusive granitic rocks alaskite (leucogranite) and mineralization associated with calcrete formations. Rössing contains significant reserves of leucogranite (Figure 3.9). The major mines Langer Heinrich and Trekkopje, located just outside the alaskite hosted uranium province, contains calcrete hosted uranium deposits (Figure 3.9) (OECD, 2014).

There are various types of granite in Namibia which are mined throughout the country. The granite companies are located within the upper Damara belt, which also contains the alaskite hosted uranium province. The mines yield different types and colours but the mining depends on economic viability and demand of the product. The company Damara Granite mine a yellowish-brown granite quarried near Rooikop, 15-km East of Walvis Bay, which is also located within the alaskite hosted uranium province. Namstone quarries red granite on the farm Rietkuil, Opuwo district (Geological Survey of Namibia, 2006). The company also quarries a light grey to white granite on Etendero 95 and pink porphyritic granite on Morewag 480, both in the Omaruru district. Marlin Granite Namibia quarries light green granite gneiss with red garnet porphyroblasts occurring 12km South East of Walvis Bay and a pinkish-yellow porphyritic granite at Okombahe, 16-km East of Uis. Marmorwerke Karibib quarries a medium to coarse grained, equigranular granite near Spitzkoppe which is situated North West of the town called Usakos (Geological Survey of Namibia, 2006). The mine also yields white granite known as Namibian Pearl, a yellow granite known as Tropical Sun and the light brown granite known as Kalahari Sand. Another quarry located in the Okahanja District near the city of Okahanja North of Windhoek is a deep reddish brown, medium to fine grained, equigranular alkali-granite known as Guldenrot (Geological Survey of Namibia, 2006). A mine located South West of Karibib produces a granite with the name of Bib which is a coarse grained red pegmatitic granite with a slightly porphyritic texture. It also produces Goas White, a uniform textured whitish-grey coarse-grained slightly porphyritic granite. The same company also quarries Omenje Black, a fine to medium grained dolerite with a greenish-black colour and ophitic texture, located South East of Omaruru (Geological Survey of Namibia, 2006). The granite Namib green was measured in this work and it was found to have elevated levels of radon. (See 5.6 for more details). According to Marmorwerke Karibib the granite Namib

Green located 15 km East of Swakopmund it would be mined on request. (Geological Survey of Namibia, 2006) The mine is on list of dormant (or abandoned) mines of Namibia and according to the GPS coordinates (22,61° South and 14.66° East) it falls within the alaskite hosted uranium province and this it will have a high concentration of uranium (www.geology.cz).

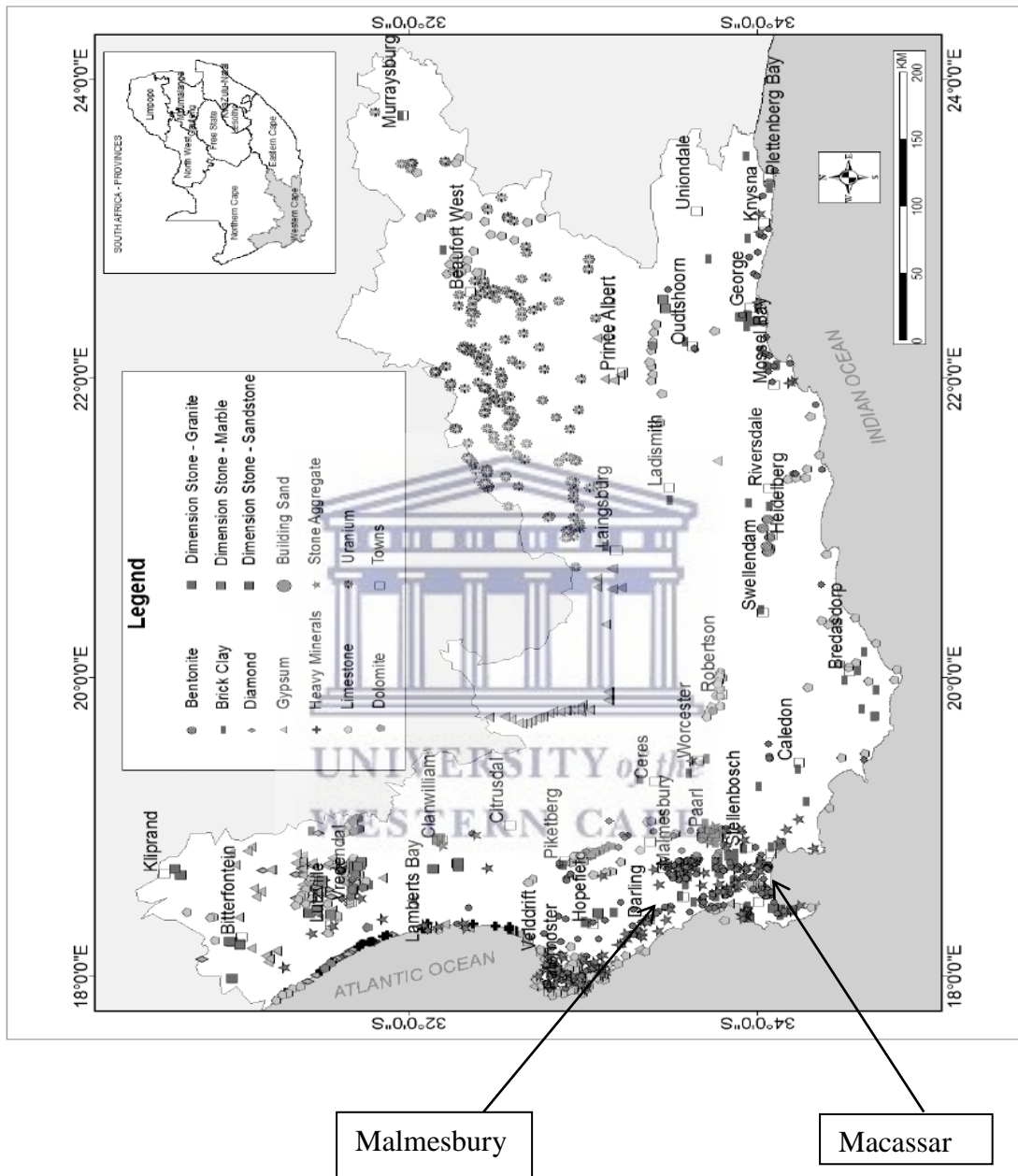


Figure 3.3 Map of the mineral potential of the Western Cape Province. (Cole DI and Ngofe 2013)

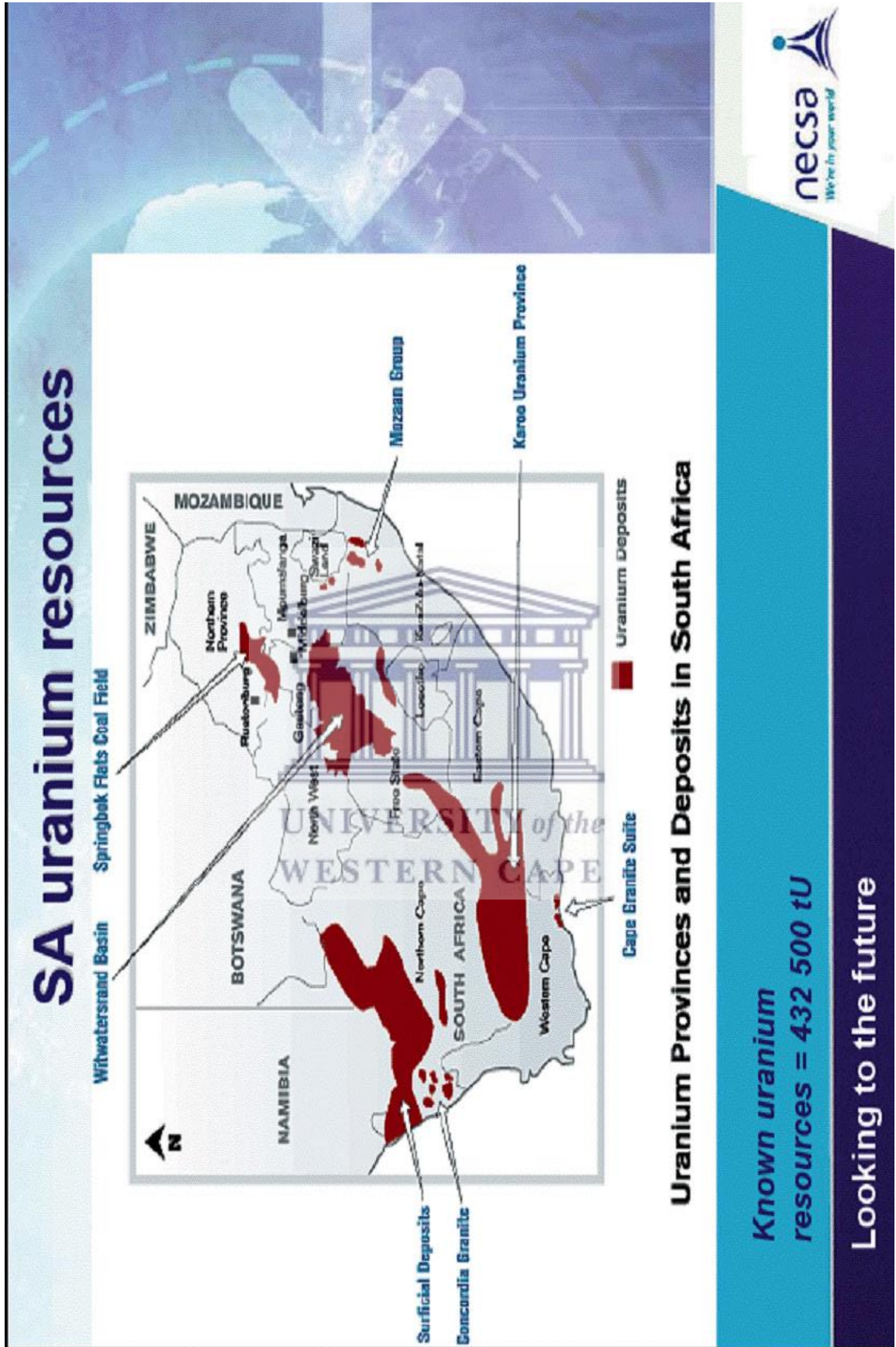


Figure 3.4 Uranium deposits in South Africa. (www.necsa.co.za/)

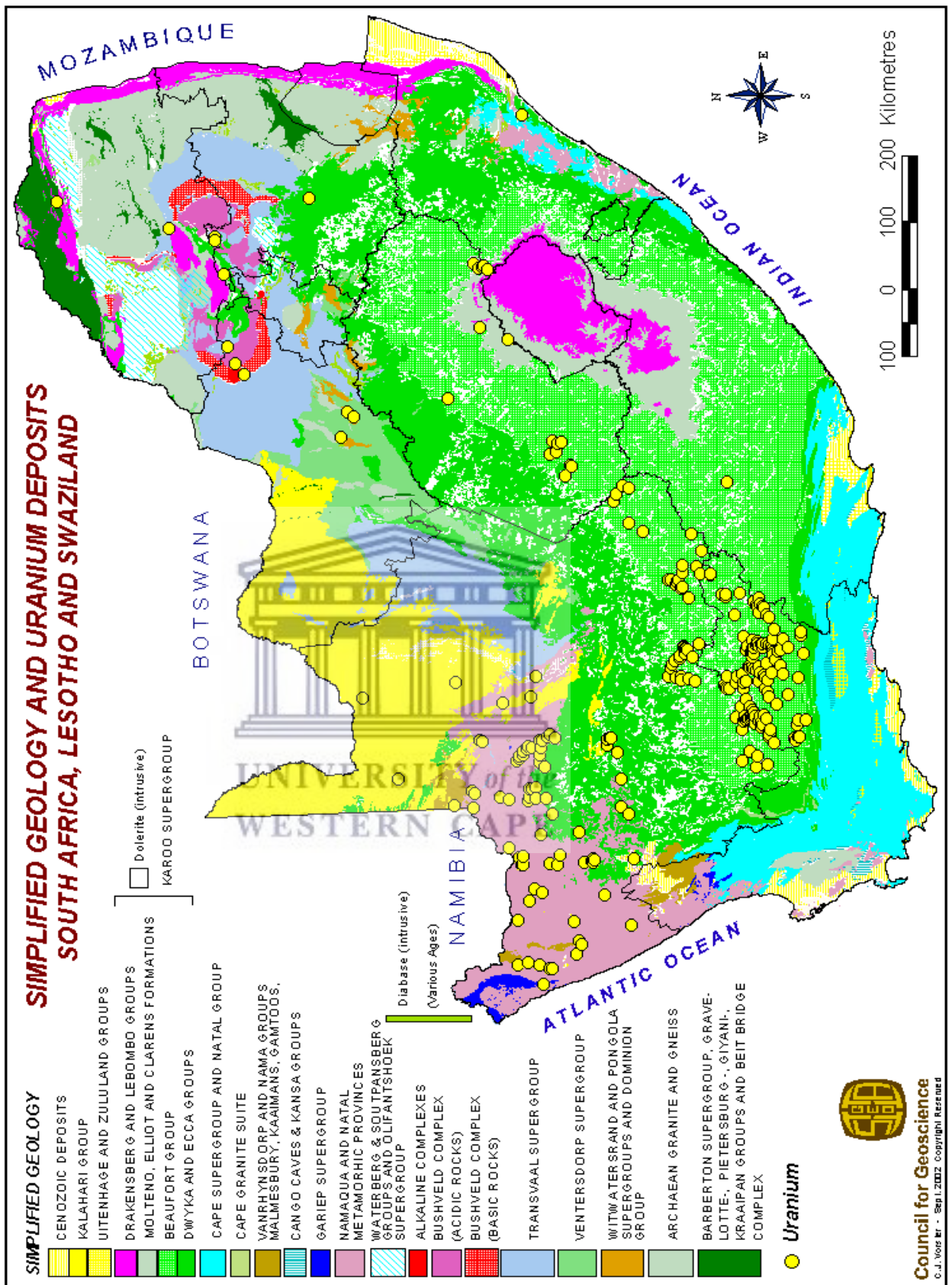


Figure 3.5 Simplified uranium deposits in South Africa, Lesotho and Swaziland.

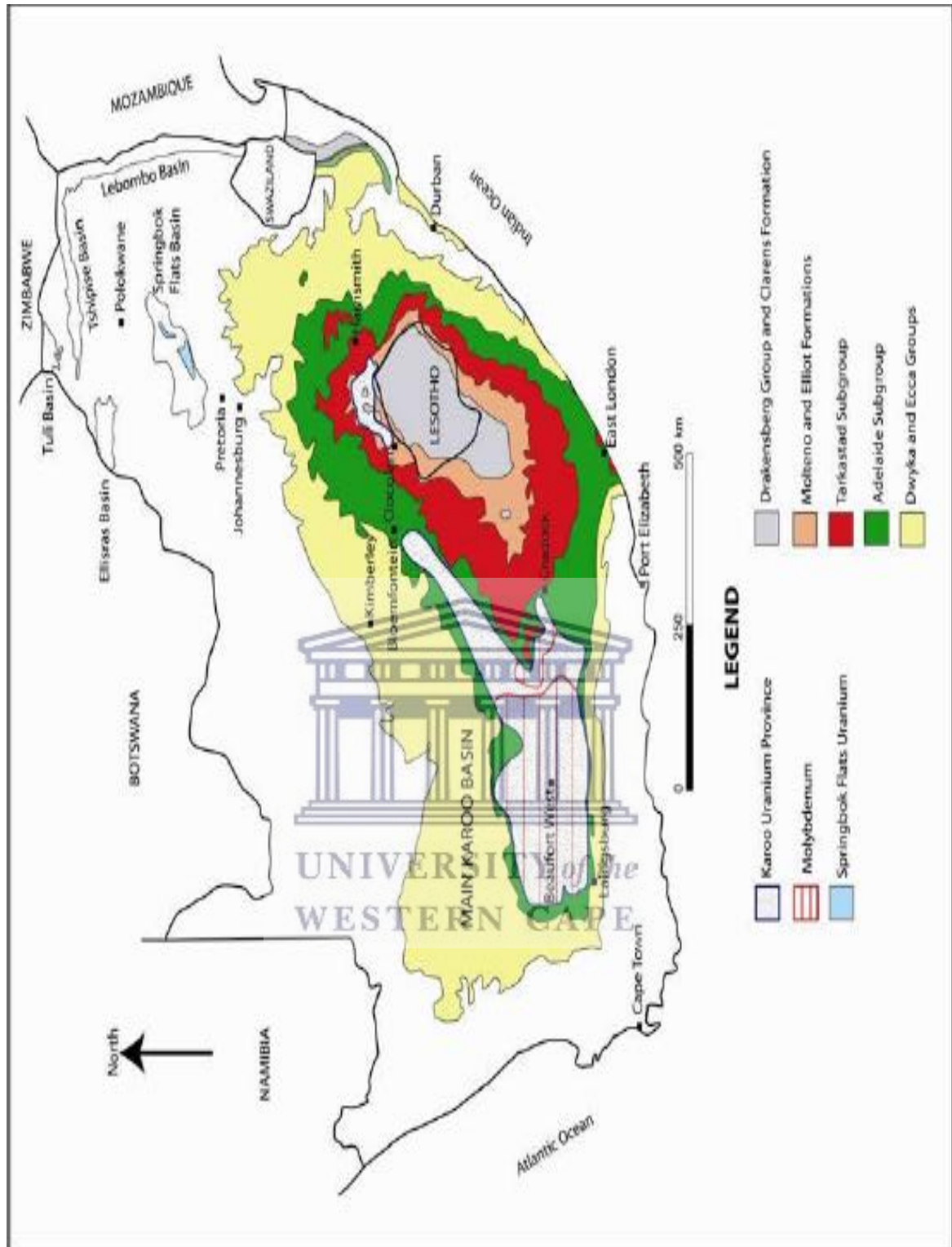


Figure 3.6 Map of South Africa showing distribution of Karoo basins and major geographical lithostratigraphic units in the main Karoo basin. (Cole D, 2009)

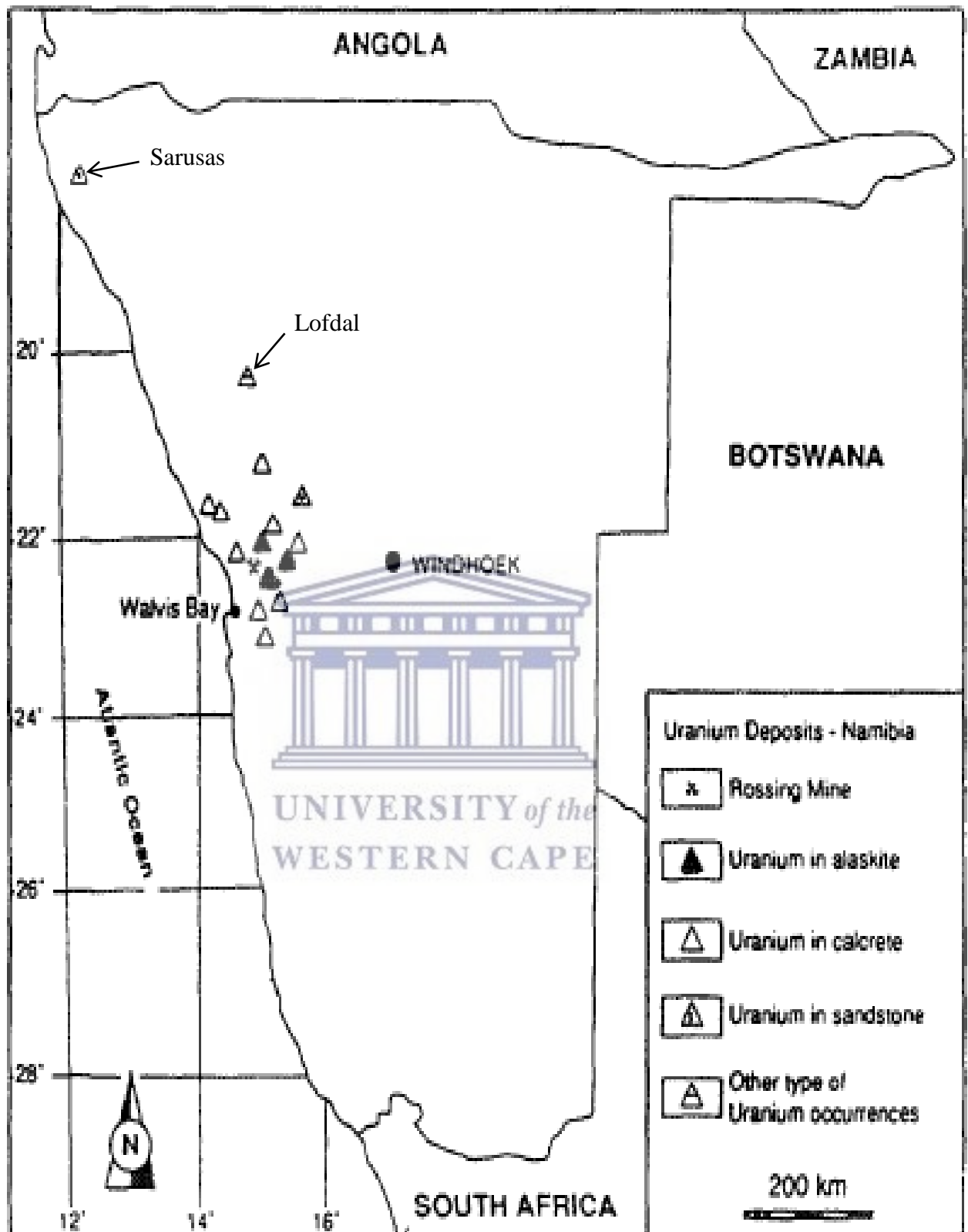


Figure 3.7 Uranium deposits of Namibia. (Mining Directorate, Ministry of Mines and Energy, 1995)

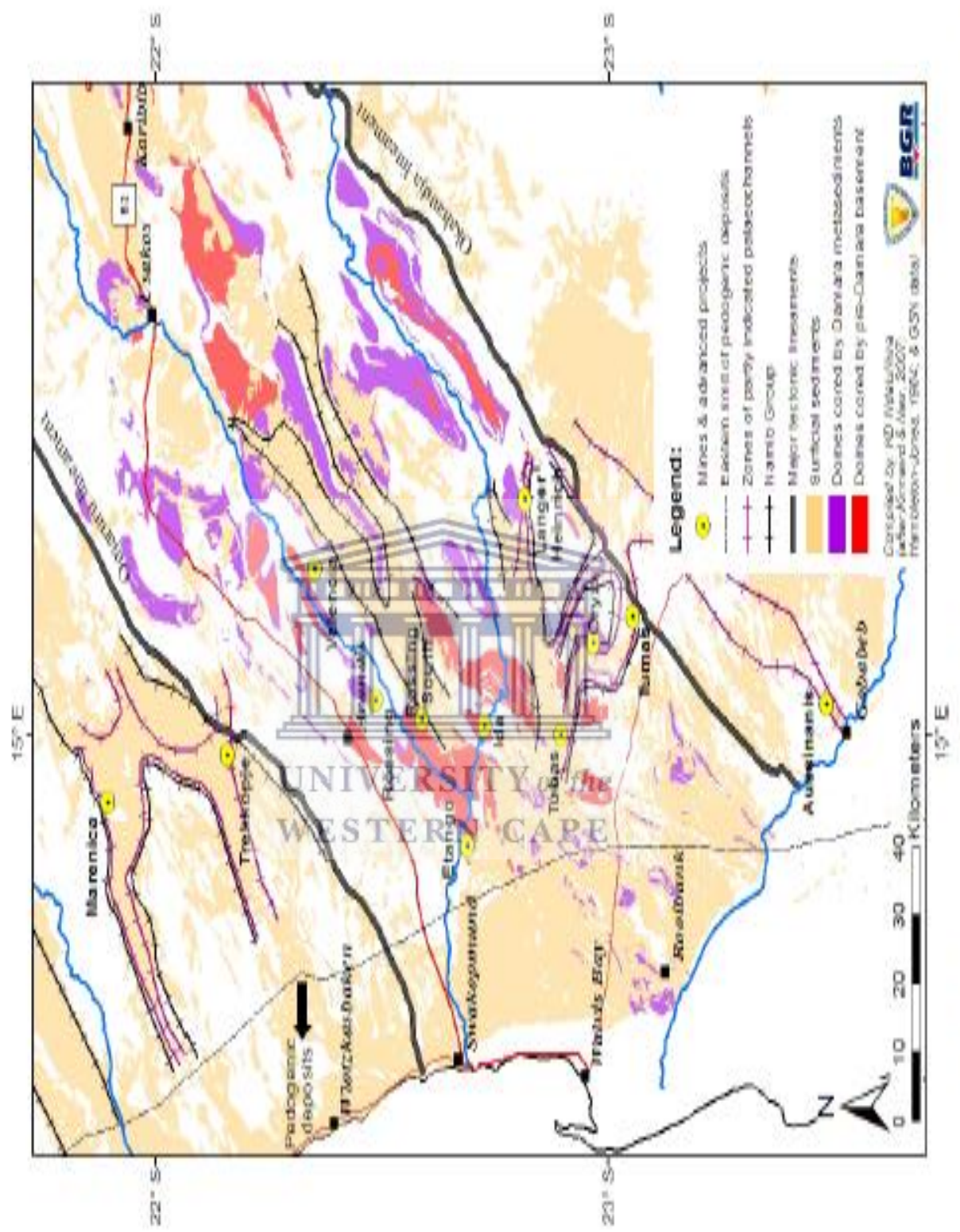


Figure 3.8: Part of the Central Zone of the Damara Belt showing domes and the location of the known uranium deposits (Geological Survey of Namibia, 2010).

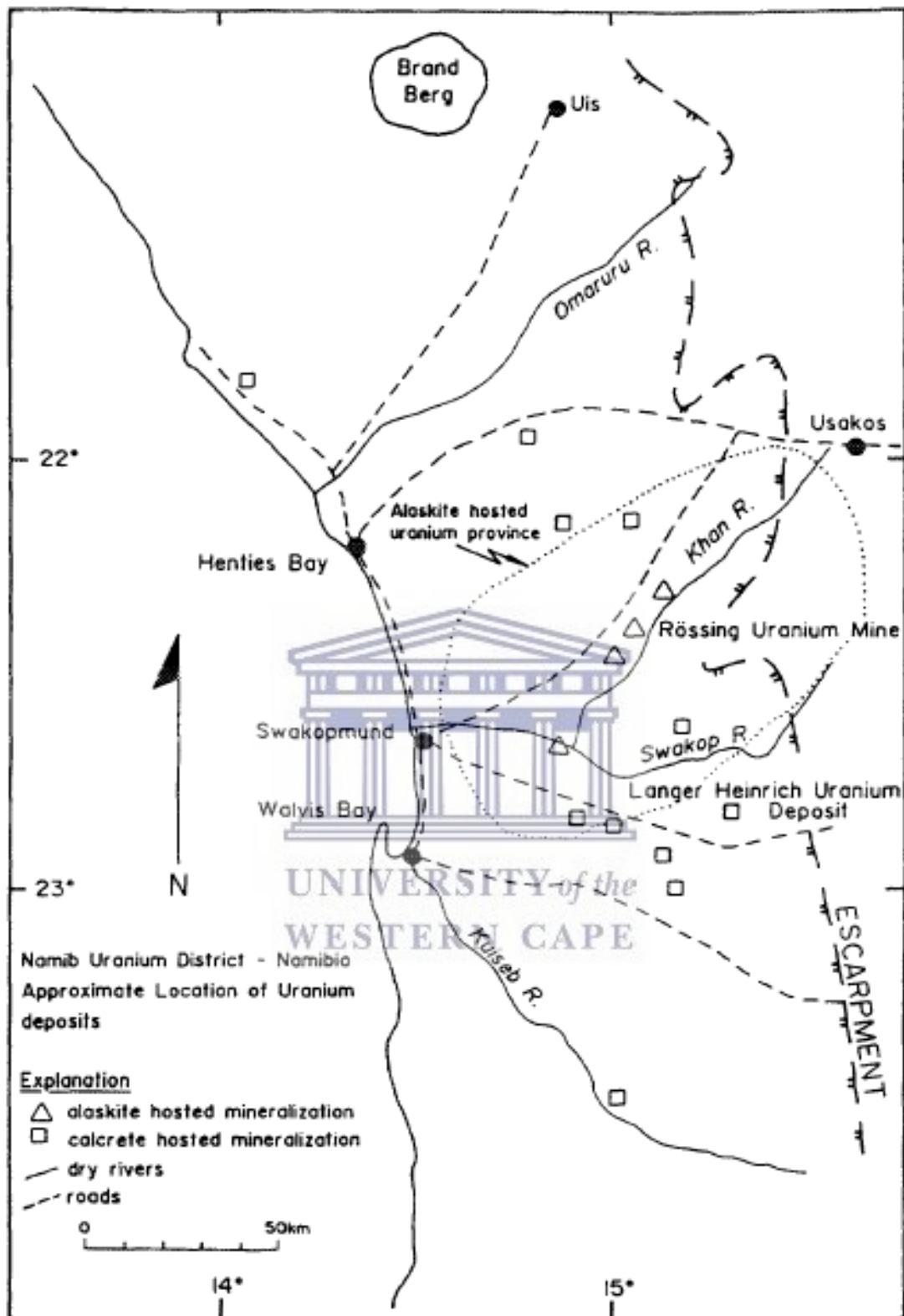


Figure 3.9 Alaskite hosted uranium province. (Mining Directorate, Ministry of Mines and Energy, 1995)

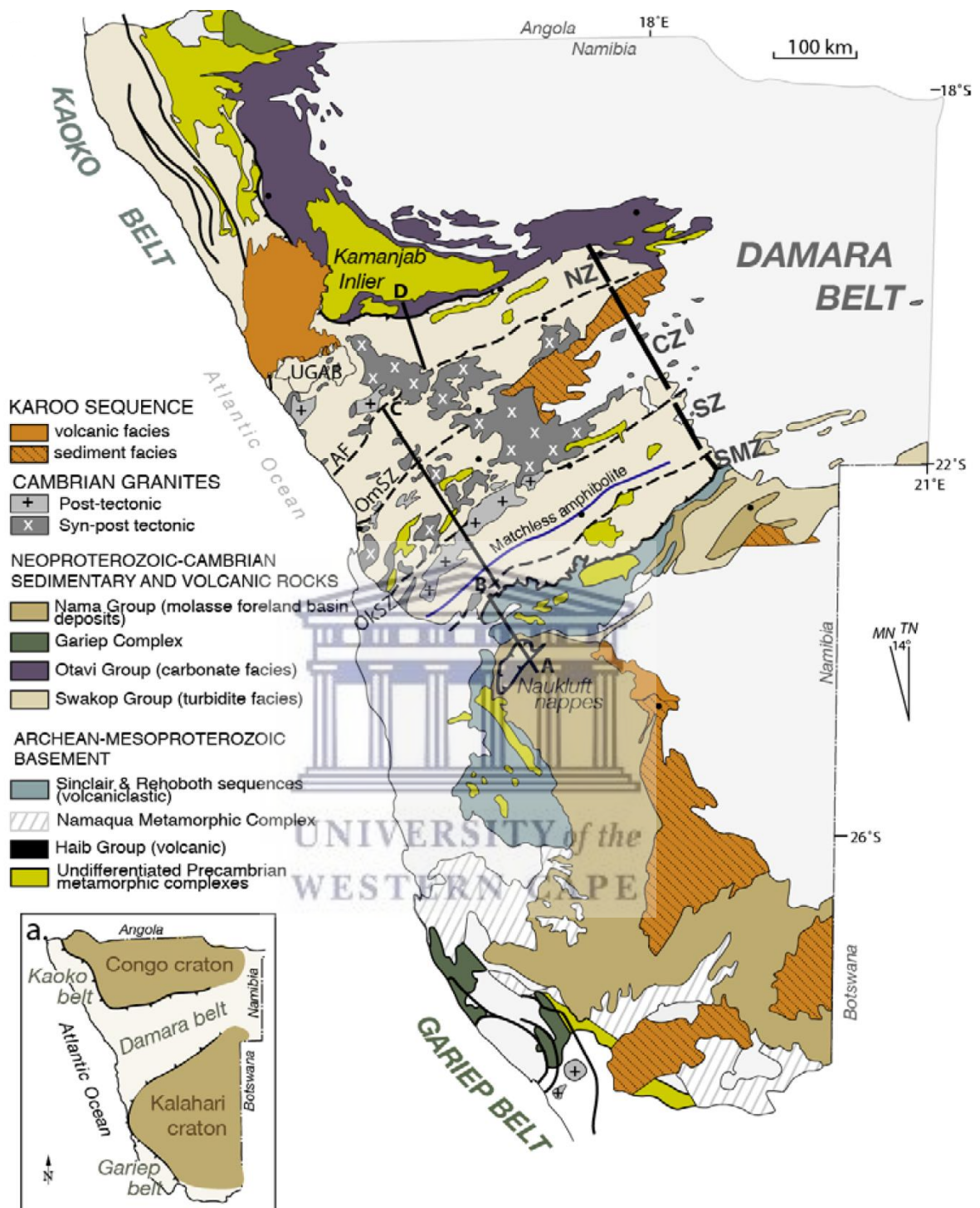


Figure 3.10 Damara belt Tectonic map of the Damara Orogen, Namibia. (Foster, Goscombe and Gray,2009)

Chapter 4: Measurement Techniques and Experimental Methods

This chapter focuses on the apparatus and measuring instruments used to measure exhalation of radon from various granite countertops and building materials. In conducting the experiments, the RAD7 continuous radon monitor was used (www.durridge.com). The HPGe was used to find the gamma radiation from the granite countertops. RAD7 with the EPERM electret system with the S-chambers and L-chambers were used to find the radon levels of the farms Blikkraal and Aardoon levels in the Beaufort West area.

4.1 RAD7 specifications

The RAD7 detector is manufactured by Durridge (See Figure 4.1) (www.durridge.com). The RAD7 detector is a continuous radon detector which works on the principle of the electrostatic collection of charged alpha-emitters on the surface of a silicon solid-state detector. The RAD7 uses a built in step up transformer to create high voltage with a range between 2000 V – 2300 V inside the conductor. The operating temperature is between 0°C and 40°C. The silicon detector signals from a spectrum showing the energy of the measured alpha particles. This spectrum is divided into channel groups or “windows” A-H corresponding to important alpha energies.

4.1.1 Setting up the RAD7 detector

The setup group is a set of commands that configures the RAD7 to perform the test according to the needs of the experiment. The RAD7 is a flexible instrument where the cycle time, recycle numbers, pump setting etc. can be changed. The detector has several built in protocols to simplify operations. These include Sniff, none, 1-day, 2day, weeks (Which is the infinite setting and it ends with user intervention) and User (The user customizing everything). The other settings are WAT - 40 and WAT - 250 for use with the RAD H₂O to measure radon in water. There is also a Thoron mode which changes the setting to counting the Thoron ²²⁰Rn decay (Durridge Co,USA, 2000).



Figure 4.1 The RAD7 inside its carrying case (DurrIDGE Co, USA, 2000).

4.1.1.1 Setting up the duration of the experiment

The sub-command >Setup Cycle is used to select the time for a single radon reading, which ranges from 2 minutes to 24 hours. The selection of 1 hour was chosen to be an ideal cycle time, since most experiments were planned to be between 40 and 90 hours long. The interval seemed appropriate for the series of experiments, since the amount of data produced would be easily studied. The >Recycle sub-command selects the number of cycles needed to complete the experiment (DurrIDGE Co,USA, 2010).

4.1.1.2 Setting up the Rad7 for radon detection

The Rad 7 uses 3 modes called Sniff, Normal and Grab. Sniff mode is used to follow the rapid changes of radon concentration in an area; this is very effective to search for radon sources or leaks (DurrIDGE Co,USA, 2010). During Sniff mode, the RAD7 reads from the ^{218}Po peak results from the "A" window and calculates the radon concentration based on this peak alone. The ^{218}Po peak result, from the α -decay of ^{218}Po that has a half-life of 3 minutes, with an alpha energy of 6 MeV (Wasco *et al.*, 2008). Normal mode achieves a higher statistical precision by counting both the ^{218}Po and ^{214}Po alpha peaks (Waska *et al.*, 2008). ^{214}Po is formed when ^{218}Po undergoes an alpha decay which forms ^{214}Pb with a half-life of approximately 27 minutes. Afterwards ^{214}Pb undergoes Beta minus decay which forms ^{214}Bi with a half-life of about 20 minutes. Afterwards ^{214}Bi undergoes Beta minus decay which forms ^{214}Po with a half-life of about 0.16 seconds and an alpha energy of 7.67 MeV. Thus Normal mode counts the average concentration between ^{218}Po and its great granddaughter ^{214}Po which is about 47 minutes apart in the ^{238}U decay chain (See Figure 2.3 and Fry and Thoennesen, 2013). Auto mode is a combination between Sniff and Normal mode. It starts off doing sniffing for 3 hours and

switches automatically to Normal mode, which is the recommended setting for long term measurements. The Grab command is less accurate than Normal or Sniff but it is used in unique situations. Grab is used to take a reading when it is not possible to spend time at the location to be tested. This can also be used when the RAD7 is busy with continuous monitoring. This is quite important when many samples need to be gathered from different rooms in a dwelling within a short time frame. This is used for very short term measuring and was not considered for use during the experiments in this work. (DurrIDGE Co,USA, 2010).

4.1.2 RAD7 experimental methods

The RAD7 serves as a sniffer for ^{222}Rn in this experiment which acts as a real time monitor to observe different radon concentration levels during the measuring period. The RAD7 measures the exhalation of radon in real time of the different materials that were used during the experiment (DurrIDGE Co,USA, 2010). The RAD7 was connected to an airtight vacuum chamber which housed the material being tested as shown in Figure 4.2. The results were stored inside the unit and analysed using software programs such as MS Excel.

4.1.2.1 Background radiation and noise check

When starting a series of experiments, it is important to do a background radiation check to see if there are no radon sources nearby the RAD7, which will affect the results of the experiment. The experiment was run with no material inside the Vacuum chamber to find the radiation emitted from the nearby environment, known as the background radiation. This must be done before running any other experiment because if the experiment runs near a radiation source, it would not display the true values of the experimental results. After the background radiation was confirmed to be at an acceptable level, a known radon source, a ^{226}Ra source, was used in this experiment. A comparison was done between the theoretical value and the actual value. If the two deviate too far from each other then the RAD7 must be sent in for calibration (DurrIDGE Co,USA, 2010). Other factors that can be used to see if the RAD7 requires calibration is Window E which is known as the High Energy Window. If the count is unusually high then the RAD7 should be sent for calibration. The other method is to check if Window O has a count of more than 30% of the total counts then the RAD7 must be sent for calibration (DurrIDGE Co,USA, 2010).

4.1.2.2 Initializing the experiment

Before monitoring takes place, the RAD7 is switched off and the sample is placed inside the chamber. This is a safety precaution, since leaving the Vacuum Chamber open could damage the RAD7 and the pump. It also collects air from the outside which will let the Relative Humidity (RH) level spike to above 20%. Both incidents will have an adverse effect on the credibility of the readings. The vacuum chamber was immediately closed tightly with bolts and nuts to make it air tight. The bolts and nuts squeeze an

“O”-ring rubber band between the lid and the vacuum chamber thereby minimizing the chances of radon leakage. This system is connected to a drying unit and the RAD7 using radon tight tubes, which are also air tight.

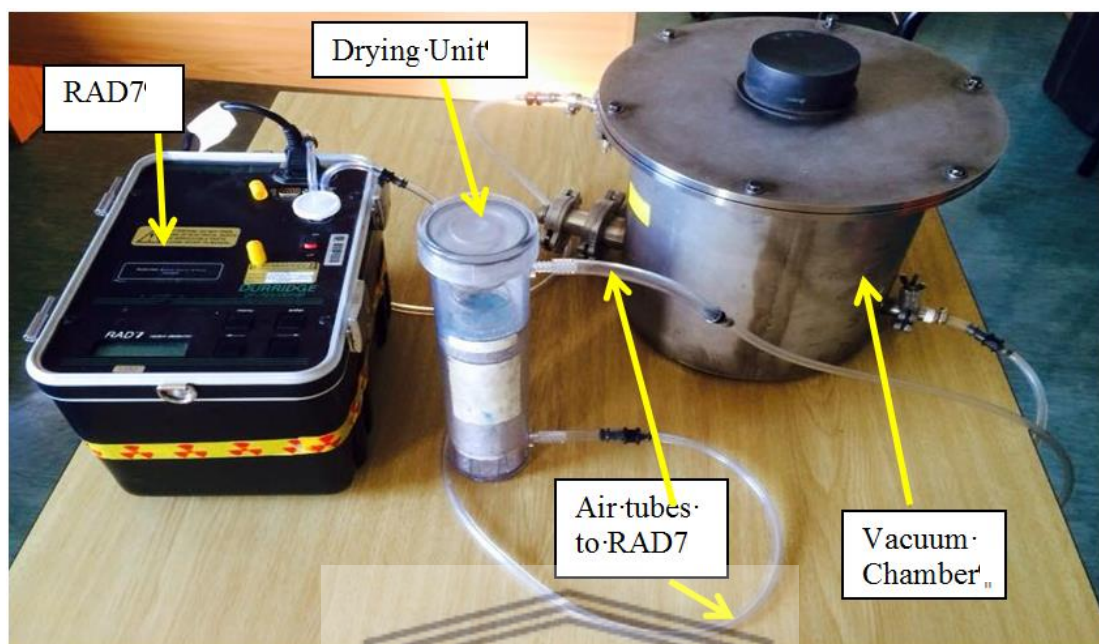


Figure 4.2 RAD7 setup for measurement.

Before monitoring starts it is recommended that the RAD7 should be purged for roughly one hour, or as needed. The RH should be less 10% at the start of the experiment, although 6% is ideal (Schubert *et al.*, 2008). To keep the RH below 10% a desiccant drying unit is required. The desiccant in a laboratory drying unit contains CaSO_4 granules, which have a high affinity for water (Burfield and Smithers, 1978). The granules are stored in an air tight tube which ensures that the moisture is absorbed before it reaches the RAD7 and it also keeps the air relatively dry inside the Vacuum chamber. When the experiment is completed, the desiccant can be stored for further use if it is kept airtight, with the use of plastic end caps. (See Figure 4.3) The granules are stored in an air tight jar before it is placed in a drying unit for use (DurrIDGE Co,USA, 2010). If the drying unit is not air tight the RAD7 will measure a sharp rise in the RH, usually above 25%.

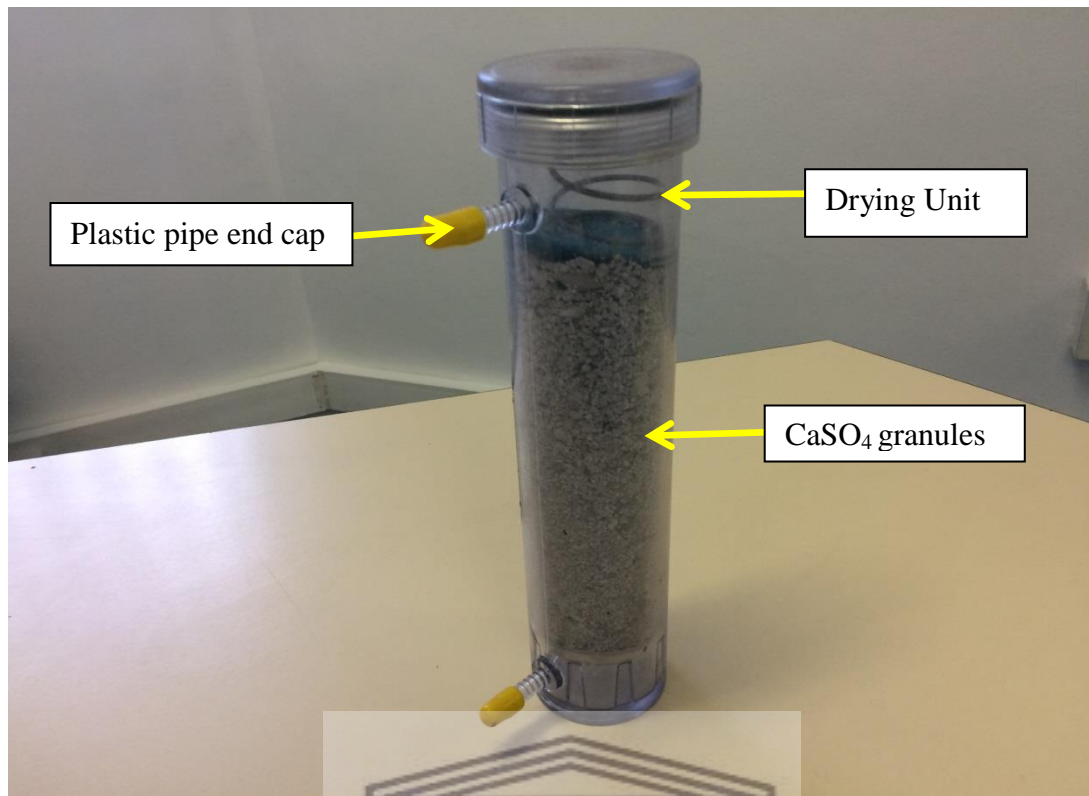


Figure 4.3 The desiccant with the plastic pipe end caps for storage.

In order to remedy this, the monitoring should be paused and the RAD7 unit should be purged until the RH is less than 10%. Purging occurs when the RAD7 is connected only to the drying unit and the RAD7 is set on purge. (See Figure 4.4) If the RH level does not go down after purging, then the desiccant should be replaced. The air, from the chamber passes through a drying unit and then to the RAD7 and back in a closed loop. The electric field, in the chamber inside the RAD7, propels the positively charged particles to the detector. The RAD7 has an internal pump that pumps air at the flow rate of 1 Litre per minute (Ravikumar *et al.*, 2006). In the detector, the alpha particles hit the active surface of the detector thus producing the signals equivalent to the energy of the alpha energy. In this operation, the RAD7 is able to differentiate different radio nuclides by their alpha energy using alpha-spectroscopy. When ^{222}Rn alpha decays it forms ^{218}Po and an alpha particle. The ^{218}Po is usually positively charged and is attracted to the detector surface that is negatively charged. The ^{218}Po then decays upon the detector's active surface. The electrical signal is proportional to the energy of the alpha particle. Different isotopes give different alpha energies and produce difference strength signals in the RAD7 detector when in Sniff mode. When in Normal mode, the concentration of ^{214}Po that is formed and which decays to ^{210}Pb and an alpha particle with an energy of 7.69 MeV is also used in the measurement. The detection of this alpha particle is also then used to get a better result. There is a 50% probability of an alpha particle to be detected by the detector (Schubert *et al.*, 2008).



Figure 4.4 Purging taking place to reduce the relative humidity inside the RAD7.

4.2 RAD7 spectrum analysis

The spectrum is a scale of alpha energies from 0 to 10 MeV. Alphas from the ^{222}Rn decay chain, fall between 6 and 9 MeV. It will be easily detected by RAD7 and deposits the energy directly into the solid state detector. The detector produces an electrical signal due to alpha radiation. The electronic circuits amplify and condition the signal, then the circuits converts the signal to digital form. The electric signal was created due to Alpha radiation and the RAD7's microprocessor picks up the signal. The RAD7 divides the spectrum's 0 to 10 MeV energy scales into a series of 200 individual counters, each representing a channel of width 0.05 MeV (Yu, Koo and Guan, 2001). When the RAD7 detects an alpha particle, it increments one of the 200 Channels by one. Theoretically the spectrum displays a peak at 6.00 MeV, which resembles a single needle-thin spike around the peak energy for ^{218}Po decays (DurrIDGE Co,USA, 2010).

4.2.1 Window information

As discussed earlier, the RAD7 has 200 Channels (See 4.2) and it also contains 8 separate windows (A to H) which divide the data into different packets. The raw spectral data contains all the data, which stores the different packets from A to H. The data can be retrieved at a later stage for later usage, even during the running of the experiment (Yu, Koo and Guan,2001).

Window A counts the radon in Sniffer mode. The total counts of alpha particles from the 6 MeV decay of ^{218}Po (with a half-life of 3 minutes) are stored in this window. This is the spectrum that will be studied in detail, in this work.

Window B is known as the Thoron 1 window. Thoron (^{220}Rn) has a half-life of approximately 56 seconds and alpha decays to ^{216}Po , which decays with an alpha energy of 6.78 MeV.

Window C counts the ^{214}Po counts which are in the radon decay chain. This Window counts the 7.69 MeV alpha particles from the decay chain. The energy counted is the great - great granddaughter of radon with an effective half-life of nearly an hour. ^{214}Po has a half-life of 0.16s (See Figure 2.3), but the decays to get to ^{214}Po includes a 26 min half-life plus a 20 min half-life decay so it takes about an hour before ^{214}Po decays are noticeable.

Window D is known as the Thoron 2 Window. The energy is around 8.78 MeV; this decay is due to the ^{212}Pb . ^{212}Pb has a half-life of about 10 hours.

Window E is known as the High Energy Window. This is a diagnostics window which ideally has a few counts and it should be very close to zero. Since this is a diagnostic window, it is also a way to check if the RAD7 is working properly. If the counts in this window are a large fraction of the counts in A or B or C or D, the RAD7 is probably not working properly and it should be sent away for calibration.

Window F collects the low Low Noise counts. This is a diagnostics window that measures the noise in the system. Since the counts are in direct proportion to temperature, the counts will be high if the RAD7 is operated at very high temperatures.

Window G collects the Medium Noise counts. A diagnostics window counts in the region around channel 30 to 40. Window G usually has a few counts, even if Window F shows a high count rate.

Window H is the High Noise or ^{210}Po counter. The counts around the energy of 5.31 MeV due to the alpha particle released due to ^{210}Po . ^{210}Po is the granddaughter of ^{210}Pb . Since ^{210}Pb has a 22-year half-life, the isotope builds up on the detector's surface over many years of normal use. Since this window is not used to calculate radon levels, it will not affect the RAD7 in any significant way or pose any threats to the reading.

Window O is a window where the RAD7 groups together the E, F, G and H Windows. It is collectively known as the "others" Window. This Window collects the High energy and Noise Window. If this window receives more than 30% of the total counts in multiple experiments, then the RAD7 should be sent back to be calibrated (Durrige Co,USA, 2010)

4.3 Reading and storing of data in the RAD7

The RAD7 stores the data in one of the 1000 memory slots which is also called cycles. The previous runs can be accessed anytime by using the read function. Even the current run with previous saved cycles can be accessed by using the read function (Durridge Co,USA, 2010).

4.3.1 Starting the test

After purging a run can be started. On the LCD information will be displayed (Information from Table 2 was used):

```
3401   Live  Sniff
00:59:37  00001
```

The 3401 gives the following information. The first 34 was the run and the second 01 was the cycle number. The middle displays Live which means that the pump is on and the RAD7 is collecting data. Sniff on the first line shows that only ^{218}Po decays are being counted for this reading (Durridge Co,USA, 2010). Thus the RAD7 counts the concentration in Window A. On the bottom row left is the count-down timer which shows the time left on the run. On the bottom right corner, it shows the number of particles counted during this run. During the run of the experiment when the countdown drops to zero then the RAD7 will display more lines of information. A typical display on the LCD of the RAD7 will look like this (Information from Table 16 was used):

```
4133  359 " 46.7 b Normal
SUN 8-FEB-15 20:27
24.5 C RH: 9% B:7.06V
```



Where 4133 are the run (41) and cycle (33) numbers, 359 is the measured radon concentration, 46.7 is the statistical uncertainty, b indicates the units (in this case Bq/cm^3). Normal mode counts both the ^{218}Po and ^{214}Po decays for the reading. The reading was set to Auto in all experiments (Durridge Co,USA, 2010).

4.3.2 The Data command set

The >Data command, is used to read data from the RAD7. The instrument has a memory of 1000 cycles which can be sub-divided into as much as a 100 Runs. A cycle is a separate storage place in the RAD7 which stores data. The run number in the Data group is from 00 to 99 (Durridge Co,USA, 2010).

4.3.3 RAD7 test status

The TEST set of commands allows the user to manipulate the run that the RAD7 is currently monitoring. The Test Status command is to quickly ascertain the status of the Run. This is an especially important command to quickly take the RH reading and if the reading is above 20% then the result will not be

considered reliable (See 4.3.3) The LCD on the RAD7 will display the following (Information of Table 3 was used):

1601 Idle Sniff
01:00:00 0000

The upper left corner once again displays the current run number and cycle number. 16 is the run number while 01 is the cycle number. Next to it is the detector status which is either (Idle or LIVE). Idle is when the RAD7 is on and the pump is switched off. The upper right corner gives the current test mode (Sniff, Normal or Grab; DurrIDGE Co,USA, 2010). If the RAD7 is set on Auto then the Setting will automatically switch from Sniff to Normal after 3 hours. (See 4.1.1 for the detailed explanation on all 3 modes) The lower left side shows the countdown timer (In hours:minutes:seconds) counts down to Zero when the detector status is live. The lower right shows the total number of counts since the beginning of the cycle. (Information of Table 3 was used):

Last reading:
1621 110 " 62.8 b

A second reading pops up on the LCD that displays the last complete reading of the current run that was stored to the RAD7. The lower left number is the run number (16) and cycle number (21). The next number 110 is the radon concentration and the number 62.8 is the uncertainty followed by the b which indicates that the unit in this case is Bq/m³. When the cycle ends then the information on this display will update to the new reading. If this is the first reading on the run then the LCD will state "No readings yet" (DurrIDGE Co,USA, 2010). When the right arrow is pressed again, a different set of information is displayed on the LCD.

UNIVERSITY of the
WESTERN CAPE
24.8°C RH:10%
B: 6.36V P: 40mA

The top left of the LCD displays the temperature in Celsius. The top right shows the Relative Humidity reading. During a run when you return to the RAD7 to check up on the RAD7, it is important to check the RH, since anything above an RH of 20% will yield unreliable results. (See 4.1.2.2 for more details.) Ideally an experiment should start with a < 6% RH. The bottom left display of the LCD shows the battery Voltage, which should be around 6 to 7.1 Volts. A battery less than 6 Volts should be recharged. In the lower right display on the LCD, the pump current value is displayed. This value varies between 0mA and 80mA. The optimal pump current value is between 40 - 70 mA. Clogging or a blocked hose will give a reading higher than 90mA, which requires an immediate replacement of the pipe (DurrIDGE Co,USA, 2010). When the right arrow is pressed again, a different set of information is displayed on the LCD.

HV: 2218V, 10%
L: 02 S: 0.21V

The following set of results show the diagnostic values of the RAD7. The top line is the high voltage reading and the next lines show the range of the values

in percentage. The lower left corner displays the leakage current, which at room temperature ranges from 0 to 10. When the temperature is quite high that causes the value to rise. A rise of noise at the lower energy end of spectrum, causes peak broadening of the peaks caused by the alpha decay of ^{218}Po . The lower right corner displays the signal voltage from the analogue circuit. The value should not fluctuate more than 0,05V from the average value (DurrIDGE Co,USA, 2010).

Press right arrow and another set of information will display on the screen:

```
W|cpm | +/- | %tot  
A| 6.0 | 4.3| 48.8
```

W is for the window data, in this case Window A. The window information was discussed in detail in 4.2.1. The cpm is the counts per minute window. The +/- displays the statistical uncertainty of the cpm value. The value %tot is the number of counts in a window as a percentage of total counts in the spectrum (DurrIDGE Co,USA, 2010).

4.4 RAD7 measurements at Aardoon and Blikkraal

At the Aardoon farmhouse, the RAD7 was placed in the television room and was purged for 30 min before monitoring started. Afterwards the RAD7 was set up to sniff radon for a period of 24 hours. The RAD7 stores the data and the results were plotted on an Excel spreadsheet, which was used to draw the spectrum. At the Blikkraal farmhouse, the RAD7 was purged for 30 min. Afterwards the RAD7 was set up to sniff radon for a period of 4 hours. Since the values of the concentration were low due to the good ventilation, the results were not used (Masia,2010).

4.5 RAD7 measurements in the UWC Nuclear physics lab

After the initial set up of the experiment was completed, (Refer to 4.1.1.1. 4.1.1.2 and Figure 4.2) the RAD7 was set up for monitoring (Refer to 4.1.2.2). The building materials and the granite counter-tops were measured at the UWC Nuclear physics lab. After the initial checks of Background and Calibration (Refer to Figure 4.2 and see 4.1.2.1) the RAD7 was ready to measure the concentrations of the different materials. The RH initially was 6% when the series of experiments started. The materials were placed in a Vacuum Chamber linked to the RAD7. The experiments ran between 40 and 160 hours. The information of the RAD7 is checked every 24 hours to monitor if the RH levels it is still under 20%. If the RH level is over 20 % then the experiment is paused and the RAD7 is purged (See 4.1.2.2) (Kappke et al., 2011). When the RAD7 brings down the RH below 10%, the experiment continues until the end or when the RH is above 20% again. After the experiment ended the RAD7 is switched off and the material removed and another material was placed in the vacuum chamber is made air tight again. Before the experiment starts again, the RAD7 is monitored to see if the RH level is below 10%. The desiccant took between 10 to 14 days of continuous running to lose its ability to dry out the moisture. The desiccant stops

absorbing moisture when the RAD7 cannot lower the RH levels even after purging. If the RAD7 is inactive for a very long time, the desiccant does not lose its ability to absorb moisture if it is in an air tight container. The RAD7 will have an increase in RH after a long period of inactivity that is why the RAD7 should be purged when starting up after a long time. In general, it took the RAD7 almost 2 hours to lower the level of the RH to 6%.

4.6 Hyper-Pure Germanium (HPGe) specifications

The Hyper-Pure Germanium (HPGe) detector (Figure 4.5) that ran the readings of the granite countertops is situated at the Environmental Radioactivity Laboratory (ERL) in iThemba LABS. The HPGe is a closed-end coaxial Canberra GC4520 (p-type, 45% relative efficiency, 2 keV FWHM resolution at 1332 keV), which is encased in a 10 cm thick lead case fitted with a 2 mm thick copper inner lining (Newman, 2008). This detector has an HPGe crystal of diameter of 6.25 cm and length of 5.99 cm and mounted on in a vertical dipstick of liquid nitrogen (LN_2) cryostat that is facing upward. The liquid nitrogen was used to cool the HPGe to optimal operating conditions, with the N_2 level checked on a weekly basis (Talha, 2008).



Figure 4.5 HPGe detector at iThemba Labs. (tlabs.ac.za)

4.6.1 Materials and measurements with the HPGe

The efficiency of the HPGe was calibrated beforehand for this geometry so that the activity concentrations of the granite countertops can be calculated. These were the same countertops that the RAD7 measured at the UWC Nuclear Physics lab (See 4.1.5) (Maleka and Newman, 2012).

4.7 EPERM electret

The EPERM is a passive radon detector system that does not require any electrical power to work and it is used to measure the average radon concentration in a dwelling. The EPERM system consists of three components namely the positively charged electret, ion chamber housing and a portable electret voltage reader (Figure 4.6 and 4.7). The device measures radon by allowing air to passively diffuse into the chamber through small holes at the top with a filter that will trap decay products (Kotrappa, Dempsey and Steiff, 1993). During the decay of radon, particles will be released and the alpha particles will ionize the air. The created electrons are attracted to the positive electret where they reduce the charge. The difference between the initial and final voltage was taken, to calculate the radon concentration. The charge is initially 700 volts and can go down to approximately 200 volts. The electrets can be differentiated with a serial number. The electrets are positively charge Teflon disks that serve as the source of an electrostatic field and sensor and it is not affected by shock, humidity and temperature. It will hold charges for a long period of time if not exposed to radiation (Righi and Bruzzi, 2006).

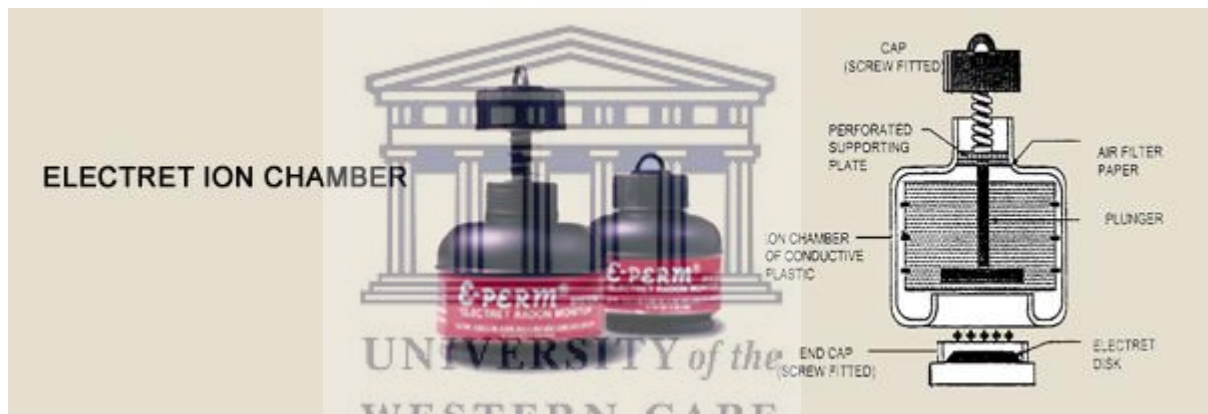


Figure 4.6 The S-Chamber Electret ion chamber (www.radelec.com).



Figure 4.7 The L-chamber Electret ion chamber. (www.radelec.com)

4.7.1 Ion chamber

The ion chamber is a holder for the electret and also forms a chamber containing the ions produced by the alpha radiation. It is made of electrically conducting plastic. The chamber has windows covered with a thin aluminised Mylar film to protect the electret from dust and other particles. The two most important commonly available ion chambers are the Short term(S) and Long Term (L) chamber (Kotrappa and Jesters, 1993).

4.7.2 Radon ion chamber measurements

Electron ion chamber measurements using the S-chamber can measure radon concentration over a short period of a few days. In this research short term electrets were deployed in the farm houses of the farms Aardorn and Blikkraal. All electrets were screwed into the bottom of the S-chamber making sure not to touch the white surface of the electrets. The EPERM systems were turned into on position by unscrewing their top screw cap in order to start the measurement. The EPERM system was placed at different areas of the dwellings. The final voltage on the electrets were read and recorded on the data logging sheet. The radon concentration from the electrets data was then calculated using the following equation. During the calculation a standard value of background of 18 Bq/m^3 was used.

$$C_{Rn} = \frac{\Delta V}{C_f \times T} - BG \quad (4.1)$$

C_{Rn} = The radon concentration in Bq/m^3

ΔV = The change in initial and final voltage

$C_f = 0.0459 + 1.5519 \times 10^{-5} \times \left(\frac{I+F}{2} \right)$ is the calibration factor of the EPERM when using an S-chamber.

The first measurements were performed with electrets in S-chambers. The 8 electrets were deployed in pairs at the Blikkraal farmhouse for 10 days. They were placed in pairs in the Lounge, TV room, Pantry and the Kitchen. At the Aardorn farm house, 12 electrets were deployed in pairs for a period of 1,06 days in TV-room, Son's bedroom, Main room and Kitchen (Masia, 2010).

Chapter 5: Discussion of results

5.1 Detectors and Materials Used

The RAD7 was the main detector used in this work to measure radon releases from building material. S-chamber, L-chamber and the HPGe-gamma ray detector were used for specific measurements to complement the Rad7 measurements. Almost all of the building materials were sourced from the greater Cape Town area, due to the high transport cost associated with transporting low cost building materials (Ngcofe and Cole, 2014). The materials sourced from the greater Cape Town area were Philippi sand, Malmesbury sand, floor tiles, roof tiles and the hornfels stones and tar. The greater Cape Town area does not have any active uranium mines or reserves. It was expected that materials sourced from these areas would yield a very low level of radon (Equity, 2014). All the granite countertops were available at a local company that source granite from various areas around the world and will be discussed in detail later. Filler material which contains uranium bearing sandstone was sourced from the Ryst-Kuil farm near Beaufort-West (Masia, 2010).

5.2 RAD7 results of diagnostics using a radium source

Since the RAD7 was set on sniff, only the 'new' radon was detected. Thus the reading was not influenced by older radon still present in the system that did not decay yet into its daughter products. So the results are not skewed because the RAD7 was previously used. The radium source was used and it increased the radon level at a nearly constant rate (see Figure 5.1) in accordance with eq. (1.33). It was compared to the theoretical yield and it was deemed suitable to measure radon. The experiment was run for 22 hours which was ample time to show that the RAD7 can detect the increase in radon.

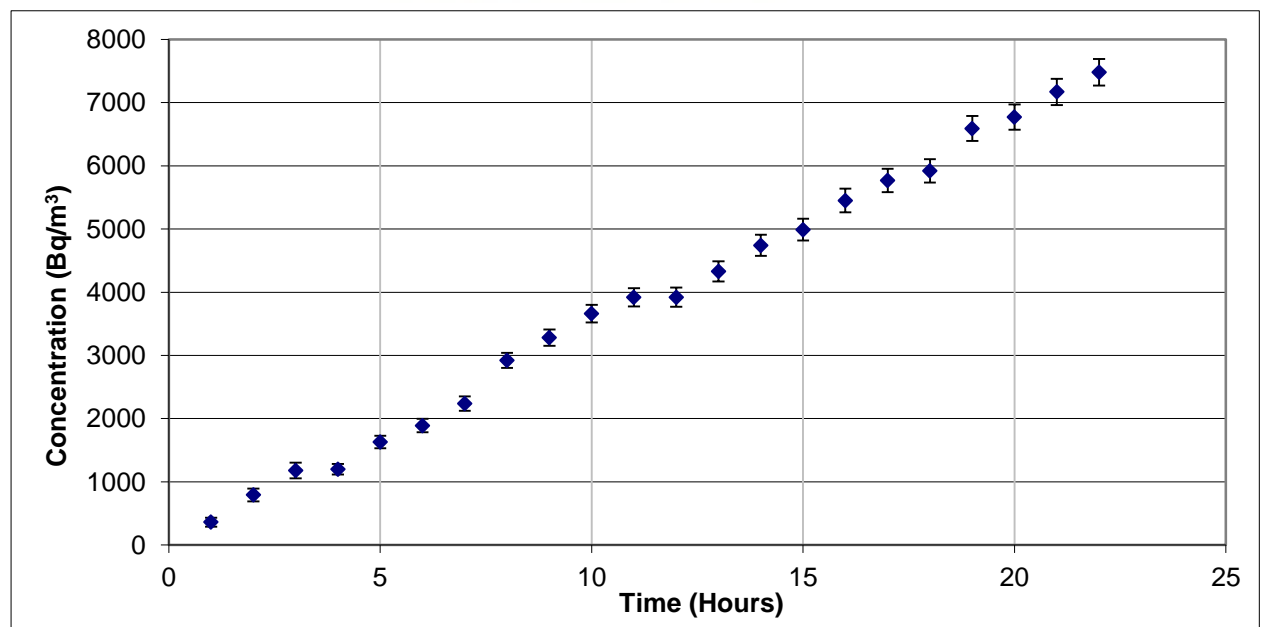


Figure 5.1 RAD7 measurement of the radium source.

Since the RAD7 was set on sniff, only the 'new' radon was detected. Thus the reading was not influenced by older radon still present in the system that did not decay yet into its daughter products. So the results are not skewed because the RAD7 was previously used. The radium source was used and it increased the radon level at a nearly constant rate in accordance with eq. (1.33). It was compared to the theoretical yield and it was deemed suitable to measure radon. The experiment was run for 22 hours which was ample time to show that the RAD7 can detect the increase in radon.

5.3 Background radiation

Before measuring any material, it is important to ensure that there is nothing in the set-up that is a source of radon. When radon is measured in a house, it is important to check that there is no extra radon source. The reason for measuring the background radiation is to find radon exhalation obtained from the measuring set-up. There are many other important uses for finding the background radiation such as detecting radon sources around a dwelling, lab or any other significant area. Background radiation is unavoidable and steps should be taken to minimize it. It is impossible to totally eliminate background radiation, since every object emits radiation. Failure to check the background radiation could affect the readings negatively, since the reading could take place near a radon source. Background gamma radiation is an important issue when measuring with the HPGe. The gamma background is a combination of cosmic, terrestrial and internal radiation. The HPGe detector does not distinguish between the three and additional equipment will be needed to measure the individual radiation. The EPERM detector does not distinguish between the three and is somewhat sensitive to gamma radiation, hence the need for a background correction in eq. (4.1) (Feblau, 2008).

5.3.1 Background Radiation in Summer

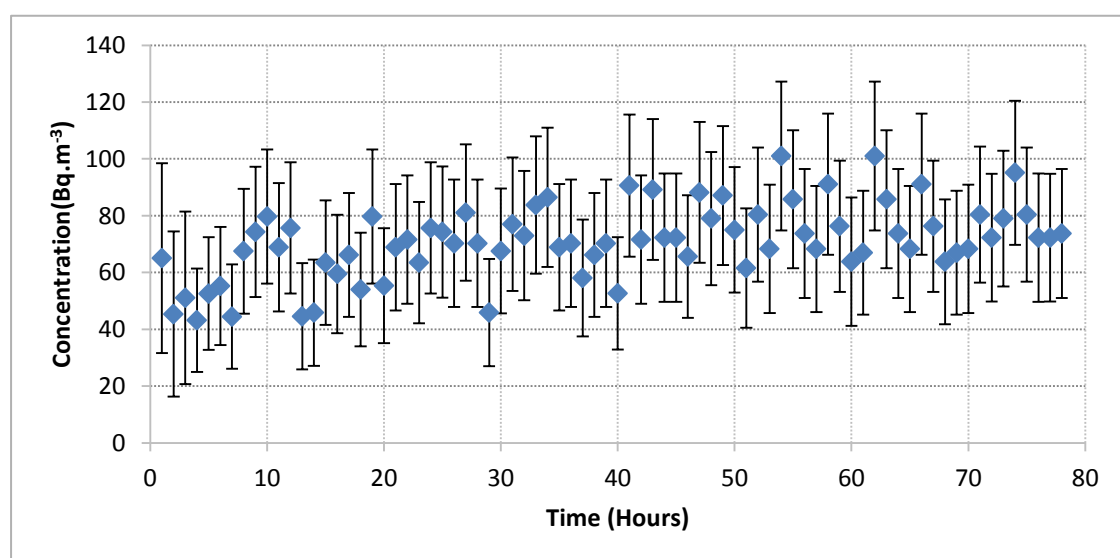


Figure 5.2 Background radiation of radon during summer.

Since all the experiments were run during summer, I used this as a benchmark for the background radon. The background radiation will constantly change due to temperature, pressure etc. Since radon in a room is known to be diurnal, this means that it has often a higher level during the day (Malakhov,1965). One expects the background radon concentration will reach its highest levels during the times between 10:00 and 14:00 (Durrige Co, USA, 2010). The background radon concentration fluctuated randomly throughout the running of the experiment (see Figure 5.2) , which means that factors such as the time of day, air pressure, temperature difference and cosmic radiation do not have a major effect on the radon level inside the vacuum chamber and RAD7 detector used in this experimental set-up. This experiment was done at the UWC Nuclear physics lab (G 30).

5.3.2 Background in Winter – Figure 5.3

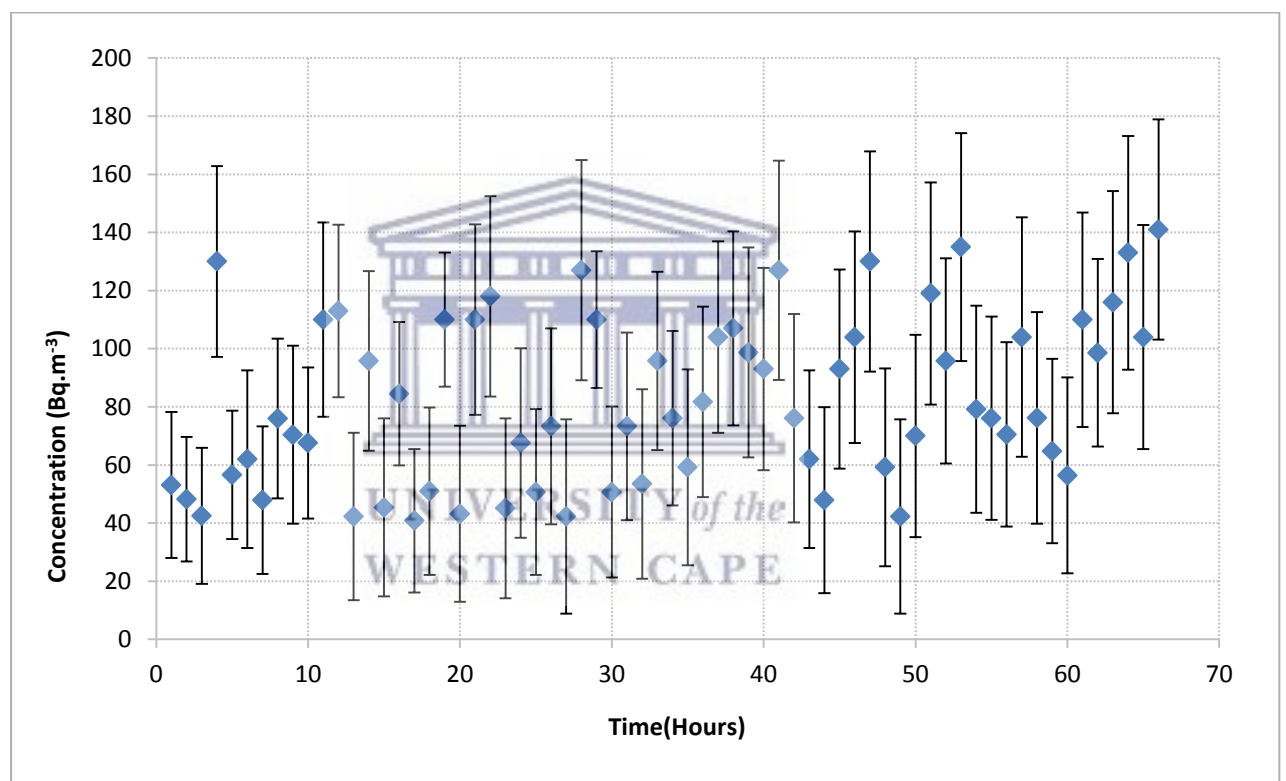


Figure 5.3 Background radiation of radon during winter.

None of the experiments were done during the winter and the result was used as comparison to compare radiation between the seasons to check if there is a significant difference between the two. I anticipated that the background radon in winter would be slightly higher than in summer. The main reason is that during winter more doors and windows are closed due to weather conditions, which causes radon to take a longer time to dissipate out of a dwelling (Ali et al.,2016). The result showed that on average there is slightly higher radon exhalation rate during winter than summer, when comparing the summer and winter background radon concentration. The similarities between the two show that both have roughly the same minimum background level of 40 Bq/m³. In winter the radon level rises above 100 Bq/m³ more times than summer. Likewise, during summer, the radon levels fluctuate erratically irrespective of

temperature, time and air pressure. In conclusion, the experiments can be done during any time of year without affecting the results in any significant way. This experiment was done at the UWC Nuclear physics lab (G 30).

5.4 Results of RAD7 measuring building materials

5.4.1 Philippi Sand

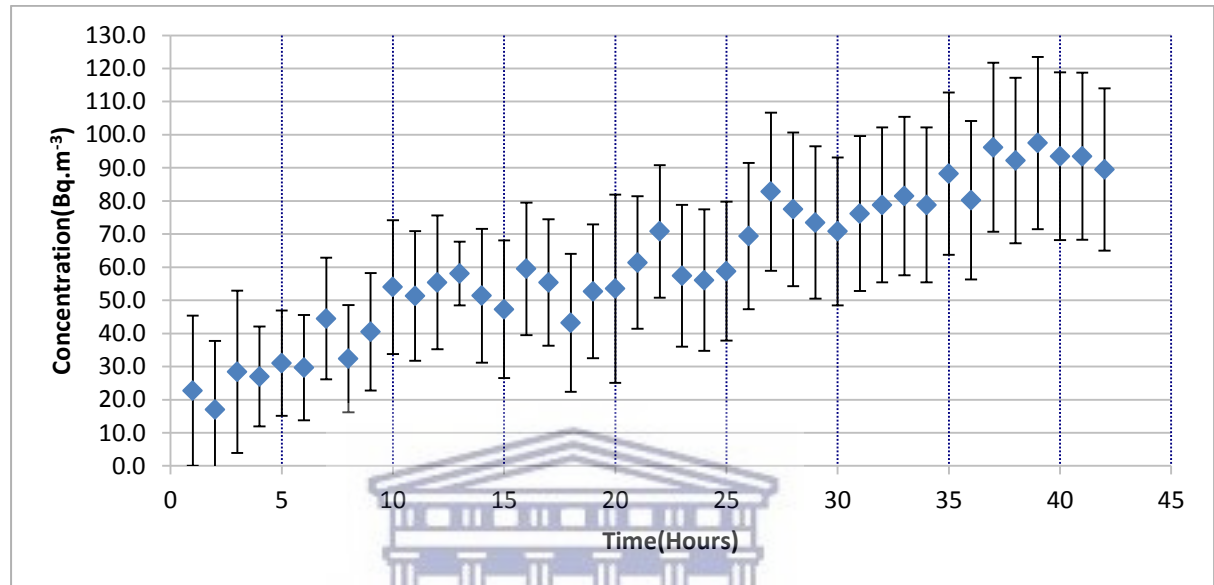


Figure 5.4 Radon exhalation from Philippi sand.

Philippi sand is mined in the Greater Cape Town area with the two biggest mines located near the towns of Philippi and Macassar in the Cape Flats area (Cole et al, 2013). There are no reasons to expect high radium concentrations in this area. The results in Figure 5.4 show that Philippi sand (Figure 5.5) is not a big radon source.

The volume inside the chamber is 12 litres which equals to 0.012m³.

First we calculate the decay constant of ²²²Rn by using equation 1.23.

$$\lambda_{222Rn} = \frac{\ln 2}{3.84 \times 24} = 7.51 \times 10^{-3} h^{-1}$$

Since the measurement was conducted over 42 hours, we use equation 1.33 that is valid for times much less than the half-life of radon, to calculate the source strength of the 2 kg Philippi sand. For the first 15 hours we get

$$C_{ac} = \frac{\lambda S t}{V}$$

$$S = \frac{V \times C_{ac}}{\lambda t} \approx \frac{0.012 \times (60 - 15)}{7 \times 10^{-3} \times 15} = 5.1 Bq$$



Figure 5.5 Philippi sand. about 2kg, placed in a pan before it was placed in the chamber to measure the radon exhalation with the RAD7.

5.4.2 Malmesbury Sand

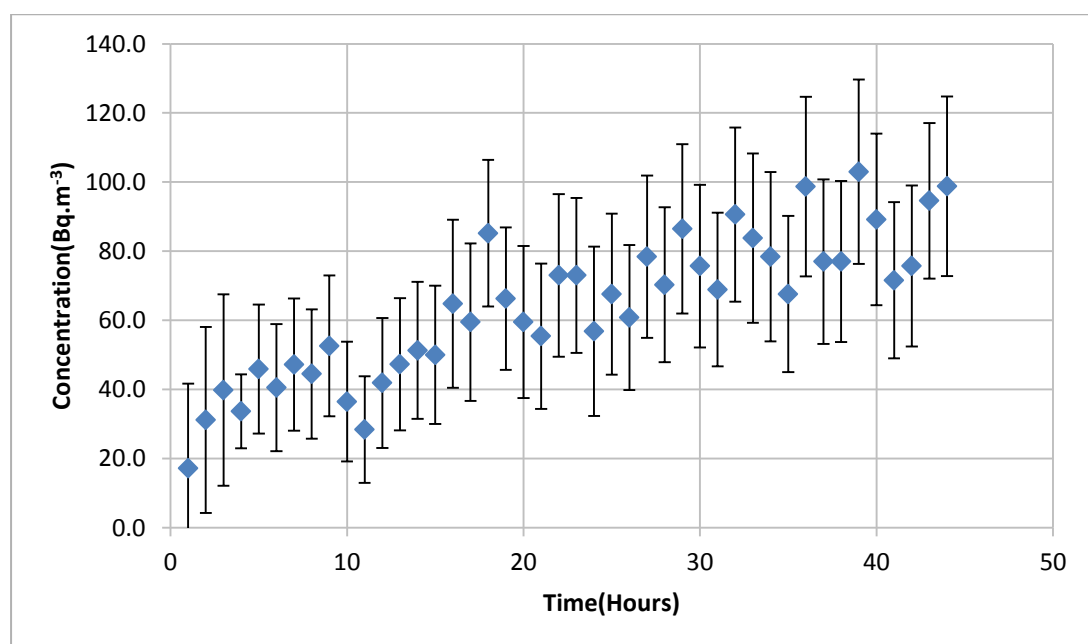


Figure 5.6 Radon exhalation of Malmesbury sand (Figure 5.7).

Malmesbury sand (Fig 5.7) is mined close to the town of Malmesbury on the West Coast of the Western Cape. This area forms part of the Greater Cape Town area. It was expected that Malmesbury sand would have a higher radon exhalation level than Phillipi sand, because it may contain eroded granite (Cole and Viljoen, 2001). However, Malmesbury Sand did not emit much radon and although it had a slightly higher exhalation than Phillipi sand. Since the measurement was conducted over 44 hours, we use equation 1.33 to calculate the source strength of the 2 kg Malmesbury sand for the first 10 hours:

$$C_{ac} = \frac{\lambda S t}{V}$$

$$S = \frac{V \times C_{ac}}{\lambda t} = \frac{0.012 \times 40}{7 \times 10^{-3} \times 10} = 6.8 Bq$$

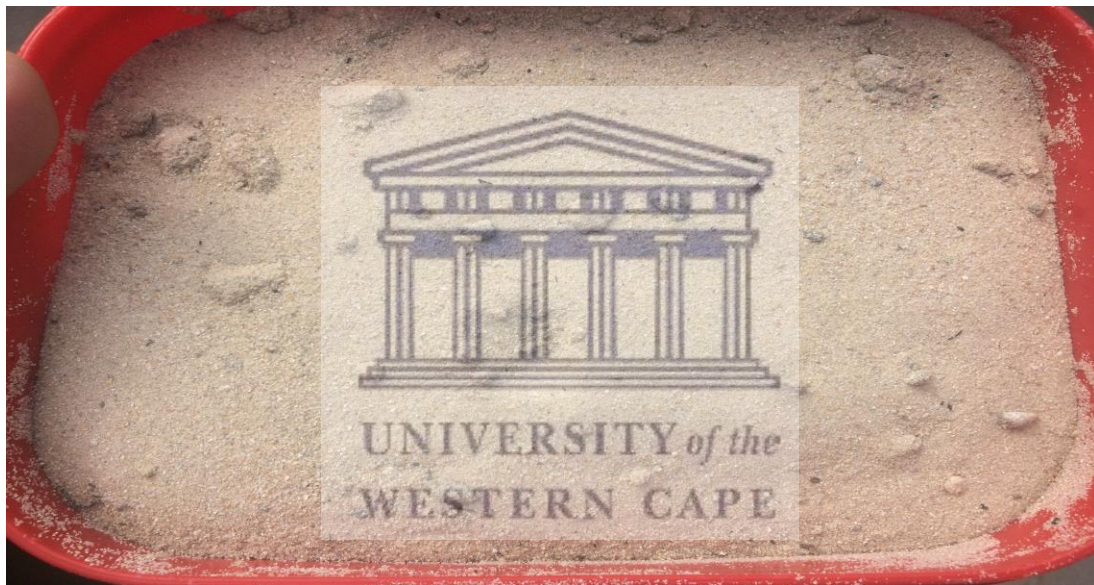


Figure 5.7 Malmesbury sand, of about 2 kg, placed in a pan before it was placed in the chamber to measure the radon exhalation.

5.4.3 Floor tile

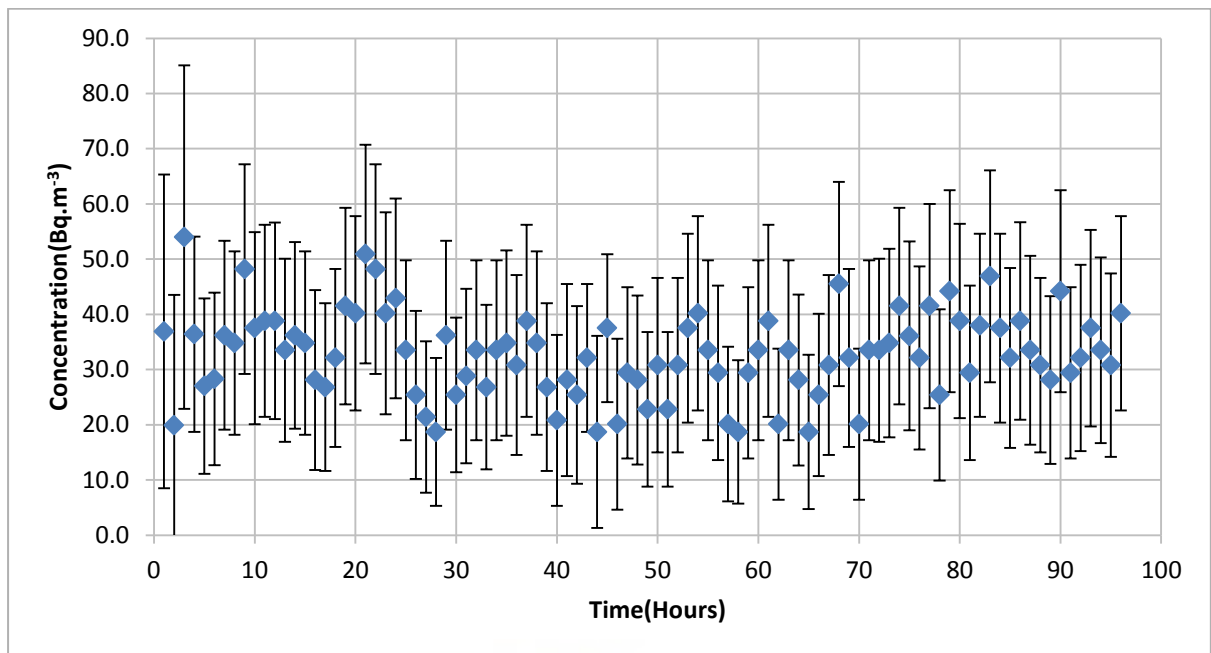


Figure 5.8 Radon exhalation of a Floor tile.

A floor tile made out of clay (consisting of mixtures of kaolin and illite) was tested for radon exhalation (Heckroodt, 1991). Porcelain tiles are normally kaolin-rich (base colour is white), normal tiles are more illite-rich and base colour is red/brown. The substance Cape Kaolin was mined in the cape granite suite near the towns of Noordhoek and Fish Hoek (www.miningweekly.com). In the Western Cape, mining also took place in Stellenbosch and Mossel Bay (www.dmr.gov.za). All these mines are currently closed. The floor tile did not release any significant amounts of radon and the level of radon was stable throughout the time.



Figure 5.9 The floor tile, with mass of 650,4g, was placed in the chamber to measure the radon exhalation.

5.4.4 Roof Tile

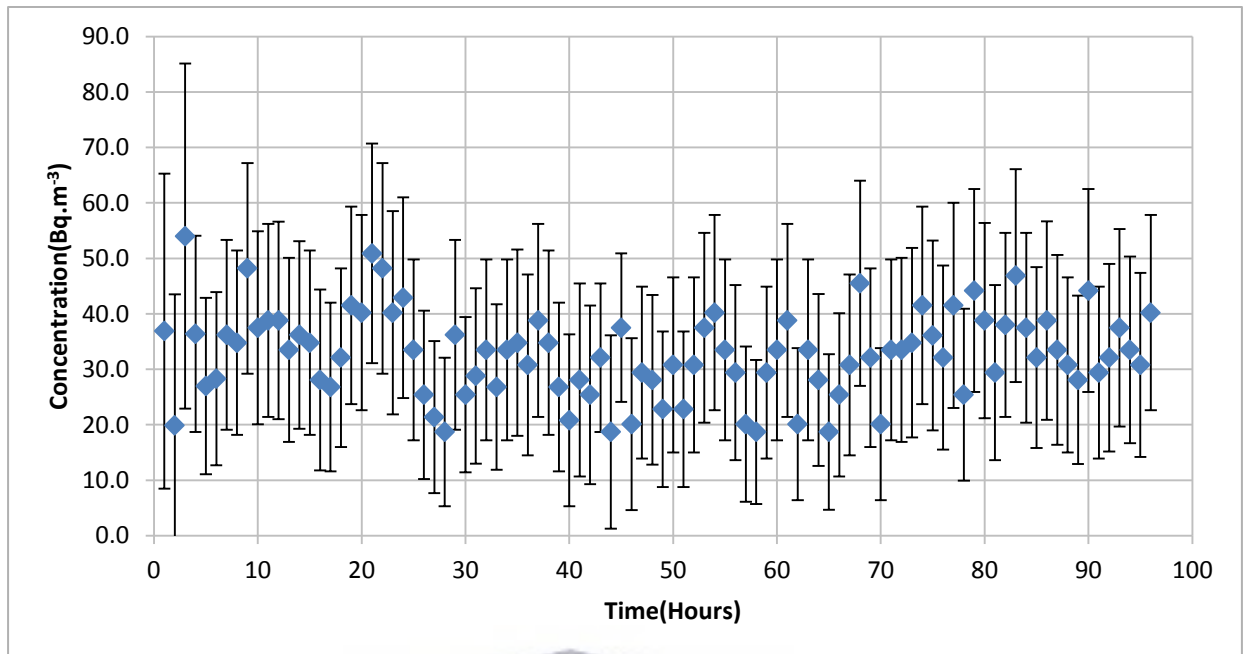


Figure 5.10 Radon exhalation of Roof tile.

The roof tile that was tested was made out of clay or concrete (sand and cement) with a waterproof glaze. The roof tile did not release any significant amounts of radon and the level of radon was stable throughout the time.

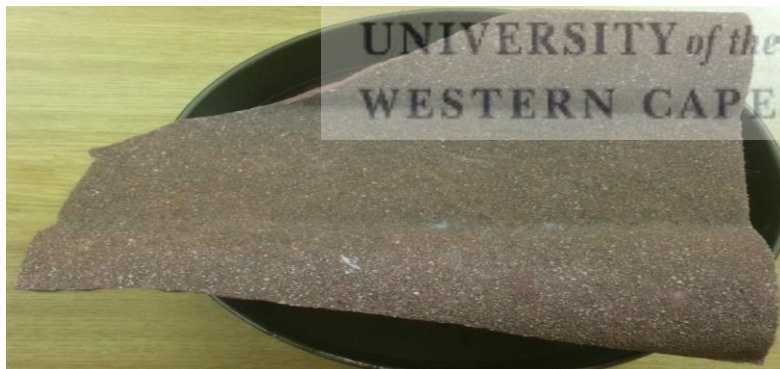


Figure 5.11 The roof tile, with mass of about 650 grams, was placed in the chamber to measure the radon exhalation.

5.4.5 Hornfels Stones

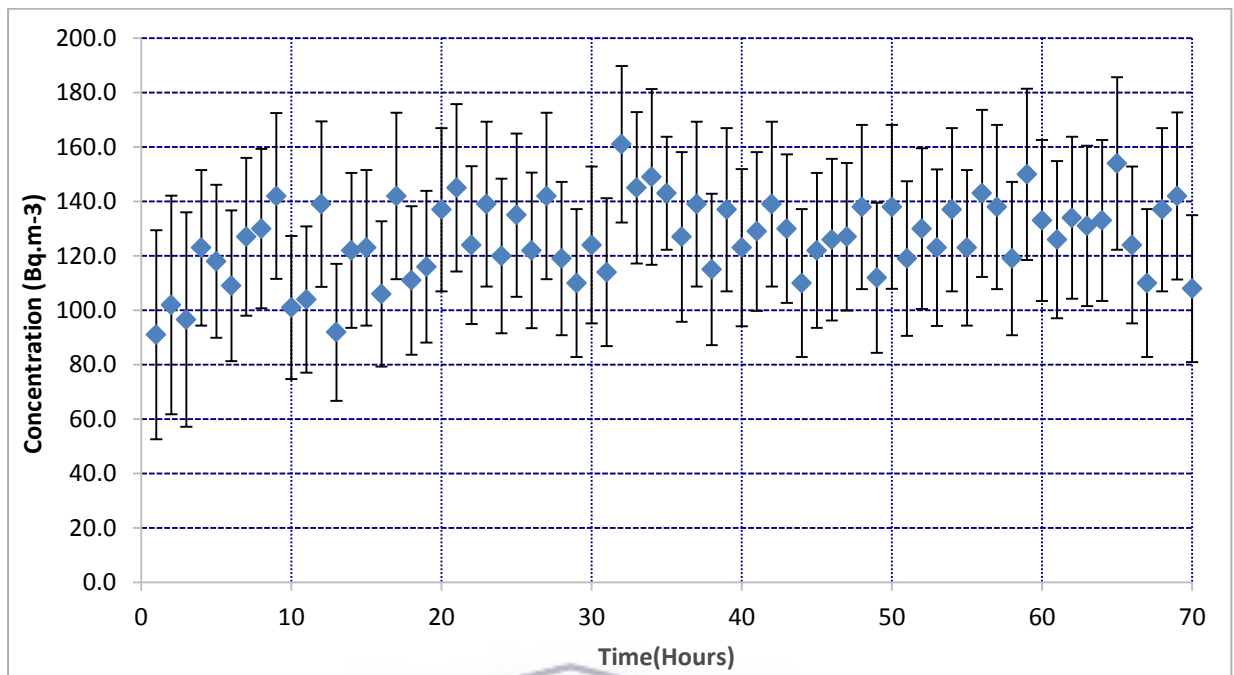


Fig 5.12 Radon exhalation from Hornfels stones.

It is expensive to transport low cost building materials (Roberts et al., 1998), so it is most likely that the source of this sample of hornfels would be from the Tygerberg Hills area, which consist of baked shale, near the suburb of Durbanville (Motsoenyane, 2010). This area is not close to any uranium sources thus it is not expected that the stones will contain elevated levels of radium. The stones would form part of the concrete mixture, especially with laying the foundation.



Figure 5.13 The Hornfels stones, with mass of 680 grams, were placed in the chamber to measure the radon exhalation.

5.4.6 Tar

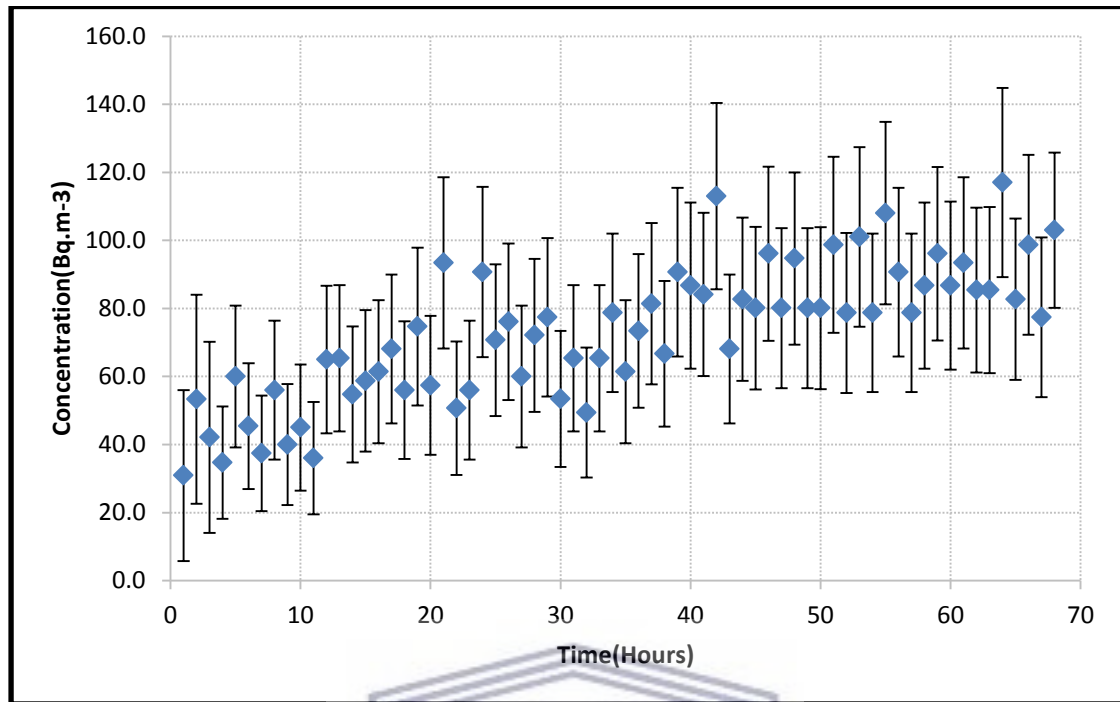


Figure 5.14 Radon exhalation of tar.

This sample was taken from tar that used to be situated around the pre-fabricated classrooms, which was going to be demolished at Livingstone High School in Claremont. This was done to build new brick classrooms. Tar consists of bitumen and small rock fragments, which could be hornfels, granite or quartzite (Fwa, 2006) (Jeffrey, 2005). In general tar is always placed outside dwellings where there is good ventilation and consequently low level of radon. Although tar is not considered a building material, the radon level was measured because there is a lot of tar situated around most classrooms around many schools across South Africa. Many people also use tar to create driveways which is situated around many houses and businesses.

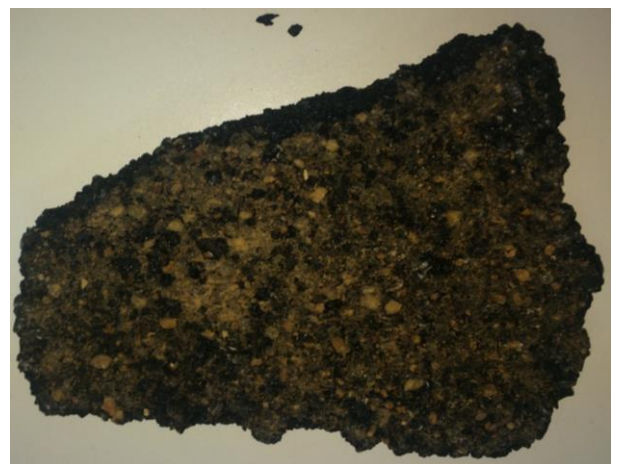


Figure 5.15 The tar piece, with mass of 966 gram, was placed in the chamber to measure the radon exhalation.

5.5 Uranium bearing sandstone from Beaufort-West

During the time of the uranium booms in the 1980's and between 2004 and 2009, many mining companies from all over the world prospected around Beaufort-West because it would be profitable to mine in new areas (<http://karoospace.co.za>). By 2010 when the price dropped dramatically, all of the companies abandoned prospecting since it would not be profitable. The price is too low and the only active uranium mines that would be feasible to develop are mines that yield Gold or Copper in South Africa (<http://world-nuclear.org>). The uranium bearing sandstone used as a sample was mined at a farm called Ryst Kuil (Heritage Western Cape, 2015). Some farmers in the area decided to use the mine tailings as filler material when building or renovating their homes. The uranium bearing sandstone was used as a cost saving matter because the prospectors did not have any use for the filler material. During 2009 there was a survey done on the radioactivity of the dwellings on the farms surrounding the area of Beaufort-West. The two farms Aardorn and Blikkraal had elevated radon levels due to using uranium bearing sandstone as filler material in their dwellings (Masia, 2010). Uranium prospecting and mining has been actively pursued in the Karoo since 1969. The uranium bearing sandstone sample used in this study originated from uranium prospecting in the Ryst Kuil farm, a prospecting site that dates back to 1978 (www.fse.org.za). When the Blikkraal farmhouse was renovated, the wooden floors were replaced with concrete slabs, which contained the uranium bearing sandstone from the Ryst Kuil farm. The Aardorn farmhouse was built in the late 1980's and the concrete used in the foundations contained sand stones which contained uranium bearing sandstone which was sourced from the Ryst Kuil farm (Masia, 2010).

5.5.1 RAD7 measurement of uranium bearing sandstone (Beaufort-West)

The soil surrounding Beaufort-West was expected to have higher levels of radon since there are a lot of uranium deposits in the area that led to the prospecting sites where stone heaps were left. The areas surrounding Beaufort-West has known uranium reserves (www.miningweekly.com b).

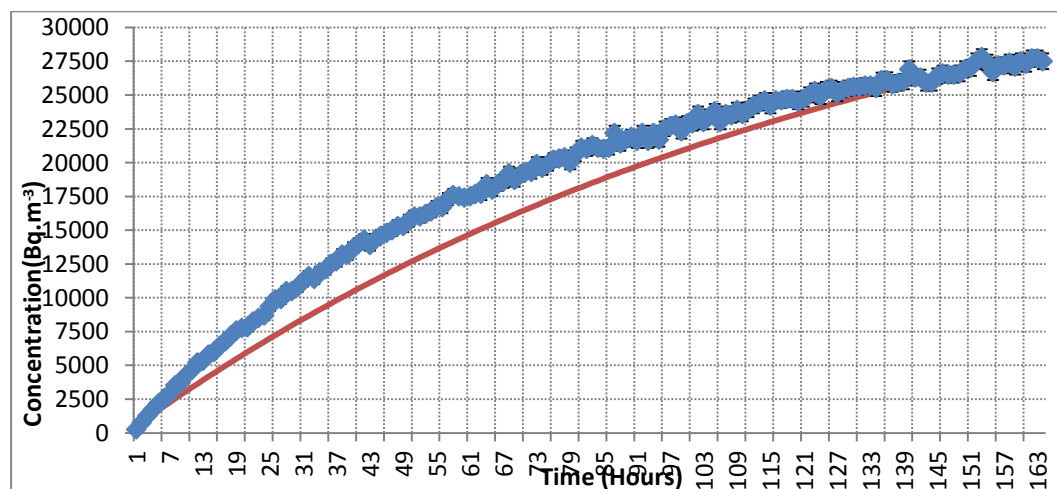


Figure 5.16 Radon exhalation of Beaufort West uranium bearing sandstone with a mass of roughly 2 kg. The top curve shows the measured data and the line is the fit to the data using Equation 1.31.

The uranium bearing sandstone emitted large amounts of radon from the start and within 2 hours the level in the chamber was over 300 Bq/m³. The concentration of radon increased at a steady rate over the duration of the experiment. This means that the uranium bearing sandstone contains a high concentration of radium which decays into radon. The only other material showing a nearly constant increase in radon concentration with no saturation was the Radium source that was measured earlier. The uranium bearing sandstone itself was measured and the radon concentration reached a high level peaking at around 27 700 Bq/m³ in the chamber as shown on figure 5.16 (Guimond, 1988).

The radon emitted can cause a large increase in the probability of developing lung cancer due to the continued exposure as a result of inhalation of radon daughters, especially in a poorly ventilated area. Care should be taken when using building materials from certain mines because mine tailings could cause health problems due to the release of radon (Vakil and Harvey, 2016). This is what happened at the farm Aardoon - see section 5.5.2 below. To calculate the source strength, we use the formula in (1.32). The Activity concentration is approximately 27500 (See Fig 5.16 and Table 10).

$$C_{ac} \approx \frac{S}{V}$$

$$27500 = \frac{S}{0.012}$$

$$S = 27500 \times 0.012 = 330 Bq$$

This shows that sandstones with a mass of about 2 kg from Beaufort West are equivalent to a source of 330 Bq. The effect of using these sandstones in the foundation of the house on the farm Aardoon is explored in the next section.



Figure 5.17 The uranium bearing sandstone, roughly 2kg, was placed in the chamber to measure the radon exhalation with the RAD7.

5.5.2 Measuring the hourly radon levels in the farm house on Aardoom

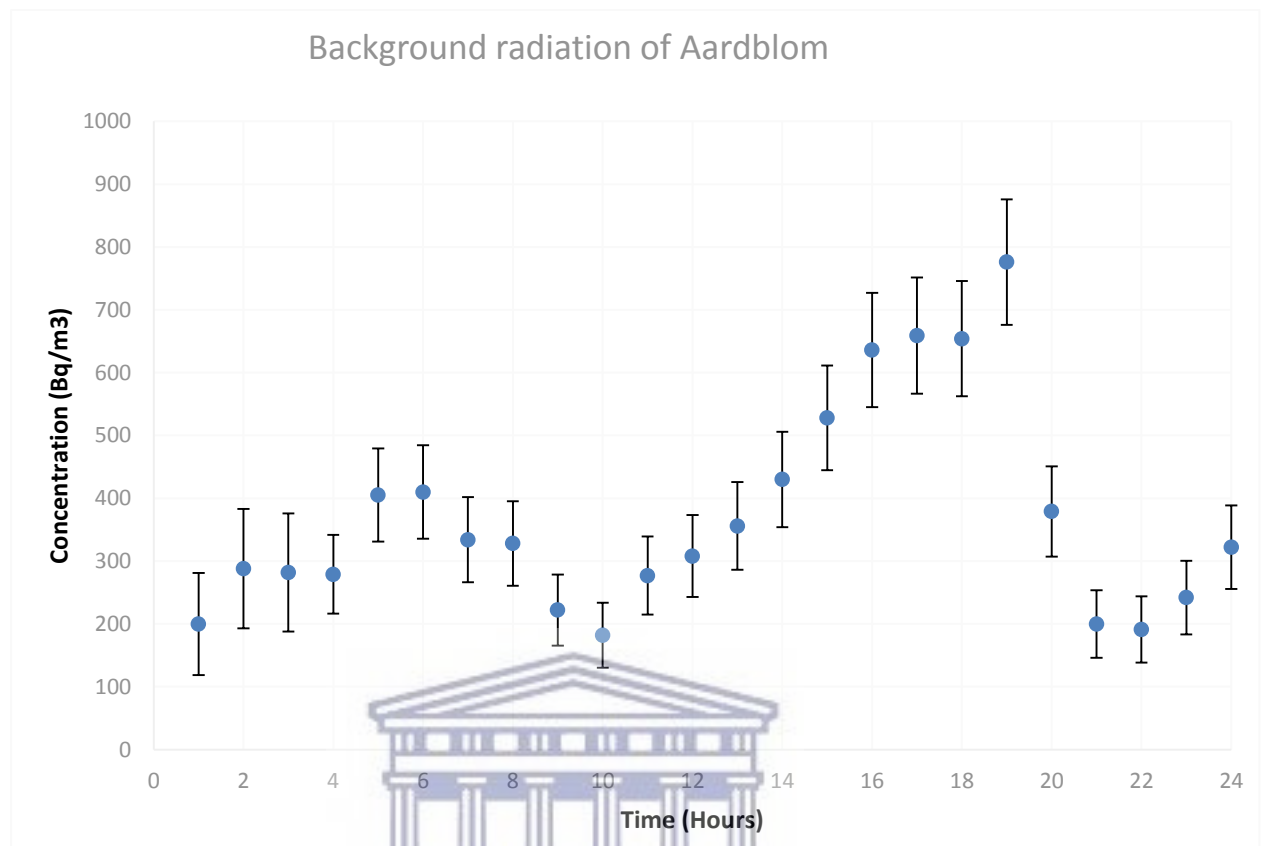


Figure 5.18 A 24-hour measurement of TV room within Aardoom. (Masia , 2010)

An example of high radon levels as a result of building materials is the house on the farm Aardoom will be shown in this section. These measurements were taken as part of the MSc work of a student at North West University (Masia, 2010). The radon concentration was measured in the TV room of the dwelling for a period of 24 hours (Masia, 2010) with the RAD7 and electret measurements were conducted in different rooms. The S-Chamber electret measurements showed a very high level of radon. Radon levels were mostly above the action level of 148 Bq/m³ in the USA. The radon level reached a peak of 776 Bq/m³ (Figure 5.18). The radon concentration has large differences over time which shows that there is a radon build up in the room during certain periods. The concentration gradually increased until the 5th hour which corresponds to the times of 11:08 and 15:08, which could be because the residents were not at home and doors were closed. There is a dip between the 5th hour and the 10th hour which corresponds to the times of 15:08 and 20:08. Since this is situated in the Karoo, it would be normal to keep doors and windows open during this time. From the 10th to the 19th hours there was a large increase in radon concentration in the room. This was during the times of 20:08 and 5:08. This corresponds to the time when doors and windows were closed during the night. During this period the radon levels reached very high levels. Between the 20th and 23rd hour which corresponds to 5:08 and 8:08, the windows and doors were open as the occupants woke up and opened doors and windows while they prepare for work. From the 23rd hour to the 24th

hour which corresponds to 8:08 and 9:08, the concentration of radon gradually increased again.

5.5.3 Radon concentration levels in the house on Aardorn.

Area	Reading 1	Reading 2	Average
Dining room	416 ± 31	349 ± 39	368 ± 29
Kitchen	388 ± 31	282 ± 26	321 ± 30
Study room	488 ± 32	536 ± 36	478 ± 34
Son bedroom	365 ± 29	431 ± 32	384 ± 30
Main bedroom	382 ± 30	384 ± 30	369 ± 30
Store	68 ± 20	49 ± 18	59 ± 19

Table 5.1: Radon measurement in the house on Aardorn using S chamber electrets (Masia, 2010).

The measurements shown in Table 5.1 were taken in the Aardorn farmhouse with the use of S-Chamber electrets. In every room except the store room the radon level was high. The dining room had an average level of $368 \pm 29 \text{ Bq/m}^3$ which is far higher than the target level. The kitchen also had a very high level of radon. The son's bedroom and the main bedroom had similar levels of radon. The study room had the highest level in the dwelling. The reason for the high level is probably that the room stays unoccupied and the windows and doors were closed most of the time. The store room has a radon level which is significantly lower than the other rooms measured. The reason for this is that it was not built by using the mine tailings from the Ryst Kuil farm (Masia, 2010). The Store room acts as a control because it shows what the radon level in this area is likely to be if there are no stones containing high levels of uranium in the foundations.

5.5.4 L -chamber measurement for Aardorn farmhouse

Location	Reading 1	Reading 2	Average
TV - room	265 ± 16	269 ± 17	267 ± 17
Son's bedroom	411 ± 24	373 ± 22	392 ± 23
Main room	259 ± 16	258 ± 16	259 ± 16
Kitchen	257 ± 16	272 ± 17	265 ± 17

Table 5.2 : L-Chamber Measurements of Aardorn (Masia S, 2010).

To investigate the radon level in houses, longer term measurements are needed. These were done with L-chambers and the results are shown in Table 5.2. The level for the TV-room, main room and kitchen is more than the action level. A RAD7 measurement was done in the TV-room for a period of 24

hours and the fluctuations was quite large (As discussed in 5.5.2 in detail). The son's bedroom had the highest level with an average of $392 \pm 23 \text{ Bq/m}^3$.

5.5.5 Radon exhalation of Blikkraal using electrets

Location	Reading 1	Reading 2	Average
Lounge	205 ± 11	183 ± 10	194 ± 11
TV room	172 ± 10	209 ± 11	190 ± 11
Pantry	315 ± 16	195 ± 11	255 ± 14
Kitchen	161 ± 9	181 ± 10	171 ± 10

Table 5.3: L-Chamber Measurements in the house on Blikkraal (Masia, 2010).

Table 5.3 shows the radon concentration of the Blikkraal farm house with use of L-Chambers. The readings showed that the Radon exhalation levels were lower than at Aardoom. The Blikkraal dwelling has a high ventilation rate, which cause the low levels of radon inside the dwelling. With the exception of the pantry, all the readings on average were below the target level.

5.6 Using the RAD7 to measure the radon exhalation of granites

Granite (a loosely used term for hard rock) counter tops are used as durable material and are usually placed in the kitchen or even used as outside furniture, such as a table or counter top. Granite is mined all over the world and it is not always possible to determine the origin of granite. Some websites and importers disclose scant details about their products and they do not disclose the origin of the mine. The names that are given to the granite counter tops do not necessarily represent the geographical names, while some names are used for marketing purposes. Granite countertops could be uniformly active, which means that it has a constant radon concentration throughout the slab. Granite countertops that contain significant hot spots (High radon concentration); give rise to various radon concentrations on the same slab. (Myatt, et al, 2010);(Chen, 2010)(Bergman, et al, 2015);(Parchocho-Torgal, 2012);(Elzain, 2014);(Saad, et al, 2008);(Zhaing, et al, 2017);(Anjos, et al, 2011);(Bala, Kumar and Mehra, 2017)

Sample	Dimension (cm)	Volume (cm ³)	Mass (kg)	Density (g/cm ³)
Santa Cecelia	(3.5 * 14.5*14.5)	735.88	1.88	2.55
Namib Green	(3.5 * 14.5*14.5)	735.88	1.77	2.41
African Red	(3.5 * 14.5*14.5)	735.88	1.84	2.50
Golden Beach	(3.5 * 14.5*14.5)	735.88	1.75	2.40
Indiana Dakota	(3.5 * 14.5*14.5)	735.88	1.88	2.55

Table 5.4: Dimensions (in cm), Volume (cm³), Mass (kg) and Density (g/cm³) for different granite samples.

Five counter top sample blocks were sourced from a local granite supplier. All the granite counter-tops have nearly identical dimensions for control purposes and it also makes it easier for simulation purpose. There will also be no need for extrapolation when simulations are done. Studies have shown that most

soil density is between 1.1 g/m^3 and 1.5 g/m^3 where the soil mainly consist of SiO_2 (Mottaet al., 2007) Granites are usually mined quite deep in the earth and the average density was approximately 2.5 g/cm^3 .

5.6.1 Golden Beach

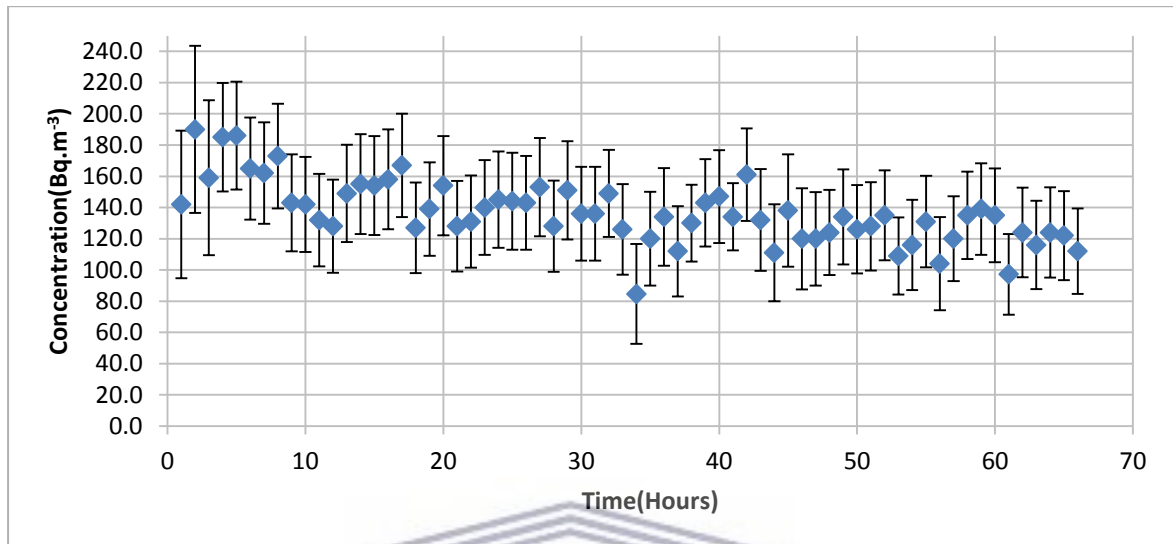


Figure 5.19 RAD7 measurement for the Golden beach sample.

The first granite sample Golden beach (Fig 5.20), showed little radon exhalation as shown in Figure 5.19. In fact, the radon released by the sample was lower than the decay of the initial radon that was present in the chamber leading to a reduction in radon readings. The country of origin for this granite is Brazil (www.stoneply.com).



Figure 5.20 The Golden beach granite used for measurements using the RAD7 and HPGe.

5.6.2 Indiana Dakota

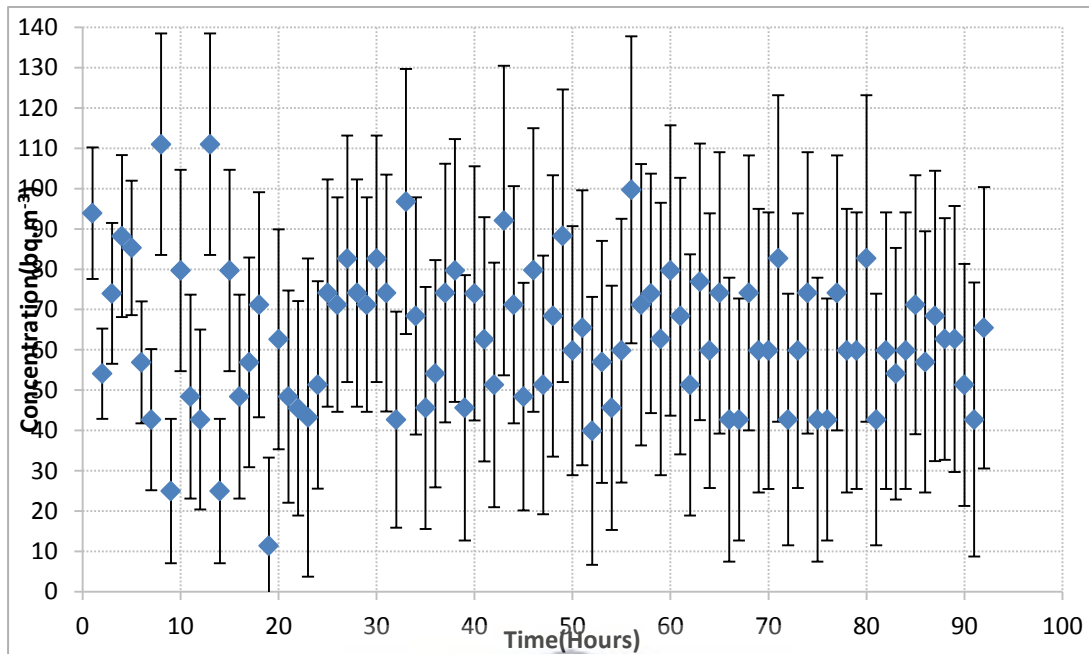


Figure 5.21 Indiana Dakota RAD7 measurement.

The radon level produced by Indiana Dakota was below detection limit. (See figure 5.21). The country of origin for this granite is India. The granite is also known as Indian Dakota and Indian Mahogany (www.stonecontact.com).

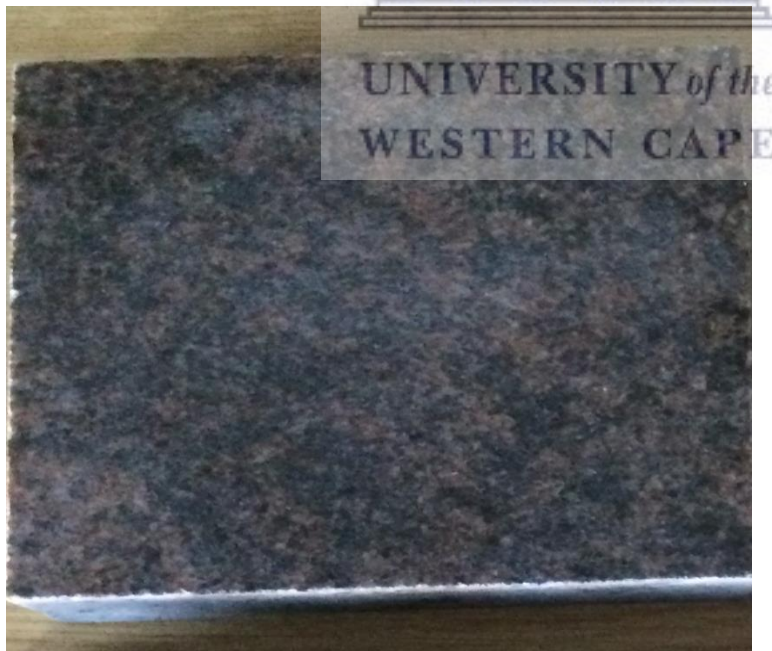


Figure 5.22 The Indiana Dakota granite used for measurements using the RAD7 and HPGe.

5.6.3 Santa Cecilia granite

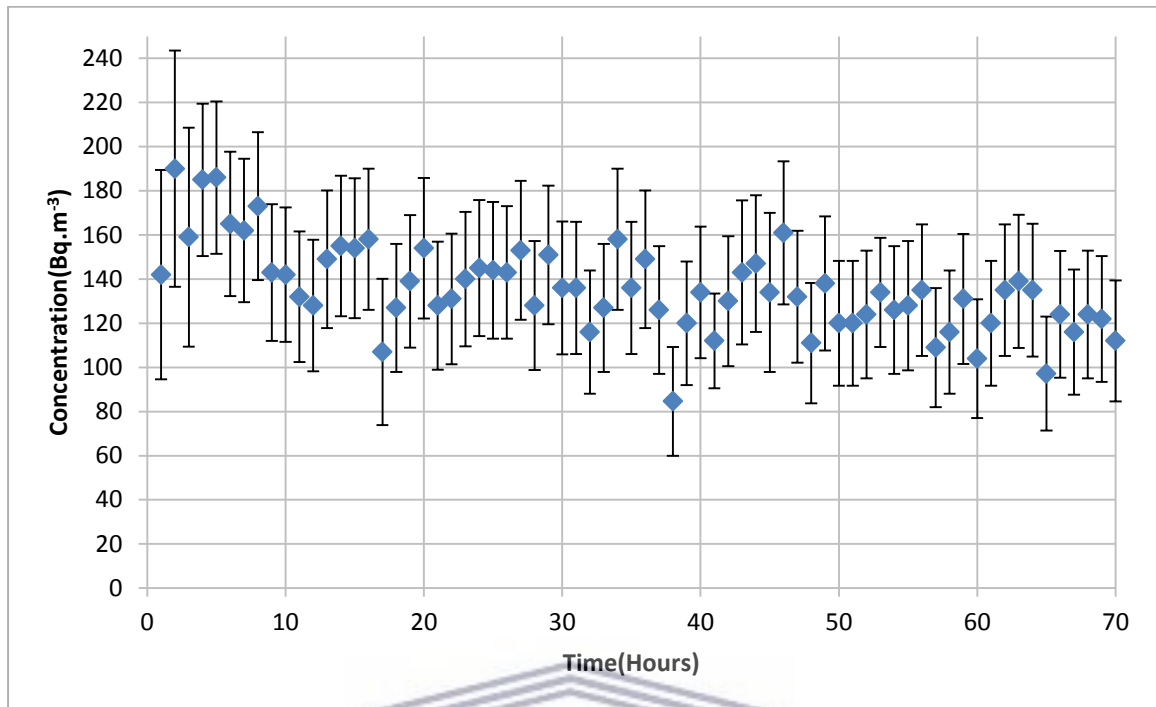


Figure 5.23 Santa Cecilia RAD7 measurement.

The radon level of Santa Cecilia was also below detection limit. (See figure 5.23). The country of origin for this granite is Brazil. (www.graniteland.com/stone)

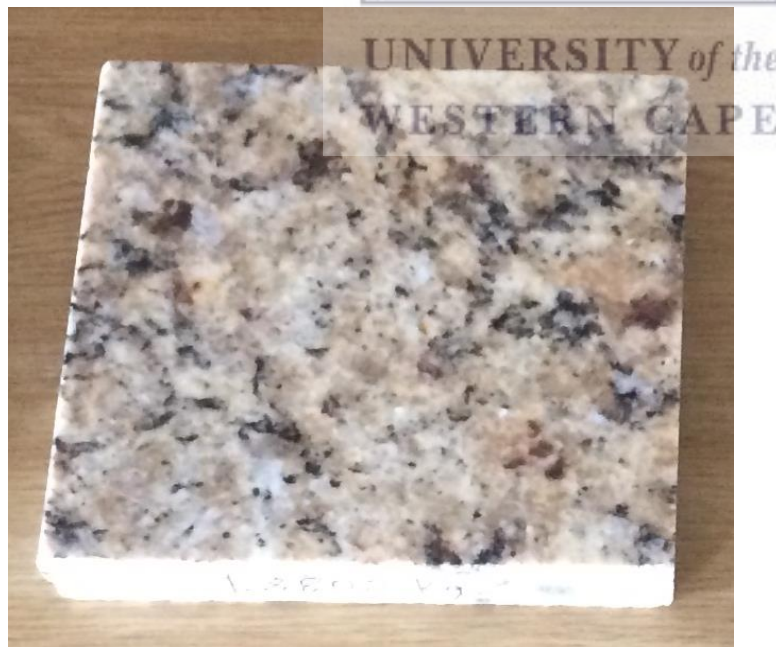


Figure 5.24 The Santa Cecilia granite used for measurements using the RAD7 and HPGe.

5.6.4 Namib green

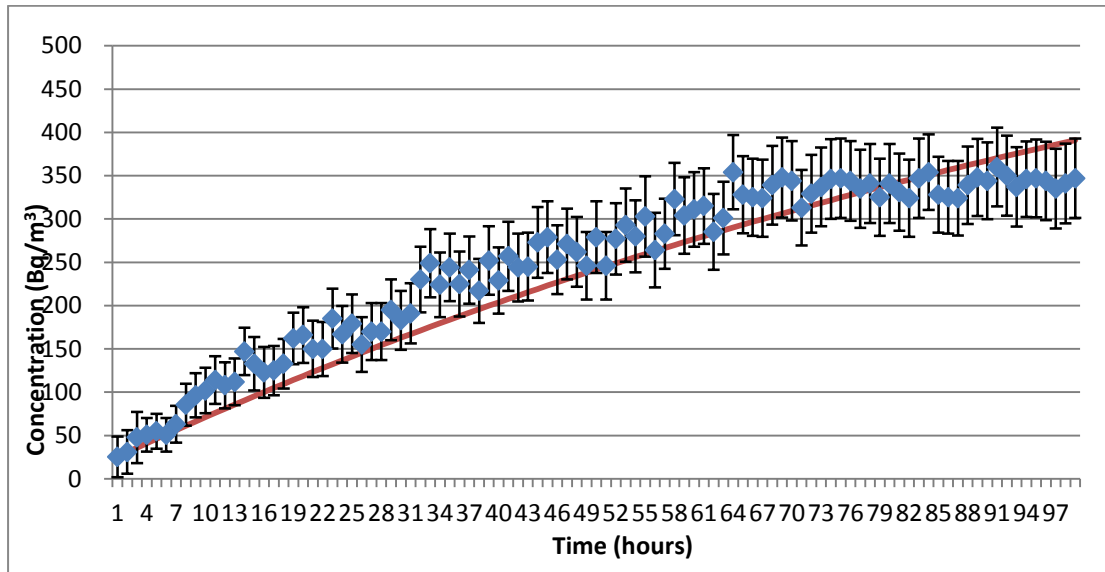


Figure 5.25 Namib Green RAD7 measurements. The top curve shows the measured data and the line is the fit to the data using Equation 1.31.

The Namib Green sample has a very high radon exhalation rate and the concentration reached around 350 Bq/m^3 after 90 hours. The radon level starts to stabilize after the 60th hour with an average radon concentration was around 320 Bq/m^3 . It is not recommended that this counter top should be installed in any dwelling with low ventilation, because of the large exhalation of this level of radon. The area of mining was located in a uranium province, which has a very high concentration of uranium and it was not unexpected that the concentration of uranium will be very high. The country of origin for this granite is Namibia, close to the town of Walvis Bay (Roesener and Schreuder, 1992). Since the measurement was conducted over only 99 hours, the concentration has not reached equilibrium so equation 1.33 can be used for the first 40 hours to calculate the source strength for the Namib green granite countertop.

$$C_{ac} = \frac{\lambda S}{V} t$$

The slope for the first 40 hours gives $\frac{232 \text{ Bq.m}^{-3}}{40 \text{ hours}}$. This implies

$$S = \frac{232 \times V}{\lambda \times 40 \times 3600} = \frac{232 \times 0.012}{2.1 \times 10^{-6} \times 40 \times 3600} = 9.2 \text{ Bq}$$

This value does not seem very big, but can contribute to the radon concentration in a room if there is a large slab of this granite.

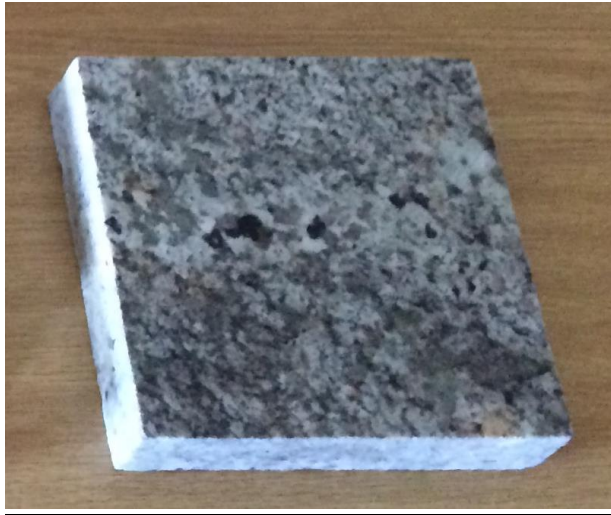


Figure 5.26 The Namib Green granite used for measurements using the RAD7 and HPGe.

5.6.5 Granite African Red

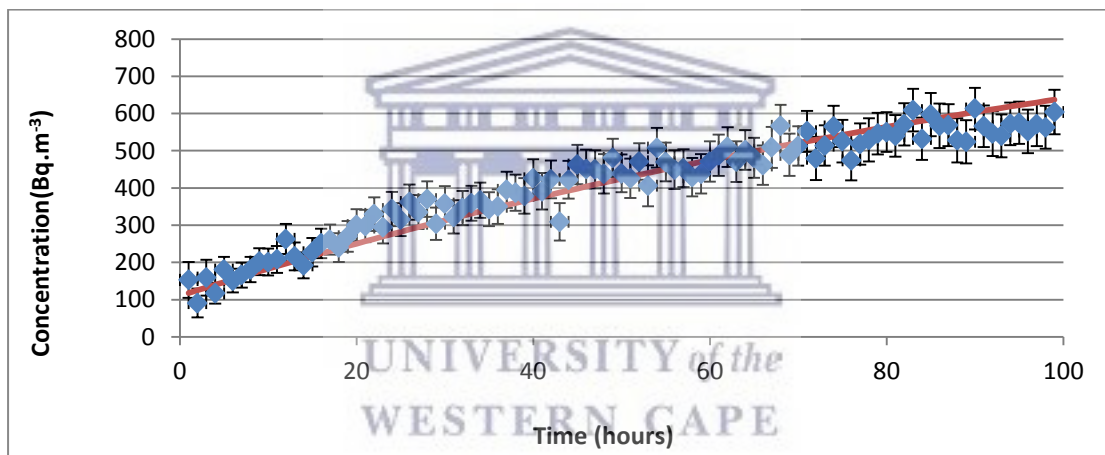


Figure 5.27 African Red RAD7 measurement. The top curve shows the measured data and the line is the fit to the data using Equation 1.31.

African Red reached 550 Bq/m³ after 70 hours and reached 609 Bq/m³ after 83 hours as shown in Figure 5.27. It is not recommended that this counter-top should be installed in any dwelling with low ventilation. The granite was mined in an area with a high concentration of uranium. African Red was possibly mined in the Springbok flats. The area has a very high concentration of uranium and it was expected that the concentration of uranium will be very high (Beceгатоet al, 2008).

Since the measurement was conducted over only 100 hours, the concentration has not reached equilibrium so equation 1.33 will again be used to calculate the source strength for the African Red granite countertop sample.

$C_{ac} = \frac{\lambda S}{V} t$ The slope for the first 20 hours (Table 16 in Appendix D) gives

$$\frac{150 \text{ Bq.m}^{-3}}{20 \text{ hours}}$$

This implies

$$S = \frac{232 \times V}{\lambda \times 40 \times 3600} = \frac{150 \times 0.012}{2.1 \times 10^{-6} \times 20 \times 3600} = 12 \text{ Bq}$$



Figure 5.28 The African Red granite used for measurements using the RAD7 and HPGe.

5.7 Overview of the HPGe readings

After completing the RAD7 measurements, the granites (Figure 5.29) were sent to iThemba Labs to measure the activity concentration of ^{238}U , ^{232}Th , ^{40}K and ^{234}Pa respectively by measuring the gamma rays from the samples. The reason for the experiment is to determine if there is a correlation between the radon measured by the RAD7 that depends on the radon that escapes from the granite and the gamma rays that depends on the radium and radon progeny in the granite. The isotopes will be discussed individually. The most significant isotope is the ^{238}U since it is the parent of the decay chain that contains ^{222}Rn (Maibane, 2017).

Sample	Activity Concentration (Bq/kg)			
	^{238}U	^{232}Th	^{40}K	^{234}Pa
Santa Cecilia	21 ± 1.8	52.5 ± 1.9	1705 ± 28	29.1 ± 12.3
Namib Green	657 ± 14	107.3 ± 3.5	2116 ± 35	714.6 ± 36
African Red	125 ± 4.1	157.9 ± 3.6	1698 ± 28	196 ± 23
Golden Beach	10 ± 2.2	160.1 ± 2.4	2131 ± 35	21.5 ± 21.5
Indiana Dakota	n/a	86.6 ± 2	1324 ± 22	n/a

Table 5.5 Overview of the general HPGe readings (Maibane, 2017).



Figure 5.29 The granite countertops used for measurements in the RAD7 and HPGe.

^{238}U exhibits high value of activity concentration compared with ^{232}Th which may be due to the higher mobility of the ^{238}U progenies such as ^{226}Ra with respect to ^{232}Th (Talavera, 2000). The activity concentration of ^{40}K was noticeably high when compared with the activity concentrations of ^{238}U and ^{232}Th . The average level in marble and granite for ^{238}U and ^{232}Th is 40 Bq/kg while ^{40}K has an average level of 400 Bq/kg (UNSCEAR, 1982). In granite the average for ^{40}K is 1200 Bq/kg, for ^{232}Th it is 84 Bq/kg and for ^{238}U 87 Bq/kg. (Wanget al., 2005). The activity of ^{40}K is quite high if compared to the ^{238}U and ^{232}Th in all granite-countertops (Maibane, 2017).

5.7.1 Uranium Activity of the granite countertops with the use of the HPGe

The measurement of gamma rays from the ^{238}U decay series is significant since ^{222}Rn forms parts of the ^{238}U decay chain. The RAD7 detector measures the energy emitted by Alpha particles, while the HPGe measures the Gamma decay energy. When the RAD7 results were compared it was expected that only the two granites African Red and Namib Green would show elevated levels of activity (Table 5.5). The granite countertops Golden Beach, Indiana Dakota and Santa Cecelia, as expected, showed activity concentrations which are below the average world levels of the activity concentration of ^{238}U of 40 Bq/kg in soil (Sroor et al., 2013). As expected the levels of African Red and Namib Green gave much higher levels than the average activity concentration of ^{238}U . When the RAD7 measurements are compared it shows that only two granite counter-tops Namib Green and African Red showed significant levels of activity. It was unexpected that the activity concentration of Namib Green was approximately 6 times the level of the African Red, while African Red has almost double the amount of radon exhalation (See Figure 5.25 and 5.27). The reason why African Red has a higher level of radon level than Namib green

despite the contradicting Gamma ray activity is that Gamma Ray activity measures the uranium that is still inside the granite countertop while RAD7 measures the amount of radon that escaped (Ebaid, 2010). The results only make sense if the Namib Green has a high radium content but the matrix does not allow the radon to escape.

5.8 Calculations of Radon exhalation from the granite

The granite African Red and Namib Green were the only two that showed significant levels of radon exhalation. The activity was calculated as in section 5.6. To calculate the exhalation rate in $Bq.m^{-2}.s^{-1}$, first find the surface area of the granite (which is in the shape of a rectangular prism) by using the formula:

$$\text{Surface Area} = (2 \times l \times b) + (2 \times b \times h) + (2 \times l \times h) \quad (5.1)$$

We find the exhalation rate by using the following formula, the radon “source strength” that is released:

$$\text{Exhalation Rate} = \frac{\text{Source}}{\text{Surface Area}} = \frac{\text{Source}}{(2 \times l \times b) + (2 \times b \times h) + (2 \times l \times h)} \quad (5.2)$$

5.8.1 Namib Green Radon exhalation calculation

Figure 5.25 shows that Namib Green reaches at around $350 Bq.m^{-3}$. In section 5.6.4 it was shown that the Namib Green sample corresponds to a source strength of $S = 9.2 Bq$ which implies that 4.2 radon atoms are produced per second, corresponding to a radon activity of $\lambda \times 4.2 Bq.s^{-1}$ that enters the room.

The surface area of the granite can be found by:

$$\text{Area (Top and bottom of granite)} = (14.5)^2 \times 2 = 420.5 cm^2$$

$$\text{Area (sides of granite)} = (14.5) \times 3.5 \times 4 = 203 cm^2$$

$$\text{Surface area} = 420.5 + 203 = 623.5 cm^2 = 0.0623 m^2$$

To find the exhalation rate, we use the equation 5.2:

$$\text{Exhalation Rate} = \frac{(7.56 \times 10^{-3}) \times 9.2}{0.0623} = 1.1 Bq.m^{-2}.h^{-1}$$

5.8.2 African Red Radon exhalation calculation

In Section 5.6.5 we found that the African Red, corresponds to a source strength of around 12 Bq.

First we find the surface area of the granite:

$$\text{Area (Top and bottom of granite)} = (14.5)^2 \times 2 = 420.5 cm^2$$

$$\text{Area (sides of granite)} = (14.5) \times 3.5 \times 4 = 203 cm^2$$

$$\text{Surface area} = 420.5 + 203 = 623.5 cm^2 = 0.0623 m^2$$

To find the exhalation rate, we use the equation 5.2:

$$\text{Exhalation Rate} = \frac{(7.56 \times 10^{-3}) \times 12}{0.0623} = 1.5 \text{ Bq.m}^{-2}.\text{h}^{-1}$$

5.9 Other investigations concerning granite countertops

A study by Llope (Llope, 2011) simulated a person standing near various countertops with different radon concentrations and estimated the dose due to gamma radiation as a result of the countertop. The measurements were done using a Sodium Iodide detector NaI(Tl) gamma spectrometer. The simulation assumed that the person was standing for 2 hours a day for 300 days a year at a distance of about 1 cm away from the source. Any measurement beyond 30 cm would become indistinguishable from the background radiation and thus 1 cm simulated the maximum radiation obtained. The result stated that the highest activity concentration for a granite countertop seen in Llope's study had a level of U-nat 55 440 Bq/kg. The two high radioactive activities found in this study were the Namib Green with a measurement of 657 Bq/kg and African Red with 129 Bq/kg. One granite countertop measured by Llope, Four seasons, had an activity rating of about 90 times more than Namib Green. The dose rate of the countertop measured by Llope was usually less than 0.1 mSv/a. This is quite low since it is 4 times lower than an average person's internal radiation, which means that these countertops are quite safe to use within a dwelling. The HPGe detector has a better resolution compared to the NaI(Tl) detector but the results will be the same for both measurements (Hossain, 2012).

A position paper by the Health Physics Society of the USA indicated that the radon exhalation from typical granite countertops comparable to the ones studied in this work are also not of major concern (hps.org/documents/Radiation_granite_countertops.pdf). They estimate that a 5 m² slab of granite with an activity of 37 Bq/kg would produce an extra 5 Bq.m⁻³ of radon activity concentration in a typical kitchen – see document for other assumptions. The granite measured in this work has much higher activity but the ventilation in houses in South Africa are usually much higher than in the USA.

Chapter 6: Conclusions

The materials measured in this study can be grouped into three different types. These were general building materials, granite countertops and mine tailings which contained uranium bearing sandstone.

6.1 General Building materials

In general building materials measured in this study had a very low radon exhalation rate. All the materials were sourced locally, which in this case is the greater Cape Town area. The Greater Cape Town area does not have significant uranium deposits, so it will make sense than the materials sourced would have a low radon exhalation. The only material sourced from an unknown location was the Floor tile and the radon concentration was also quite low. Radon emanation from concrete is normally reduced with various coverings for floors and walls, namely tiles, paint, carpeting etc. (Brodhead, 2008)

6.2 Granite Countertops

The Granite countertops used in this study were available locally but sourced from different areas around the world. According to studies done on granite, it was established that granite has significant variation in emanation rates between surfaces confirmed in our work. (Brodhead, 2008)

The three granite counter tops with low radon concentrations were Golden Beach, Santa Cecelia and Indiana Dakota. The Golden Beach and Santa Cecelia were both quarried in Brazil, while Indiana Dakota was quarried in India. The two Brazilian granite countertops had very similar concentrations. The two granite countertops with elevated radon exhalation were the African Red and Namib Green. African Red was possibly mined in the Springbok Flats area which was located in parts of the Gauteng, North West and Limpopo provinces. The African Red granite counter-top produced a maximum concentration of 550 Bq/m^3 within the chamber and the source strength of the sample was found to be 12 Bq. The Namib Green granite countertop was mined 15 km East of Swakopmund Namibia. Namib green produced concentration of 350 Bq/m^3 within the chamber and the source strength was 9.2 Bq. The concentration of radon within African Red and Namib Green will not pose an immediate danger to anyone in the vicinity of the respective granite countertops. A well ventilated dwelling would lower the radon level significantly. A study by Llope simulated a person standing near various countertops with different activity concentrations. The granite countertop measured by Llope, "Four seasons", had a gamma activity rating of about 90 times more than Namib Green. The dose rate of the countertop measured by Llope was around 0.1 mSv/a . This is quite low since it is 5 times lower than an average person's internal radiation, which means that these countertops are quite safe to use within a dwelling. The gamma source strengths of both the African Red and Namib Green will not pose any threats to anyone in the vicinity.

A similar estimate using the guidelines of the HPS in the USA (see Section 5.9) indicates that the additional radon from granite countertops with the radon exhalation found in this work will only increase the radon in a room by a few Bq.m⁻³.

6.3 Uranium bearing sandstone from the Ryst-Kuil farm, Beaufort-West

Uranium bearing sandstone from the Ryst-Kuil farm was used as filler material, and as coarse aggregate in concrete, for the surrounding dwellings in neighbouring farms. According to a study (Masia, 2010, Scholtz, 2006), the farm houses Aardoorn and Blikkraal had elevated levels of radon. The uranium bearing sandstone itself with a mass of around 2 kg was measured and the radon concentration produced was at a very high level and peaked at around 27 700 Bq/m³ with an equivalent source strength of 320 Bq. The radon concentration at the Aardoorn dwelling had average ventilation and certain rooms had very high radon concentrations. During the 24 hour RAD7 reading, the radon concentration peaked at 776 Bq/m³, almost certainly as a result of the filler material used in the foundations.

6.4 Recommendations

All the locally sourced building materials measured had very low levels of radon exhalation and will not pose any radiological threat. According to the study done by Masia (Masia, 2010), concerning the dwellings of Blikkraal and Aardoorn, which used the same filler material from the Ryst-Kuil farm, which contained uranium, this material can cause significant radon concentrations. Since Blikkraal had adequate ventilation, the radon concentration was relatively low despite the presence of the uranium bearing sandstone. By contrast Aardoorn had a high radon concentration do to the fact that the ventilation does not allow radon to dissipate fast enough and more uranium bearing sandstone was used from the description of the owners. This causes radon build-up, especially during the evenings when doors and windows are closed. It is recommended that a dwelling must be well ventilated.

Some of the granite countertops measured in this work showed considerable radon exhalation, but comparing to the work of Llope (Llope, 2011) even granite countertops with much higher levels of radon do not pose a threat to the user, even at close proximity due to gamma radiation (Llope, 2011) or radon exhalation.

References :

Abdelouas, A., Lutze, W., Gong, W., Nuttall, E.H., Strietelmeier, B.A. and Travis, B.J., (2000) Biological reduction of uranium in groundwater and subsurface soil. *Science of the Total Environment*, Volume 250 Issue 1, pages 21-35.

Abu-Jarad F (1988) Application of Nuclear Track Detectors for radon related measurements. *Nucl Tracks Radiat Measurement*, Volume 15, pages 525-534.

Abu-Jarad F, Fremlin JH, Bull R (1980) A Study of radon emitted from building materials using SSNTD. *Phys Med Biol*, Volume 25, pages 683-694.

Ackland Len (2002) *Making a Real Killing: Rocky Flats and the Nuclear West*

Åkerblom, G., Mellander, H. (1997) Geology and radon. In *Radon measurements by etched track detectors*, Editors S.A. Durrani and R. Ilić, World Scientific Publishing Co. Pty. Ltd.

Al-Hamarneh, I. and Awadallah, M. (2009) Soil radioactivity levels and radiation hazard assessment in the highlands of Northern Jordan. *Radiation Measurements*, Volume 44 Issue 1, pages 102-110

Al-Jarallah M, Fazul-Rehman I, Musazay MS, Aksoy A. (2005) Correlation between radon exhalation and radium content in granite samples used as construction material in Saudi Arabia. *Radiat Meas* 40: pages 625– 629

Alavanja M.C.R. (2002) Biologic damage resulting from exposure to tobacco smoke and from radon: implication for preventive interventions. *Oncogene* Volume 21, pages 7365 - 7375.

Ali, N., Muhammad, W., Khattak, N.U., Khan, E.U., Rajput, M.U., Akram, M., Hussain, S. and Mujahid, S.A., (2016) Radon doses in the indoor environments of Murree and Islamabad, Pakistan: A comparison of active and passive techniques. *Indoor and Built Environment*, Volume 25, Issue 6, pages 883-894.

Amin, R.M. and Eissa, M.F., (2008) Radon level and radon effective dose rate determination using SSNTDs In Sannur cave, Eastern desert of Egypt. *Environmental monitoring and assessment*, Volume 143 Issue 1, pages 59-65

Anderson, C.L., (1996) *Economics and the Environment*. Council for Economic Education.

Anjos, R., Juri Ayub, J., Cid, A., Cardoso, R. and Lacerda, T. (2011) External gamma-ray dose rate and radon concentration in indoor environments covered with Brazilian granites. *Journal of Environmental Radioactivity*, Volume 102 Issue 11, pages 1055-1061

Archer, V.E., (1988) Lung cancer risks of underground miners: cohort and case-control studies. *The Yale journal of biology and medicine*, Volume 61 Issue 3, page 183.

Babonneau, N., Delacourt, C., Cancouët, R., Sisavath, E., Bachelery, P., Mazuel, A., Jorry, S.J., Deschamps, A., Ammann, J. and Villeneuve, N., (2013). Direct sediment transfer from land to deep-sea: Insights into shallow multibeam bathymetry at La Réunion Island. *Marine Geology*, Volume 346, pages 47-57

Bala, P., Kumar, V. and Mehra, R. (2017). Measurement of radon exhalation rate in various building materials and soil samples. *Journal of Earth System Science*, Volume 126 Issue 2).

Bashir M, Ibeanu I G E, Zakari Y I and Sadiq U,(2013) Assessment of Radiological Risk in Flooded Soil Samples of Kudenda, Kaduna State Nigeria. *International Journal of Engineering Science Invention* ISSN (Online): 2319 – 6734, ISSN (Print): 2319 – 6726 www.ijesi.org Volume 2 Issue 10, pages 69-74

Becegato, V.A., Ferreira, F.J.F. and Machado, W.C.P., 2008. Concentration of radioactive elements (U, Th and K) derived from phosphatic fertilizers in cultivated soils. *Brazilian Archives of Biology and Technology*, Volume 5 Issue16, pages 1255-1266.

Beir VI, Report of the Committee on the Biological effects of Ionizing Radiation (1999) Health Effects of Exposure to radon. Natl. Res. Council. Natl. Acad. Press, Washington, DC.

Bergman, L., Lee, J.,Sadi,B., Chen, J.:(2015) Radon exhalation from sub-slab aggregate used in home construction in Canada, *Radiation Protection Dosimetry*, Volume 164, Issue 4, Pages 606–611

Berlin M and Rudell B (1986). In *Handbook on the Toxicity of Metals*, 2nd edn (eds Friberg L, Nordberg G F & Vouk V B), pages 623-637. Elsevier Science Publications: New York

Bertrand, B.A., David, V., Becker, K., Stanley, J.G., Bennett, G.P., Ken, K., Henry, R., Edward, B., Silberstein, Edward, W., (1994) Radon update: facts concerning environmental radon levels, mitigation strategies, dosimetry effects and guides. *J. Nucl. Med.* Volume 35 Issue 2, pages 368–385

Birky, B. (2014). *Health Physics and Radiological Health*. Philadelphia: Wolters Kluwer.

Blatt, J.M. and Weisskopf, V.F., (2012). *Theoretical nuclear physics*. Springer Science & Business Media.

Bleise, A., Danesi, P.R. and Burkart, W., (2003). Properties, use and health effects of depleted uranium (DU): a general overview. *Journal of environmental radioactivity*, Volume 64 Issue 2, pages 93-112.

Boyes, W. (2003). *Instrumentation reference book*. Boston: Butterworth-Heinemann.

Borgoni, Riccardo, et al. "Hierarchical modeling of indoor radon concentration: how much do geology and building factors matter?" *Journal of environmental radioactivity* 138 (2014): 227-237.

Bossey, P. (2003) The radon emanation power of building materials, soils and rocks. *Applied Radiation and Isotopes*, Volume 59, pages 389 – 392.

Boyes, W. (2003). *Instrumentation reference book*. Boston: Butterworth-Heinemann.

Brodhead, B. (2008). *Measuring Radon and Thoron emanation from concrete and granite with continuous Radon monitors and EPERMS*.

Burfield, D.R. and Smithers, R.H., 1978. Desiccant efficiency in solvent drying. Issue 20, pages 3966-3968.

Bushberg, J.T. and Boone, J.M., 2011. The essential physics of medical imaging. Lippincott Williams & Wilkins.

Cancio, D., Gutierrez, J., Ruiz, C. and Sainz, A., (1994). Radiological considerations related with the restoration of a phosphogypsum disposal site in Spain. In Remediation and Restoration of Radioactively Contaminated Sites in Europe (Proc. Int. Symp. Antwerp, 1993), Rep. XI-5027/94, European Commission, Brussels.

Carroll, William Larkin, and Jonathan L Finlay. Cancer in Children and Adolescents. 1st ed. Sudbury, MA: Jones and Bartlett Publishers, 2010. Print.

Carvalho, F.P., 1995. ^{210}Po and ^{210}Pb intake by the Portuguese population: the contribution of seafood in the dietary intake of ^{210}Po and ^{210}Pb . Health Physics, Volume 69 Issue 4, pages 469-480

Carvalho, F.P. and Oliveira, J.M., 2006. Polonium in cigarette smoke and radiation exposure of lungs. Czechoslovak Journal of Physics, Volume 56, pages 697-703.

Chang B.U., Koh S.M., Kim Y.J., Seo J.S., Yoon Y.Y., Row J.W., Lee D.M. (2008) Nationwide survey on the natural radionuclides in industrial raw minerals in South Korea. Journal of Environmental Radioactivity Volume 99, pages 455-460

Chauhan RP and Chakarvarti SK (2002) radon Exhalation rates from soils and stones as building materials. Indian Journal of Pure & Applied Physics, Volume 39 pages 491-495.

Chen, CJ, Weng PS, Chu TH. (1993) Radon exhalation rate from various building materials. Health Phys Volume 64 pages 613– 619;

Chen, J., et al., (2010) Radon exhalation from building materials for decorative use, J. Environ. Radioact., doi : 10.1016/j.jenvrad.2010.01.005

Cho, G., Kim, J.H., Park, T.S. and Cho, K., (2017). Proposing a Simple Radiation Scale for the Public: Radiation Index. Nuclear Engineering and Technology, Volume 49 Issue 3, pages 598-608.

Choi, H. and Mazzone, P., (2014). Radon and lung cancer: assessing and mitigating the risk. Cleveland Clinic journal of medicine, Volume 81 Issue 9, pages 567-575.

Cinelli, G., Tondeur, F., Dehandschutter, B., Bossew, P., Tollefsen, T. and De Cort, M., (2017). Mapping uranium concentration in soil: Belgian experience towards a European map. Journal of environmental radioactivity, Volume 166, pages 220-234.

Cogliano, V.J., Baan, R., Straif, K., Grosse, Y., Lauby-Secretan, B., El Ghissassi, F., Bouvard, V., Benbrahim-Tallaa, L., Guha, N., Freeman, C. and Galichet, L.,(2011). Preventable exposures associated with human cancers. Journal of the National Cancer Institute, Volume 103 Issue 24, pages 1827-1839

Cole, D.I. (2009). A Review of uranium Deposits in the Karoo Supergroup of South Africa. (#80047)

Cole DI. (2013) The metallogeny of the Calvinia area. Explanation and metallogenic map of sheet 3118 (scale 1: 250 000). Pretoria: Council for Geoscience; pages 77.

Cole DI, Ngofoe and Halenyane K. (2013) Mineral commodities in the Western Cape province, South Africa. Report number 2013-0165. Pretoria: Council for geosciences,

Cole, D.I., and Viljoen J. H. A. (2001) "Building sand potential of the Greater Cape Town area." Bulletin of the Council for Geoscience.

Conde, M. and Kallis, G. (2012). The global uranium rush and its Africa frontier. Effects, reactions and social movements in Namibia. *Global Environmental Change*, Volume 22 Issue 3, pages 596-610.

Cothorn, C. and Smith, J. (1987). *Environmental radon*. New York: Plenum Press.

CSIR Environmental Management Services, (2012). Desktop Palaeontological Assessment of a proposed Solar Photovoltaic Facility near Glen, Bloemfontein, FS Province. Bloemfontein.

de González, A.B., Mahesh, M., Kim, K.P., Bhargavan, M., Lewis, R., Mettler, F. and Land, C., 2009. Projected cancer risks from computed tomographic scans performed in the United States in 2007. *Archives of internal medicine*, Volume 169 Issue 22, pages 2071-2077.

de Meijer, R.J., Lindsay, R., Maleka, P., Newman, R.T. (2001) Proposal to assess the integral radon production of gold-mine dumps. Internal report, iThemba LABS.

Deka PC, Bhattachargee BK, Sharma BK, Goswami TD (2001) Measurement of Indoor radon Progeny Levels in Some Dwellings of North Kamrup in Brahmaputra Valley Regions of Assam. *Indian J Environmental Protection*, Volume 21 pages 24-28

Dlamini, T.C., (2014). Radionuclides and toxic elements transfer from the Princess Dump to the surrounding vegetation in Roodepoort South Africa: Potential radiological and toxicological impact on humans (Doctoral dissertation).

Durrani, S. and Ilić, R. (1997). *Radon measurements by etched track detectors*. Singapore: World Scientific.

Durrige Company Inc, (2000) . Reference Manual Version 6.0.1, RAD7™ Electronic Radon Detector.

Ebaid, Y.Y. (2010) Use of gamma-ray spectrometry for uranium isotopic analysis in environmental samples. *Romanian Journal*, 55, 69-74.

Ebbs, S. D.; Kochian, L. V., (1998) . Phytoextraction of zinc by oat (*Avena sativa*), barley (*Hordeum vulgare*), and Indian mustard (*Brassica juncea*). *Environ. Sci. Technol.*, Volume 32 Issue 6: pages 802–806

Eff-Darwich A, Viñas R., Soler V., de la Nuez J., Quesada M.L. (2008) Natural air ventilation in underground galleries as a tool to increase radon sampling volumes for geological monitoring. *Radiation Measurements* Volume 43 pages 1429–1436

El-Bahi SM (2004) Assessment of radioactivity and radon exhalation rate in Egyptian cement. *Health Physics*, Volume 86 pages 517-522.

Elzain, A. (2014). Radon exhalation rates from some building materials used in Sudan. *Indoor and Built Environment. IOSR Journal of Environmental Science, Toxicology and Food Technology (IOSR-JESTFT)* e-ISSN: 2319-2402, p- ISSN: 2319-2399 Volume 9, Issue 3 Ver. III (Mar. 2015), pages 62-67

Equity, A. (2014). College physics textbook equity edition volume 3 of 3. [Place of publication not identified]: Lulu Com.

Faheema M., Mujahid (2008) S.A. Assessment of radiological hazards due to the natural radioactivity in soil and Building material samples collected from six districts of the Punjab province-Pakistan. *Radiation Measurements* Volume 43 pages 1443–1447.

Feblau, P. E. (1994) "Perimeter Radiation "Monitors." Passive Nondestructive Assay of Nuclear Materials. Volume 41 Issue 4 pages 922 – 926

Fermi, E., Amaldi, E., D'Agostino, O., Rasetti, F. and Segrè, E., (1934). Artificial radioactivity produced by neutron bombardment. *Proceedings of the Royal Society of London. Series A, Containing Papers of a Mathematical and Physical Character*, Volume 146 Issue 857, pages 483-500.

Field R.W. (1999) Radon Occurrence and Health Risk (Adapted from Field RW, *Occupational Medicine Secrets*, Hanley and Belfus, Philadelphia,.

Finch, W. (1996). Uranium provinces of North America. Washington: US Gov. Print. Off.

Foster, D., Goscombe, B. and Gray, D. (2009). Rapid exhumation of deep crust in an obliquely convergent orogen: The Kaoko Belt of the Damara Orogen. *Tectonics*, Volume 28 Issue 4.

Fourie, C.J.S., Henry, G. and Maré, L.P., (2009), September. The structure of the Karoo-age Ellisras Basin in Limpopo Province, South Africa in the light of new airborne geophysical data: a preliminary report. In 11th SAGA Biennial Technical Meeting and Exhibition.

Frimmel, H.E., Schedel, S. and Brätz, H., (2014). Uraninite chemistry as forensic tool for provenance analysis. *Applied Geochemistry*, Volume 48, pages 104-121.

Fuchs, S., Williams-Jones, A.E. and Przybyłowicz, W.J., (2016). The origin of the gold and uranium bearing sandstones of the Black Reef Formation, Transvaal Supergroup, South Africa. *ore, Geology Reviews*, Volume 72, pages 149-164.

Fuller, C.C., Bargar, J.R., Davis, J.A. and Piana, M.J., (2002). Mechanisms of uranium interactions with hydroxyapatite: Implications for groundwater remediation. *Environmental Science & Technology*, Volume 36 Issue 2, pages 158-165.

Fry, C., and M. Thoennessen. (2013) "Discovery of Actinium, Thorium, Protactinium, and uranium Isotopes". *Atomic Data and Nuclear Data Tables* Volume 99 Issue 3 pages 345-364.

- Fwa, T. F. ,(2006)The Handbook of Highway Engineering. 1st ed. Boca Raton: Taylor & Francis
- Gablin G. (2004) Grain size in radiometric measurements of ground. In the proceedings of NORM IV conference Szczyrk, Poland. pages 101-102.
- Gadd, M.S., Borak, T.B. (1995) In-situ determination of the diffusion coefficient of ^{222}Rn in concrete. Health Physics, Volume 68, Issue 6, pages 817 – 822.
- Gaisser, T.K. and Stanev, T., (2000). Cosmic rays. The European Physical Journal C-Particles and Fields, Volume 15 Issue 1, pages 150-156.
- Ganguly, J. (2008). Thermodynamics in earth and planetary sciences. Berlin: Springer.
- Geddes, I. and Campbell, C. (2015). Higher Geography for CfE., Hodder and Gibson 2014.
- Geological Survey of Namibia (2006). Namibian Dimension Stone. Windhoek, Namibia.
- Gray, D., Foster, D., Meert, J., Goscombe, B., Armstrong, R., Trouw, R. and Passchier, C. (2008). A Damara orogen perspective on the assembly of South Western Gondwana. Geological Society, London, Special Publications, Volume 294, Issue 1, pages 257-278
- Gresse, P.G. & Theron, J.N. (1992). The geology of the Worcester area. Explanation of Geological Sheet Volume 3319, pages 79, tables. Council for Geoscience, Pretoria
- Guimond, R.J. (1988). "Reducing radon risk: The approach in the United States". Radiation Protection Dosimetry. Volume 24, Issue ¼, pages 483-485.
- Haddon, I.G. and McCarthy, T.S., (2005). The Mesozoic–Cenozoic interior sag basins of Central Africa: The Late-Cretaceous–Cenozoic Kalahari and Okavango basins. Journal of African Earth Sciences, Volume 43, Issue 1, pages 316-333.
- Hamed, A.M.H., (2016). Evaluation of Radioactivity and other Related Elements in Some Areas of South Kordofan State (Doctoral dissertation, Sudan University of Science and Technology).
- Hansen, M.V. (1981) World uranium resources. Int.At.Energy Agency Bull.Volume 3, Issue 2 pages 3-10,.
- Hassan N , Hosoda M, Ishikawa T, Tokonami S, Fukushi M, Hafez A and Khalil E." (2009), ^{222}Rn Exhalation Rate from Egyptian Building Materials Using Active and Passive Methods", Jpn. J. Health Phys., Volume 44, Issue 1, pages106 - 111
- Hawkesworth, C., Menzies, M. and van Calsteren, P. (1986). Geochemical and tectonic evolution of the Damara Belt, Namibia. Geological Society, London, Special Publications, Volume 19, Issue 1, pages305-319.
- Heckroodt, R. O. (1991) "Clay and clay materials in South Africa." J. South. Afr. Inst. Min. Metall Volume 91, pages 343-363.
- Heinrjch, E., (1970). The palabora carbonatitic omptex-a unique copper deposit.

Heritage Western Cape (2015). Built environment assesment: Proposed uranium mining and associated infrastructure on portions of the farms Quaggasfontein and Ryst Kuil. Beaufort-West: Peninsula Energy Ltd., pages 1-30.

Hill, R.S., Theron, J.N., Cole, D.I., Roberts, D.L. and Mulholland, B.J., (1992). The geology and mineral resources of the Greater Cape Town region. Report, Geological Survey of South Africa, 28p.

Hore-Lacy, I. (2016). Uranium for nuclear power.

Horn GFJ, Strydom JH. Clay In: Wilson MGC, Angaeusser CR, (1998) editors. The mineral resources of South Africa: Handbook. Pretoria: Council for Geoscience; pages 106 - 135

Hosny, T., Al-Anezi, E. and Khalil, M.M., (2017). Basic Radiation Physics. In Basic Science of PET Imaging pages 3-35 Springer International Publishing.

Hossain, I. (2012). Efficiency and resolution of HPGe and NaI(Tl) detectors using gamma-ray spectroscopy. Scientific Research and Essays, Volume 7, Issue 1.

Hůlka, Jiří, Jaroslav Vlček, and Jiří Thomas. (2008) "Natural radioactivity in building materials – Czech experience and European legislation." International Symposium Las Vegas.

Hunter, G.K., (1987). An ion-exchange mechanism of cartilage calcification. Connective tissue research, Volume 16, Issue 2, pages 111-120.

Hunter-Smith, L., (2012). Levels of Naturally Occurring Radioactive Material in Bottled Natural Mineral Water (Doctoral dissertation, University of Surrey Guildford).

Jahn, B.M. and Condie, K.C., (1995). Evolution of the Kaapvaal Craton as viewed from geochemical and Sm_Nd isotopic analyses of intracratonic pelites. Geochimica et Cosmochimica Acta, Volume 59, Issue 11, pages 2239-2258.

Jakhu, R., Mehra, R. and Mittal, H. (2016). Exposure assessment of natural uranium from drinking water. Environ. Sci.: Processes Impacts, Volume 18, Issue 12, pages 1540-1549.

Jashank, Mily, Jayalakshmi M. Nair, and Rajendra S. Khairnar. (2016) "Analysis of radon Gas Variation As A Precursor Of Earthquake Prediction Using RAD7". International Journal of Advanced Research Volume 4, Issue 7, pages 518-524. Print.

Jeffrey, L.S., (2005). Characterization of the coal resources of South Africa. Journal of the Southern African Institute of Mining and Metallurgy, Volume 105, Issue 2, pages 95-102.

Jojo PJ, Rawat A, Prasad R (1994) Enhancement of trace uranium in fly ash. Nucl Geo Phys, Volume 8, pages 55-61.

Jones, E. and Childers, R. (1990). Contemporary college physics. Reading, Mass.: Addison-Wesley Pub. Co.

Kamiya, K., Shimizu, K., Igarashi, A. and Kobashi, H., 2015. Visual and refractive outcomes of small incision lenticule extraction for the correction of myopia: 1-year follow-up. *BMJ open*, Volume 5, Issue 11, p.e008268.

Kant K, Rashmi, Sonkawade RG, Sharma GS, Chauhan RP, Chakarvarti SK (2009) Seasonal variation of radon, thoron and their progeny levels in dwellings of Haryana and Western Uttar Pradesh. *Iran J Radiat Res*, Volume 7, pages 79 - 84.

Kant K, Upadhyay S.B., Sonkawade R.G., Chakarvarti S.K., (2006) Radiological risk assessment of use of phosphate fertilizers in soil Iran. *J. Radiat. Res.*, Volume 4, Issue 2, pages 63-70

Kappke, J., Paschuk, S., Rocha, Z., Corrêa, J., Denyak, V., Santos, T. and Reque, M. (2011). Radium activity measurements in bottled mineral water. *ASSOCIAÇÃO BRASILEIRA DE ENERGIA NUCLEAR - ABEN*.

Karam, P.A. and Leslie, S.A., (1999). Calculations of background beta-gamma radiation dose through geologic time. *Health physics*, Volume 77, Issue 6, pages 662-667.

Khan AJ, Tyagi RK, Prasad R., (1992). Measurement of radon exhalation rates from some building materials. *Nucl Tracks Radiat Meas*, Volume 20, pages 609-610.

Kitto M, Green J. (2005) "radon emanation from granite countertops. In: *Proceedings of an International Symposium.*" San Diego, CA: Am Assoc radon Sci Technol;.

Knoll G.F. (2000), *Radiation Detection and Measurement*, 3rd ed. John Wiley & Sons, New York, pages 48-52.

Kok, Kenneth D. (2016). *Nuclear Engineering Handbook*, Second Edition. 1st ed. Milton: CRC Press. Print.

Kotrappa P., (1999) Review of Electret ion chamber technology for measuring technologically enhanced natural radioactivity.

Kotrappa, P., Dempsey, J.C. and Steiff, L.R., (1993). Recent advances in electret ion chamber technology for radiation measurements. *Radiation Protection Dosimetry*, Volume 47, Issues 1-4, pages 461-464.

Kotrappa, P. and Jesters, W.A., (1993). Electret ion chamber radon monitors measure dissolved ^{222}Rn in water. *Health physics*, Volume 64, Issue 4, pages 397-405.

Kotrappa, P. and Frederick S. (2009) "Radon exhalation rates from building materials using electret ion chamber radon monitors in accumulators." *Health physics* Volume 97, Issue 2, pages 163-166.

Kovler, K., Haquin, G., Manasherov, V., Ne'eman, E. and Lavi, N. (2002). Natural radionuclides in building materials available in Israel. *Building and Environment*, Volume 37, Issue 5, pages 531-537.

Kreuzer M, McLaughlin J. Radon. (2010), In: *WHO Guidelines for Indoor Air Quality: Selected Pollutants*. Geneva: World Health Organization;

Kruger, S.J., (1981), A mineralogical investigation of the ash fraction of coal from the Springbok Flats Coalfield (in Afrikaans), M.Sc. thesis, Rand Afrikaans University (now Johannesburg University), Johannesburg, 166 p.

Lang, K. (2006). Parting the cosmic veil. New York: Springer.

Lauria D.C., Ribeiro F.C.A., Conti C.C., Loureiro F.A., (2009) Radium and uranium levels in vegetables grown using different farming management systems. Journal of Environmental Radioactivity Volume 100, pages 176–183.

Lilley J.S. (2001), Nuclear Physics, Principles and Applications, John Wiley & Sons, New York. pages 13-15.

Lindsay R, Newman RT, and Speelman WJ. (2008) "A study of airborne radon levels in Paarl houses (South Africa) and associated source terms, using electret ion chambers and gamma-ray spectrometry." Applied Radiation and Isotopes Volume 66, Issue 11, pages 1611-1614.

Liptak, B. and Venczel, K. (2016). Instrument and automation engineers' handbook. 5th ed. CRC Press.

Llope, W. (2011). Activity concentrations and dose rates from decorative granite countertops. Journal of Environmental Radioactivity, Volume 102, Issue 6, pages 620-629.

Loubser, T., (2007). Uranium 2007: Resources, Production and Demand (The Red Book). A Joint Report by the OECD Nuclear Energy Agency, South Africa and the International Atomic Energy Agency (IAEA). OECD Publishing, 422 pp.

Loureiro C.O., and Abriola L.M., Martin J.E., Sextro R.G. (1990) Three-Dimensional Simulation of radon Transport into Houses with Basements under Constant Negative Pressure. Environ. Sci. Technol., Volume 24, pages 1338-1348.

Lubin, J., Boice, J., Edling, C., Hornung, R., Howe, G., Kunz, E., Kusiak, R., Morrison, H., Radford, E., Samet, J., Tirmarche, M., Woodward, A. and Yao, S. (1995). Radon-Exposed Underground Miners and Inverse Dose-Rate (protraction Enhancement) Effects. Health Physics, Volume 69, Issue 4, pages 494-500

Lust, Merle, and Enn Realo. (2012) "Assessment of natural radiation exposure from building materials in Estonia." Proceedings of the Estonian Academy of Sciences Volume 61, Issue 2, pages 107-112.

Lyle, S., (2007). Kansas Geological Survey. ^{222}Rn , pages 3-825.

Maibane, K.F.(2017). "Validation of Gamma Ray Spectrometry Process Used To Determine the Radionuclides and Radioactivity Levels in Decorative Granite Countertops". Masters Thesis. University of the Western Cape.

MALAKHOV, S. G. et al. (1966) "Diurnal Variations Of radon And Thoron Decay Product Concentrations in the Surface Layer of the Atmosphere and Their Washout by Precipitations". Tellus Volume 18, Issue 2-3, pages 643-654.

Maleka, P.P and Newman, R.T. (2012) Report on radiometric analyses of iThemba LABS liquid standard sources.

Markkanen, M. and Arvela, H. (1992) radon emanation from soils. Radiation Protection Dosimetry, Volume 45, Issue 1, pages 269 – 272

Marques A.L. and Dos Santos W., Geraldo L.P. (2004) Direct measurements of radon activity in water from various natural sources using nuclear track detectors. Applied Radiation and Isotopes Volume 60, pages 801–804.

Martini JEJ. Limestone and dolomite resources of the Republics of South Africa, Bophuthathatswana, Ciskei, Transkei and Venda. Geological Survey 9. Pretoria : Department of Energy and Mineral Affairs; 1987.

Martini JEJ and Wilson MGC. Limestone and dolomite, in Wilson MGC, Anhaeusser CR, editors. The mineral resources of South Africa: Handbook. Pretoria: Council for geosciences; 1998. p 433 – 440

Masia, S. (2010). Assessment of radiological dose to the inhabitants from radon emanation in houses at Beaufort-West District. MSc. Northwest University.

Masterson, R. (2017). Nuclear engineering fundamentals. CRC Press, 2016.

Myatt, T.A., Allen, J.G., Minegishi, T., Mccarthy, W.B., Stewart, J.H., Macintosh, D.L. and Mccarthy, J.F., (2010). Assessing exposure to granite countertops--part 1: Radiation. Journal of Exposure Science and Environmental Epidemiology, Volume 20, Issue 3, page 273.

Mazur J, Kozak K, Horwacik T, Haber R, Zdziarski T(2004) Influence of meteorological conditions on radon measurements in soil-Preliminary results. In the proceedings of NORM IV conference Szczyrk, Poland, page 77-78.

Mechenich, C. and Shaw, B.H., (1996). Do deeper wells mean better water?. University of Wisconsin--Extension, Cooperative Extension.

Minerals Bureau, (1987). Construction materials in the Western Cape. Memorandum, Minerals Bureau, 10/87, Page 16.

Mining Directorate, Ministry of Mines and Energy (1995). THE uranium resources and production of namibia. Windhoek, Namibia, pages 49-60.

Mohamed A., Ahmed A.A., Ali A.E., Yuness M. , (2008) Attached and Unattached Activity Size Distribution of Short-Lived radon Progeny ^{214}Pb and Evaluation of Deposition Fraction. Journal of Nuclear and Radiation Physics, Volume 3, Issue 2, pages 101-108

Moss MA (1985) Chronic low level uranium exposure via drinking water — clinical investigations in Nova Scotia. Halifax, Nova Scotia, Dalhousie University (M.Sc. thesis).

Motsoenyane, W.M., (2010). Operating mines and quarries and mineral processing plants in the Republic of South Africa, 2010. Directory, Department of Mineral Resources, D1/2010, page 155.

Motta Cabrera S.C., Bryan J., Komishke B. and Kantzas A., (2007) Study of the Settling Characteristics of Tailings Using Nuclear Magnetic Resonance (NMR) Technique

Nain M, Chauhan RP, Chakarvarti SK (2006). Alpha radioactivity in Indian cement samples. Iran J. Radiat Res, Volume 3, Issue 1, pages 71-176.

Nazaroff W.W., Doyle S.M., Nero A.V. and Sextro R.G. (1987), Potable Water as a Source of Airborne ^{222}Rn in U.S. Dwellings: A Review and Assessment. Health Physics Volume 52, Issue.3 (March), pages 281-295,

NCRP (1984). National Council on Radiation Protection and Measurements. Control of Air Emissions of Radionuclides, NCRP Statement No. 6 (National Council on Radiation Protection and Measurements, Bethesda, Maryland).

Ngcofe, L. and Cole, D.I., (2014). The distribution of the economic mineral resource potential in the Western Cape Province. South African Journal of Science, Volume 110, Issue 1-2, pages 1-4.

Nel, L. (2012). The geology of the Springbok Flats. PhD thesis, Department of Geology, University of the Free State.

Nelson, G. and Reilly, D., (1991). Gamma-ray interactions with matter. Passive Nondestructive Analysis of Nuclear Materials, Los Alamos National Laboratory, NUREG/CR-5550, LAUR-90-732, pages 27-42.

Nero, A.V. (1988) radon and its decay products in indoor air: An overview. Editors W. Nazaroff and A. Nero, John Wiley and Sons, Inc., pages 1 – 53

Nero, A.V. and Nazaroff, W.W. (1984). Characterizing the source of radon indoors. Radiation Protection Dosimetry, Volume 7, Issue 1-4, pages 23 – 39.

Newman R.T., Lindsay R., Maphoto, K.P., Mlwiilo, N.A., Mohanty, A.K., Roux D.G. et al. (2008). Determination of soil, sand and ore primordial radionuclide concentrations by full-spectrum analyses of high-purity germanium detector spectra. Applied Radiation and Isotopes. UNIVERSITY of the

Nielson, K.K., Rogers, V.C., Holl, R.B. (1996) Contributions of building materials to indoor radon levels in Florida buildings, USEPA Research and Development project summary, EPA/600/SR-96/107.

O'donoghue, J.A., Bardies, M. and Wheldon, T.E., (1995). Relationships between tumor size and curability for uniformly targeted therapy with beta-emitting radionuclides. Journal of Nuclear Medicine, Volume 36, Issue 10, pages 1902-1909.

OECD (2014). Uranium 2014: Resources, Production and Demand.

Pacheco-Torgal, F. (2012). Indoor radon: An overview on a perennial problem. Building and Environment, Volume 58, pages 270-277.

Papastefanou C. Radioactivity of Tobacco Leaves and Radiation Dose Induced from Smoking. Int. J. Environ. Res. Public Health 2009, Volume 6, Issue 2, pages 558-567.

Pertlik, F; Rodgers, J.J.W.; Haack, U.K. and J.A.S. Adams. (1978). Uranium. In Wedepohl (Ed), 1978, Handbook of Geochemistry, Volume 2, Issue 4.

Peterson, S., (2015). 1. Interaction of Radiation with Matter.

Podgorsak, E.B., (2005). Treatment machines for external beam radiotherapy. Radiation Oncology Physics: A Handbook for Teachers and Students. IAEA, Vienna, Austria, pages 123-160.

Povh, B., Rith, K. and Zetsche, F., (1995) Particles and nuclei (Vol. 1). Berlin: Springer.

Prueitt R.L., Goodman J.E., Valberg P.A., (2009), Radionuclides in cigarettes may lead to carcinogenesis via p16INK4a inactivation. Journal of Environmental Radioactivity, Volume 100, Issue 157–161.

Rajasekaran, G., (2016). The Story of the Neutrino. arXiv preprint arXiv:1606.08715.

Ravikumar P, Davis D, Somashekar RK and Prakash KL., (2015) Measurement of radon activity in soil gas using RAD7 in the Environs of Chitradurga District, Karnataka, India Elixir Earth Sci. Volume 80, pages 31078-31082

Righi, S. and Bruzzi, L., (2006), Natural radioactivity and radon exhalation in building materials used in Italian dwellings. Journal of Environmental Radioactivity, Volume 88, Issue 2, pages 158-170.

Roberts DL, Botha GA, Maud RR, Pether J., (1998), Coastal Cenozoic deposits. In: Johnson MR, Anhaeusser CR, Thomas RJ, editors. The geology of South Africa : Handbook. Pretoria: Council for Geoscience; pages 433-440

Roesener H and Schreuder CP., (1992). Uranium, 7.1-1-7.1-55. In: Geological Survey of Namibia. (1992). The Mineral Resources of Namibia. 1.1-1-9-17pp.

Rosner, T., (2007). The environmental impact of seepage from gold mine tailings dams near Johannesburg, South Africa (Doctoral dissertation, University of Pretoria).

Rossouw, M. (2016). Environmental screening study of for a proposed LNG terminal and saldanha and associate pipeline infrastructures to Atlantis and Cape Town. [online] CSIR p240 https://www.westerncape.gov.za/assets/departments/economic-development-tourism/Ing_ess_chapter_78_conclusions.pdf [Accessed 10 Apr. 2016].

Roux PL., (1998), Aggregates. In: Wilson MGC, Anhaeusser CR, editors. The mineral resources of South Africa Handbook. Pretoria: Council for Geosciences; pages 40 – 45.

Saad, A.F., Abdallah, R.M. and Hussein, N.A., (2013). Radon exhalation from Libyan soil samples measured with the SSNTD technique. Applied Radiation and Isotopes, Volume 72, pages 163-168.

Samuelsson, C., Petterson, H. (1984) Exhalation of ^{222}Rn from porous materials. Radiation Protection Dosimetry, Volume 7, Issue 1 – 4, pages 95 – 100

Savidou A., Kehagia K., Eleftheriadis K. Concentration levels of ^{210}Pb and ^{210}Po in dry tobacco leaves in Greece. Journal of Environmental Radioactivity 85 (2006) 94-102.

Scholtz, N, Scholtz, OF and Potgieter, GP (2006), Potential environmental impact from inadequate remediation of uranium mining in the Karoo Uranium Province, South Africa, in Uranium in the Environment: Mining impact and consequences, Ed by Merkel BJ and Hasche-Berger A. Springer Science and Business Media 2006.

- Schubert M., Schmidt A., Paschke A., Lopez A., Balcázar M. (2008) In situ determination of radon in surface water bodies by means of hydrophobic membrane tubing. *Radiation Measurements*, Volume 43, pages 111–120
- Shahbazi-Gahrouei, D., Gholami, M. and Setayandeh, S., (2013) . A review on natural background radiation. *Advanced biomedical research*, Volume 2, Issue 1, page 65.
- Singh BP , Pandit B, Bhardwaj VN, Singh P, Kumar R (2010) Study of radium and radon exhalation rate in some solid samples using solid state nuclear track detectors.
- Singh J., Singh H., Singh S., Bajwa B.S. (2008) Estimation of uranium and radon concentration in some drinking water samples. *Radiation Measurements*, Volume 43 ,pages S523–S526.
- Smethurst, M.A., Strand, T., Sundal, A.V. and Rudjord, A.L., (2008). Large-scale radon hazard evaluation in the Oslofjord region of Norway utilizing indoor radon concentrations, airborne gamma ray spectrometry and geological mapping. *Science of the total environment*, Volume 407, Issue 1, pages 379-393.
- South African Bureau of Standards, (1994). Standard specification for aggregates from natural sources - aggregates for concrete. Report, Council of the South African Bureau of Standards, pages 1083-1994.
- Sroor, Amany T. et al. (2013), "Radiological Hazards for Marble and Granite Used At Shak El Thouban Industrial Zone in Egypt". *Journal of Environmental Protection*, Volume 04, Issue 12, pages 41-48.
- Stieglitz T. (2005) Submarine groundwater discharge into the near-shore zone of the Great Barrier Reef, Australia, *Marine Pollution Bulletin* 51, pages 51–59
- Surbeck H. Dissolved gases as natural tracers in karst hydrogeology; radon and beyond. Center of Hydrogeology (CHYN), University of Neuchâtel, Emile-Argand 11, CH-2007 Neuchâtel, Switzerland.
- Talavera, L., (2000). Dependency-based feature selection for clustering symbolic data. *Intelligent Data Analysis*, Volume 4, Issue 1, pages 19-28.
- Talha,S.A., Lindsay R., Newman, R.T., de Meijer, R.J., Maleka, P., Hlatshwayo, I.N. et al. (2008) Gamma-ray spectrometry of radon in water and the role of radon to representatively sample aquifers.(*Proceedings of IAEA International Conference on Enviromental Radioactivity , 23-27 April 2007 , Vienn, Austria*).
- Těšínská, E. (2009) "Epidemiological studies of lung carcinoma incidence in uranium miners (accumulation and retrospective use of diagnostic data)." *Prague medical report*, Volume 110, Issue 2, pages 165-172.
- Theron, J.N.,(1984). The geology of Cape Town and environs: Explanation and Geological Maps of Sheets 3318CD and DC, and 3418AB, AD and BA (1:50 000). Geological Survey of South Africa, pages 77
- Ting, D.S.K.,(2010) . WHO handbook on indoor radon: a public health perspective.
- Toth, F. (2011). *Geological Disposal of Carbon Dioxide and Radioactive Waste: A Comparative Assessment*. Dordrecht: Springer Netherlands.

United Nations., (2009) Scientific Committee on the Effects of Atomic Radiation. Effects of ionizing radiation: UNSCEAR 2006 Report to the General Assembly, with scientific annexes. Vol. 2. United Nations Publications.

UNSCEAR,(1982). Ionising Radiation Sources and Biological Effects. United Nations Scientific Committee on the Effects of Atomic Radiation. A/37/45, New York.

Urosevic V., Nikezic D., Vulovic S., (2008), A theoretical approach to indoor radon and thoron distribution. Journal of Environmental Radioactivity, Volumw 99, pages 1829–1833.

Uys, J. (2007). Lithostratigraphy, depositinal environments and sedimentology of the Permian Vryheid formation (Karoo Supergroup), Arnot North, Witbank coalfield, South Africa. MSc. University of Johannesburg.

Vakil M.D., C.C.F.P., F.C.F.P., Dr. Cathy and Dr. Linda Harvey B.Sc., M.Sc., M.D. "Human Health Implications of the Nuclear Energy Industry". Physicians for the Environment. N.P., 2009. 21 Nov. 2016.

Van Strijp, L.T.,(1998) . Brickmaking materials in The Mineral Resources of South Africa (M.G.C. Wilson and C.R. Anhaeusser, editors). Handbook, Council for Geoscience, Volume 16, pages 85-89.

Vinson D.S., Campbell T.R., Vengosh A., (2008), radon transfer from groundwater used in showers to indoor air. Applied Geochemistry, Volume 23, pages 2676–2685.

Vogiannis, E.G. and Nikolopoulos, D., (2014). Radon sources and associated risk in terms of exposure and dose. Frontiers in public health, 2.

Wagner, T. (1994). In our backyard. [Place of publication not identified]: John Wiley & Sons.

WANG, Nanping et al., (2005), "Determination Of Radioactivity Level Of ^{238}U , ^{232}Th And ^{40}K In Surface Medium In Zhuhai City By In-Situ Gamma-Ray Spectrometry". Journal of Nuclear Science and Technology, Volume 42, Issue10, pages 888-896.

Waska H., Kim S., Kim G, Peterson R.N., Burnett W.C., (2008) An efficient and simple method for measuring ^{226}Ra using the scintillation cell in a delayed coincidence counting system (RaDeCC). Journal of Environmental Radioactivity, Volume 99, pages 1859–1862.

Weinstein, N.D. and Sandman, P.M., (1992). A model of the precaution adoption process: evidence from home radon testing. Health psychology, Volume 113, page 170

Whicker, F.W. and Schultz, V., (1982). Radioecology: nuclear energy and the environment, Volume 1, pages 75-150, Boca Raton, FL: CRC press.

Wilson, Janice, et al. (2014) "Synergistic cytotoxicity and DNA strand breaks in cells and plasmid DNA exposed to uranyl acetate and ultraviolet radiation." Journal of Applied Toxicology.

Wronkiewicz, D.J.,(1989). Geochemistry and provenance of sediments from the Pongola Supergroup, South Africa: evidence for a 3.0-Ga-old continental craton. Geochimica et Cosmochimica Acta, Volume 53, Issue 7, pages 1537-1549.

Yngveson A., Williams C., Hjerpe A., Lundeberg J., Söderkvist P. and Pershagen G., (1999), page 53, Mutations in Lung Cancer Associated with Residential radon Exposure. *Cancer Epidemiol Biomarkers Prev.* Volume 8, page 433–438.

Yu, K.N., V.S.Y Koo, and Z.J. Guan., (2001), "A Simple And Versatile $^{222}\text{Rn}/^{220}\text{Rn}$ Exposure Chamber". *Nuclear Instruments and Methods in Physics Research A* Volume 481, Issue 2002, pages 749-755. Print.

Zavodska, L., Kosorinova, E., Scerbakova, L. and Lesny, J.,(2008). *Environmental chemistry of uranium.* HV ISSN, pages 1418-7108.

Zhang L., Yang J., Guo Q., (2017) ; Study on a step-advanced filter monitor for continuous radon progeny measurement, *Radiation Protection Dosimetry*, Volume 173, Issue 1-3, 1, Pages 259–262,

Zhuo W., Guo Q., Chen B., Cheng G. Estimating the amount and distribution of radon flux density from the soil surface in China. *Journal of Environmental Radioactivity* 99 (2008) 1143-1148.

Websites:

http://isite.lps.org/sputnam/chem_notes/Unit1latoms/DecaySeriesU238.jpg

<http://largeigneousprovinces.org/sites/default/files/BushveldLIP.pdf>

<http://tlabs.ac.za/?s=hpge>

http://uotechnology.edu.iq/petrol_tech/scholistic%20plans/rocks4.pdf

<https://www.atsdr.cdc.gov/>

<http://www.biomation.com/radon/eperm.htm>

<http://www.chemicool.com/elements/radon.html> [Accessed 19 Apr. 2015].

http://www.daviddarling.info/images/binding_energy.jpg

<http://www.durridge.com>

<http://www.ems.psu.edu/~radovic/Chapter14.pdf>

<http://www.epa.gov/radon>. "Consumers Guide To radon Reduction". N.p., 2017. Web. 1 Apr. 2017.

<http://www.fse.org.za/Downloads/uranium%20MINING%20KAROO.pdf>

http://www.geology.cz/igcp594/training-courses/27-annex_g-namibian_abandoned_mines_inventory.xlsx

<http://www.graniteland.com/stone/santa-cecilia>

<https://www.ijg-research.net/wp-content/uploads/IJG-Economic-Outlook-2017-1.pdf>

http://www.infomine.com/library/publications/docs/DMESouthAfrica/DME_Annual_Report_0405.pdf

<http://www.karooinvest.co.za/2701/index.html>

<http://metadata.berkeley.edu/nuclear-forensics/images/U238.png>

a <https://www.mindat.org/loc-158050.html>

b <https://www.mindat.org/loc-271556.html>

<https://minerals.usgs.gov/minerals/pubs/mcs/2016/mcs2016.pdf>

a

<http://www.miningweekly.com/article/power-generation-still-driving-uranium-demand-but-environmental-health-concerns-persist-2016-01-29>

b

http://www.miningweekly.com/article/exploration-and-development-firm-gets-more-prospecting-rights-for-ryst-kuil-channel-2006-11-17/rep_id:3650

a, <https://www.mirion.com/introduction-to-radiation-safety/man-made-sources-of-radiation/>

b, <https://www.mirion.com/introduction-to-radiation-safety/types-of-ionizing-radiation/>

<http://www.namibiareearth.com/lofdal.asp>

<http://www.nationalradondefense.com/radon-information/what-is-radon.html>

<https://www.nuclear-power.net/nuclear-power/reactor-physics/atomic-nuclear-physics/nuclear-stability/>

<https://www.nrc.gov/reading-rm/basic-ref/students/for-educators/06.pdf>

<http://www.nrc.gov/reading-rm/basic-ref/teachers/06.pdf>

<http://www.nrc.gov/about-nrc/radiation.html>

<http://www.nrc.gov/about-nrc/radiation/around-us/sources/nat-bg-sources.html>

<https://www.physicsforums.com/threads/derivations-of-the-decay-constant-equation.213312/>

<http://www.remtekenvironmental.com/radon1.html>

<https://www.revolv.com/main/index.php?s=uranium%20in%20Africa>

<http://www.stonecontact.com/indian-dakota-granite>

<https://www.stoneply.com/en/stones/golden-beach>

<http://www.thevillager.com.na/articles/417/uranium-discovered-in-Kunene/>

<http://www.uraniumseek.com/news/uraniumSeek/1453752320.php>

<http://www.wise-uranium.org/upnattrk.html>

a:<http://www.world-nuclear.org/information-library/nuclear-fuel-cycle/mining-of-uranium/world-uranium-mining-production.aspx>

b:<http://www.world-nuclear.org/information-library/country-profiles/countries-g-n/namibia.aspx>

c:<http://www.world-nuclear.org/information-library/current-and-future-generation/nuclear-power-in-the-world-today.aspx>

d:<http://world-nuclear.org/information-library/nuclear-fuel-cycle/uranium-resources/uranium-markets.aspx>

e:<http://www.world-nuclear.org/nuclear-basics/how-is-uranium-ore-made-into-nuclear-fuel.aspx>



UNIVERSITY *of the*
WESTERN CAPE

APPENDICES

APPENDIX A: Measurements using the RAD7

Table 1 : RAD7 measurement of Radium Source (Figure 5.1)

Name of Product	Time	Time	RAD 7	Reading	Error	model
Radium source	1	18:58	2801	362	71,3	688
Date	2	19:58	2802	793	101	1025
18-Dec-14	3	20:58	2803	1180	123	1359
Mass	4	21:58	2804	1200	83,9	1690
200 grams	5	22:58	2805	1630	97,6	2019
Starting Time	6	23:58	2806	1890	105	2345
17:58	7	00:58	2807	2240	114	2669
	8	01:58	2808	2920	120	2991
	9	02:58	2809	3280	130	3310
	10	03:58	2810	3660	138	3626
	11	04:58	2811	3920	146	3941
	12	05:58	2812	3920	152	4252
	13	06:58	2813	4330	159	4562
	14	07:58	2814	4740	167	4869
	15	08:58	2815	4990	172	5174
	16	09:58	2816	5450	188	5477
	17	10:58	2817	5770	185	5777
	18	11:58	2818	5920	187	6075
	19	12:58	2819	6590	198	6371
	20	13:58	2820	6770	201	6664
	21	14:58	2821	7170	207	6956
	22	15:58	2822	7480	212	7245

Table 2 : RAD7 measurement of Background Radiation (Summer) (Figure 5.2)

Name of Product	Time	RAD 7	Hours	Reading	Error
Background Radiation	16:37	3401	1	65,1	33,4
Date	17:37	3402	2	45,4	29,1
12-Jan-15	18:37	3403	3	51,1	30,4
Mass	19:37	3404	4	43,2	18,2
n/a	20:37	3405	5	52,6	19,8
Starting Time	21:37	3406	6	55,3	20,8
15:37	22:37	3407	7	44,5	18,4
	23:37	3408	8	67,5	22
	00:37	3409	9	74,3	22,9

	01:37	3410	10	79,7	23,6
	02:37	3411	11	68,9	22,6
	03:37	3412	12	75,7	23,1
	04:37	3413	13	44,6	18,7
	05:37	3414	14	45,9	18,7
	06:37	3415	15	63,5	21,9
	07:37	3416	16	59,5	20,8
	08:37	3417	17	66,2	21,8
	09:37	3418	18	54	20
	10:37	3419	19	79,7	23,6
	11:37	3420	20	55,4	20,2
	12:37	3421	21	68,9	22,2
	13:37	3422	22	71,6	22,6
	14:37	3423	23	63,5	21,4
	15:37	3424	24	75,7	23,1
	16:37	3425	25	74,3	23,1
	17:37	3426	26	70,3	22,4
	18:37	3427	27	81,1	24
	19:37	3428	28	70,3	22,4
	20:37	3429	29	45,9	18,9
	21:37	3430	30	67,6	22
	22:37	3431	31	77	23,5
	23:37	3432	32	73	22,8
	00:37	3433	33	83,8	24,2
	01:37	3434	34	86,5	24,5
	02:37	3435	35	68,9	22,2
	03:37	3436	36	70,3	22,4
	04:37	3437	37	58,1	20,6
	05:37	3438	38	66,2	21,8
	06:37	3439	39	70,3	22,4
	07:37	3440	40	52,7	19,8
	08:37	3441	41	90,6	25
	09:37	3442	42	71,6	22,6
	10:37	3443	43	89,2	24,8
	11:37	3444	44	72,3	22,6
	12:37	3445	45	72,3	22,6
	13:37	3446	46	65,6	21,6
	14:37	3447	47	88,2	24,8
	15:37	3448	48	79	23,4
	16:37	3449	49	87,1	24,4
	17:37	3450	50	75	22,1
	18:37	3451	51	61,6	21
	19:37	3452	52	80,4	23,6

	20:37	3453	53	68,3	22,6
	21:37	3454	54	101	26,2
	22:37	3455	55	85,8	24,3
	23:37	3456	56	73,7	22,7
	00:37	3457	57	68,3	22,2
	01:37	3458	58	91,1	24,9
	02:37	3459	59	76,3	23,1
	03:37	3460	60	63,8	22,6
	04:37	3461	61	67	21,8
	05:37	3462	62	101	26,2
	06:37	3463	63	85,8	24,3
	07:37	3464	64	73,7	22,7
	08:37	3465	65	68,3	22,2
	09:37	3466	66	91,1	24,9
	10:37	3467	67	76,3	23,1
	11:37	3468	68	63,8	22
	12:37	3469	69	67	21,8
	13:37	3470	70	68,3	22,6
	14:37	3471	71	80,4	23,9
	15:37	3472	72	72,3	22,5
	16:37	3473	73	79	23,9
	17:37	3473	74	95,1	25,4
	18:37	3473	75	80,4	23,6
	19:37	3473	76	72,3	22,6
	20:37	3473	77	72,3	22,5
	21:37	3473	78	73,7	22,7

Table 3: RAD7 measurement of Background Radiation (Winter) (Figure 5.3)

Name of Product	Time	RAD 7	Time	Reading	Error
Background Radiation (winter)	21:43	1601	1	53,1	25,1
Date	22:43	1602	2	48,2	21,4
12-Jun-15	23:43	1603	3	42,5	23,4
Mass	00:43	1604	4	130	32,8
n/a	01:43	1605	5	56,6	22,1
Starting Time	02:43	1606	6	62	30,6
20:43	03:43	1607	7	47,9	25,4
	04:43	1608	8	76	27,5
	05:43	1609	9	70,4	30,6
	06:43	1610	10	67,6	26
	07:43	1611	11	110	33,4
	08:43	1612	12	113	29,7
	09:43	1613	13	42,3	28,8

	10:43	1614	14	95,8	30,9
	11:43	1615	15	45,4	30,6
	12:43	1616	16	84,5	24,7
	13:43	1617	17	40,8	24,7
	14:43	1618	18	51	28,8
	15:43	1619	19	110	23,1
	16:43	1620	20	43,2	30,3
	17:43	1621	21	110	32,8
	18:43	1622	22	118	34,5
	19:43	1623	23	45,1	30,9
	20:43	1624	24	67,6	32,6
	21:43	1625	25	50,7	28,5
	22:43	1626	26	73,3	33,7
	23:43	1627	27	42,3	33,4
	00:43	1628	28	127	37,9
	01:43	1629	29	110	-23,5
	02:43	1630	30	50,7	29,4
	03:43	1631	31	73,3	32,3
	04:43	1632	32	53,5	32,6
	05:43	1633	33	95,8	30,7
	06:43	1634	34	76,1	30
	07:43	1635	35	59,2	33,7
	08:43	1636	36	81,7	32,8
	09:43	1637	37	104	32,9
	10:43	1638	38	107	33,4
	11:43	1639	39	98,7	36,1
	12:43	1640	40	93	34,8
	13:43	1641	41	127	37,7
	14:43	1642	42	76,1	35,8
	15:43	1643	43	62	30,6
	16:43	1644	44	47,9	32
	17:43	1645	45	93	34,2
	18:43	1646	46	104	36,4
	19:43	1647	47	130	37,9
	20:43	1648	48	59,2	34
	21:43	1649	49	42,3	33,4
	22:43	1650	50	70	34,8
	23:43	1651	51	119	38,2
	00:43	1652	52	95,8	35,3
	01:43	1653	53	135	39,2
	02:43	1654	54	79,2	35,6
	03:43	1655	55	76,1	35
	04:43	1656	56	70,5	31,7

	05:43	1657	57	104	41,2
	06:43	1658	58	76,2	36,4
	07:43	1659	59	64,8	31,7
	08:43	1660	60	56,4	33,7
	09:43	1661	61	110	36,9
	10:43	1662	62	98,6	32,3
	11:43	1663	63	116	38,2
	12:43	1664	64	133	40,2
	13:43	1665	65	104	38,5
	14:43	1666	66	141	37,9



UNIVERSITY *of the*
WESTERN CAPE

APPENDIX B: Radon concentrations of Building materials

Table 4: RAD7 measurement of Phillipi Sand (Figure 5.4)

Name of Product	Time	RAD 7	Time	Reading	Error
Phillipi Sand	16:26	3101	1	22,7	22,7
Date	17:26	3102	2	17,0	20,7
21-Dec-14	18:26	3103	3	28,4	24,5
Mass	19:26	3104	4	27,0	15,1
2000 gram	20:26	3105	5	31,0	15,9
Starting Time	21:26	3106	6	29,7	15,9
18:06	22:26	3107	7	44,5	18,4
	23:26	3108	8	32,4	16,2
	00:26	3109	9	40,5	17,7
	01:26	3110	10	54,0	20,2
	02:26	3111	11	51,3	19,6
	03:26	3112	12	55,4	20,2
	04:26	3113	13	58,1	9,6
	05:26	3114	14	51,4	20,2
	06:26	3115	15	47,3	20,8
	07:26	3116	16	59,5	20,0
	08:26	3117	17	55,4	19,1
	09:26	3118	18	43,2	20,8
	10:26	3119	19	52,7	20,2
	11:26	3120	20	53,5	28,4
	12:26	3121	21	61,4	20,0
	13:26	3122	22	70,8	20,0
	14:26	3123	23	57,4	21,4
	15:26	3124	24	56,1	21,4
	16:26	3125	25	58,8	21,0
	17:26	3126	26	69,4	22,1
	18:26	3127	27	82,8	23,9
	19:26	3128	28	77,5	23,2
	20:26	3129	29	73,5	23,0
	21:26	3130	30	70,8	22,3
	22:26	3131	31	76,2	23,4
	23:26	3132	32	78,8	23,4
	00:26	3133	33	81,5	23,9
	01:26	3134	34	78,8	23,4
	02:26	3135	35	88,2	24,5
	03:26	3136	36	80,2	23,9
	04:26	3137	37	96,2	25,5
	05:26	3138	38	92,2	25,0
	06:26	3139	39	97,5	26,0

	07:26	3140	40	93,5	25,3
	08:26	3141	41	93,5	25,2
	09:26	3142	42	89,5	24,5

Table 5: RAD7 measurement of Malmesbury Sand (Figure 5.6)

Name of Product	Time	Number	Time	Reading	Error
Malmesbury	19:06	3001	1	17,2	24,5
Date	20:06	3002	2	31,2	26,9
19-Dec-14	21:06	3003	3	39,8	27,7
Mass	22:06	3004	4	33,7	10,7
2000g	23:06	3005	5	45,9	18,7
Starting Time	00:06	3006	6	40,5	18,4
18:06	01:06	3007	7	47,2	19,1
	02:06	3008	8	44,5	18,7
	03:06	3009	9	52,6	20,4
	04:06	3010	10	36,5	17,3
	05:06	3011	11	28,4	15,4
	06:06	3012	12	41,9	18,8
	07:06	3013	13	47,3	19,1
	08:06	3014	14	51,3	19,8
	09:06	3015	15	50,0	20
	10:06	3016	16	64,8	24,3
	11:06	3017	17	59,5	22,8
	12:06	3018	18	85,2	21,2
	13:06	3019	19	66,3	20,6
	14:06	3020	20	59,5	22
	15:06	3021	21	55,4	21
	16:06	3022	22	73,0	23,5
	17:06	3023	23	73,0	22,4
	18:06	3024	24	56,8	24,5
	19:06	3025	25	67,6	23,3
	20:06	3026	26	60,8	21
	21:06	3027	27	78,4	23,5
	22:06	3028	28	70,3	22,4
	23:06	3029	29	86,5	24,5
	00:06	3030	30	75,7	23,5
	01:06	3031	31	68,9	22,2
	02:06	3032	32	90,6	25,2
	03:06	3033	33	83,8	24,5
	04:06	3034	34	78,4	24,5
	05:06	3035	35	67,6	22,6
	06:06	3036	36	98,7	26
	07:06	3037	37	77,0	23,8

	08:06	3038	38	77,0	23,3
	09:06	3039	39	103,0	26,7
	10:06	3040	40	89,2	24,8
	11:06	3041	41	71,6	22,6
	12:06	3042	42	75,7	23,3
	13:06	3043	43	94,6	22,5
	14:06	3044	44	98,8	26

Table 6: RAD7 measurement of a floor tile (Figure 5.8)

Name of Product	Run/cycle	Time of Reading	Duration Hour	Reading	Error
Floor Tile	3201	10:52	1	36,9	28,4
Date	3202	11:52	2	19,9	23,6
23-Dec-14	3203	12:52	3	54,0	31,1
Mass	3204	13:52	4	36,4	17,7
590.7 grams	3205	14:52	5	27,0	15,9
Starting Time	3206	15:52	6	28,3	15,6
9:52	3207	16:52	7	36,2	17,1
	3208	17:52	8	34,8	16,6
	3209	18:52	9	48,2	19,0
	3210	19:52	10	37,5	17,4
	3211	20:52	11	38,8	17,4
	3212	21:52	12	38,8	17,8
	3213	22:52	13	33,5	16,6
	3214	23:52	14	36,2	16,9
	3215	00:52	15	34,8	16,6
	3216	01:52	16	28,1	16,3
	3217	02:52	17	26,8	15,2
	3218	03:52	18	32,1	16,1
	3219	04:52	19	41,5	17,8
	3220	05:52	20	40,2	17,6
	3221	06:52	21	50,9	19,8
	3222	07:52	22	48,2	19,0
	3223	08:52	23	40,2	18,3
	3224	09:52	24	42,9	18,1
	3225	10:52	25	33,5	16,3
	3226	11:52	26	25,4	15,2
	3227	12:52	27	21,4	13,7
	3228	13:52	28	18,7	13,4
	3229	14:52	29	36,2	17,1
	3230	15:52	30	25,4	14,0
	3231	16:52	31	28,8	15,8
	3232	17:52	32	33,5	16,3

	3233	18:52	33	26,8	14,9
	3234	19:52	34	33,5	16,3
	3235	20:52	35	34,8	16,8
	3236	21:52	36	30,8	16,3
	3237	22:52	37	38,8	17,4
	3238	23:52	38	34,8	16,6
	3239	00:52	39	26,8	15,2
	3240	01:52	40	20,8	15,5
	3241	02:52	41	28,1	17,4
	3242	03:52	42	25,4	16,1
	3243	04:52	43	32,1	13,4
	3244	05:52	44	18,7	17,4
	3245	06:52	45	37,5	13,4
	3246	07:52	46	20,1	15,5
	3247	08:52	47	29,4	15,5
	3248	09:52	48	28,1	15,3
	3249	10:52	49	22,8	14,0
	3250	11:52	50	30,8	15,8
	3251	12:52	51	22,8	14,0
	3252	13:52	52	30,8	15,8
	3253	14:52	53	37,5	17,1
	3254	15:52	54	40,2	17,6
	3255	16:52	55	33,5	16,3
	3256	17:52	56	29,4	15,8
	3257	18:52	57	20,1	14,0
	3258	19:52	58	18,7	13,0
	3259	20:52	59	29,4	15,5
	3260	21:52	60	33,5	16,3
	3261	22:52	61	38,8	17,4
	3262	23:52	62	20,1	13,7
	3263	00:52	63	33,5	16,3
	3264	01:52	64	28,1	15,5
	3265	02:52	65	18,7	14,0
	3266	03:52	66	25,4	14,7
	3267	04:52	67	30,8	16,3
	3268	05:52	68	45,5	18,5
	3269	06:52	69	32,1	16,1
	3270	07:52	70	20,1	13,7
	3271	08:52	71	33,5	16,3
	3272	09:52	72	33,5	16,6
	3273	10:52	73	34,8	17,1
	3274	11:52	74	41,5	17,8
	3275	12:52	75	36,1	17,1

	3276	13:52	76	32,1	16,6
	3277	14:52	77	41,5	18,5
	3278	15:52	78	25,4	15,5
	3279	16:52	79	44,2	18,3
	3280	17:52	80	38,8	17,6
	3281	18:52	81	29,4	15,8
	3282	19:52	82	38,0	16,6
	3283	20:52	83	46,9	19,2
	3284	21:52	84	37,5	17,1
	3285	22:52	85	32,1	16,3
	3286	23:52	86	38,8	17,9
	3287	00:52	87	33,5	17,1
	3288	01:52	88	30,8	15,8
	3289	02:52	89	28,1	15,2
	3290	03:52	90	44,2	18,3
	3291	04:52	91	29,4	15,5
	3292	05:52	92	32,1	16,9
	3293	06:52	93	37,5	17,8
	3294	07:52	94	33,5	16,8
	3295	08:52	95	30,8	16,6
	3296	09:52	96	40,2	17,6

Table 7: RAD7 measurement of a Roof tile (Figure 5.10)

Name of Product	Time	RAD 7	Time	Reading	Error
Roof Tile	20:11	4401	1	68,0	34,1
Date	21:11	4402	2	59,6	32,3
14-Feb-15	22:11	4403	3	31,2	25,3
Mass	23:11	4404	4	74,2	22,9
650.4 gram	00:11	4405	5	40,5	17,7
Starting Time	01:11	4406	6	59,3	20,8
19:11	02:11	4407	7	63,4	21,4
	03:11	4408	8	45,9	18,7
	04:11	4409	9	63,4	18,2
	05:11	4410	10	45,9	18,7
	06:11	4411	11	43,2	18,2
	07:11	4412	12	52,6	19,8
	08:11	4413	13	54,0	20,2
	09:11	4414	14	58,0	20,6
	10:11	4415	15	54,0	26,0
	11:11	4416	16	67,5	22,6
	12:11	4417	17	70,2	20,4
	13:11	4418	18	56,7	22,7

	14:11	4419	19	72,9	22,7
	15:11	4420	20	71,6	23,4
	16:11	4421	21	78,3	23,4
	17:11	4422	22	75,6	23,1
	18:11	4423	23	64,8	22,0
	19:11	4424	24	56,7	20,4
	20:11	4425	25	54,0	20,2
	21:11	4426	26	48,6	19,3
	22:11	4427	27	64,8	21,8
	23:11	4428	28	55,3	20,4
	00:11	4429	29	54,0	20,0
	01:11	4430	30	70,2	22,4
	02:11	4431	31	71,5	22,0
	03:11	4432	32	58,0	20,6
	04:11	4433	33	62,1	21,2
	05:11	4434	34	64,8	21,6
	06:11	4435	35	62,1	21,2
	07:11	4436	36	62,1	21,4
	08:11	4437	37	75,6	23,1
	09:11	4438	38	81,0	23,5
	10:11	4439	39	60,7	21,0
	11:11	4440	40	72,0	22,7
	12:11	4441	41	67,5	22,0
	13:11	4442	42	66,1	21,8
	14:11	4443	43	59,4	20,8
	15:11	4444	44	62,1	21,2
	16:11	4445	45	59,4	21,0
	17:11	4446	46	52,6	19,8
	18:11	4447	47	62,1	21,2
	19:11	4448	48	55,3	20,2
	20:11	4449	49	67,5	22,4
	21:11	4450	50	56,7	20,4
	22:11	4451	51	74,3	23,1
	23:11	4452	52	71,6	22,6
	00:11	4453	53	68,9	22,2
	01:11	4454	54	66,1	21,8
	02:11	4455	55	76,9	23,3
	03:11	4456	56	68,8	22,4
	04:11	4457	57	70,2	22,7
	05:11	4458	58	66,1	21,8
	06:11	4459	59	51,3	19,6
	07:11	4460	60	54,0	20,6
	08:11	4461	61	74,6	23,4

	09:11	4462	62	64,8	21,6
	10:11	4463	63	52,7	20,2
	11:11	4464	64	48,6	19,8
	12:11	4465	65	52,6	20,0
	13:11	4466	66	47,2	19,1
	14:11	4467	67	54,0	20,4
	15:11	4468	68	70,2	22,5
	16:11	4469	69	54,0	20,0
	17:11	4470	70	56,7	20,4
	18:11	4471	71	60,7	21,2
	19:11	4472	72	79,6	23,6
	20:11	4473	73	68,8	22,2
	21:11	4474	74	70,2	22,4
	22:11	4475	75	51,3	16,9
	23:11	4476	76	49,9	19,8
	00:11	4477	77	68,8	22,4
	01:11	4478	78	60,7	21,0
	02:11	4479	79	60,8	21,4
	03:11	4480	80	51,3	19,8
	04:11	4481	81	56,7	20,8
	05:11	4482	82	35,1	20,2
	06:11	4483	83	35,4	17,5
	07:11	4484	84	56,7	22,1
	08:11	4485	85	64,8	22,0
	09:11	4486	86	56,6	20,6
	10:11	4487	87	58,0	20,8
	11:11	4488	88	59,4	21,2
	12:11	4489	89	58,8	20,8
	13:11	4490	90	76,9	23,3
	14:11	4491	91	70,2	22,4
	15:11	4492	92	55,3	22,4
	16:11	4493	93	47,2	20,6
	17:11	4494	94	63,4	19,1
	18:11	4495	95	45,9	21,6
	19:11	4496	96	59,4	19,3
	20:11	4497	97	74,3	23,3

Table 8: RAD7 measurement of Hornfels Stones (Figure 5.12)

Name of Product	Time	RAD 7	Time	Reading	Error
Stones	15:13	3301	1	91,0	38,4
Date	16:13	3302	2	102,0	40,2
21-Dec-14	17:13	3303	3	96,6	39,4
Mass	18:13	3304	4	123,0	28,6
680.2 gram	19:13	3305	5	118,0	28,1
Starting Time	20:13	3306	6	109,0	27,7
18:06	21:13	3307	7	127,0	29,0
	22:13	3308	8	130,0	29,3
	23:13	3309	9	142,0	30,5
	00:13	3310	10	101,0	26,3
	01:13	3311	11	104,0	26,9
	02:13	3312	12	139,0	30,4
	03:13	3313	13	91,9	25,2
	04:13	3314	14	122,0	28,5
	05:13	3315	15	123,0	28,6
	06:13	3316	16	106,0	26,7
	07:13	3317	17	142,0	30,6
	08:13	3318	18	111,0	27,3
	09:13	3319	19	116,0	27,9
	10:13	3320	20	137,0	30,0
	11:13	3321	21	145,0	30,8
	12:13	3322	22	124,0	29,0
	13:13	3323	23	139,0	30,3
	14:13	3324	24	120,0	28,4
	15:13	3325	25	135,0	30,0
	16:13	3326	26	122,0	28,6
	17:13	3327	27	142,0	30,6
	18:13	3328	28	119,0	28,2
	19:13	3329	29	110,0	27,2
	20:13	3330	30	124,0	28,8
	21:13	3331	31	114,0	27,2
	22:13	3332	32	161,0	28,8
	23:13	3333	33	145,0	27,8
	00:13	3334	34	149,0	32,3
	01:13	3335	35	143,0	20,8
	02:13	3336	36	127,0	31,2
	03:13	3337	37	139,0	30,3
	04:13	3338	38	115,0	27,8
	05:13	3339	39	137,0	30,0
	06:13	3340	40	123,0	28,9
	07:13	3341	41	129,0	29,2

	08:13	3342	42	139,0	30,3
	09:13	3343	43	130,0	27,3
	10:13	3344	44	110,0	27,2
	11:13	3345	45	122,0	28,5
	12:13	3346	46	126,0	29,7
	13:13	3347	47	127,0	27,1
	14:13	3348	48	138,0	30,2
	15:13	3349	49	112,0	27,6
	16:13	3350	50	138,0	30,1
	17:13	3351	51	119,0	28,4
	18:13	3352	52	130,0	29,5
	19:13	3353	53	123,0	28,8
	20:13	3354	54	137,0	30,0
	21:13	3355	55	123,0	28,6
	22:13	3356	56	143,0	30,7
	23:13	3357	57	138,0	30,2
	00:13	3358	58	119,0	28,2
	01:13	3359	59	150,0	31,5
	02:13	3360	60	133,0	29,6
	03:13	3361	61	126,0	28,9
	04:13	3362	62	134,0	29,8
	05:13	3363	63	131,0	29,5
	06:13	3364	64	133,0	29,6
	07:13	3365	65	154,0	31,7
	08:13	3366	66	124,0	28,8
	09:13	3367	67	110,0	27,2
	10:13	3368	68	137,0	30,0
	11:13	3369	69	142,0	30,7
	12:13	3370	70	108,0	27,0

Table 9: RAD7 measurement of Tar (Figure 5.14)

Name of Product	Time	RAD 7	Time	Reading	Error
Tar	20:13	4601	1	30,9	25,1
Date	21:13	4602	2	53,3	30,7
23-Feb-15	22:13	4603	3	42,1	28,1
Mass	23:13	4604	4	34,7	16,5
966.2 gram	00:13	4605	5	60,0	20,8
Starting Time	01:13	4606	6	45,4	18,5
20:03	02:13	4607	7	37,4	17,0
	03:13	4608	8	56,0	20,4
	04:13	4609	9	40,0	17,8
	05:13	4610	10	45,0	18,5

	06:13	4611	11	36,0	16,5
	07:13	4612	12	65,0	21,7
	08:13	4613	13	65,4	21,5
	09:13	4614	14	54,7	20,0
	10:13	4615	15	58,7	20,8
	11:13	4616	16	61,4	21,0
	12:13	4617	17	68,1	21,9
	13:13	4618	18	56,0	20,2
	14:13	4619	19	74,7	23,2
	15:13	4620	20	57,4	20,4
	16:13	4621	21	93,4	25,2
	17:13	4622	22	50,7	19,6
	18:13	4623	23	56,0	20,4
	19:13	4624	24	90,7	25,0
	20:13	4625	25	70,7	22,3
	21:13	4626	26	76,1	23,0
	22:13	4627	27	60,0	20,8
	23:13	4628	28	72,1	22,5
	00:13	4629	29	77,4	23,3
	01:13	4630	30	53,4	20,0
	02:13	4631	31	65,4	21,5
	03:13	4632	32	49,4	19,1
	04:13	4633	33	65,4	21,5
	05:13	4634	34	78,7	23,3
	06:13	4635	35	61,4	21,0
	07:13	4636	36	73,4	22,6
	08:13	4637	37	81,4	23,7
	09:13	4638	38	66,7	21,4
	10:13	4639	39	90,7	24,8
	11:13	4640	40	86,7	24,4
	12:13	4641	41	84,1	24,0
	13:13	4642	42	113,0	27,4
	14:13	4643	43	68,1	21,9
	15:13	4644	44	82,7	24,0
	16:13	4645	45	80,1	23,9
	17:13	4646	46	96,1	25,6
	18:13	4647	47	80,1	23,5
	19:13	4648	48	94,7	25,3
	20:13	4649	49	80,1	23,5
	21:13	4650	50	80,1	23,8
	22:13	4651	51	98,7	25,9
	23:13	4652	52	78,7	23,5
	00:13	4653	53	101,0	26,4

	01:13	4654	54	78,7	23,3
	02:13	4655	55	108,0	26,8
	03:13	4656	56	90,7	24,8
	04:13	4657	57	78,7	23,3
	05:13	4658	58	86,7	24,4
	06:13	4659	59	96,1	25,5
	07:13	4660	60	86,7	24,7
	08:13	4661	61	93,4	25,2
	09:13	4662	62	85,4	24,2
	10:13	4663	63	85,4	24,4
	11:13	4664	64	117,0	27,8
	12:13	4665	65	82,7	23,7
	13:13	4666	66	98,7	26,4
	14:13	4667	67	77,4	23,5
	15:13	4668	68	103,0	22,8

Table 10: RAD7 measurement of Beaufort-West uranium bearing sandstone (Figure 5.16)

Name of Product	Time	RAD 7	Time	Reading	Error	model
Beaufort Sand	16:55	4501	1	250	59,0	545,00
Date	17:55	4502	2	770	94,0	837,78
15-Dec-15	18:55	4503	3	1270	126,0	1128,36
Mass	19:55	4504	4	1740	147,0	1416,75
2000 gram	20:55	4505	5	2190	165,0	1702,96
Starting Time	21:55	4506	6	2560	177,0	1987,02
18:06	22:55	4507	7	2890	188,0	2268,94
	23:55	4508	8	3530	208,0	2548,74
	00:55	4509	9	3730	213,0	2826,43
	01:55	4510	10	4260	227,0	3102,03
	02:55	4511	11	4660	237,0	3375,55
	03:55	4512	12	5200	251,0	3647,01
	04:55	4513	13	5330	254,0	3916,43
	05:55	4514	14	5800	265,0	4183,81
	06:55	4515	15	6000	269,0	4449,19
	07:55	4516	16	6450	279,0	4712,56
	08:55	4517	17	6770	286,0	4973,95
	09:55	4518	18	7170	295,0	5233,38
	10:55	4519	19	7590	303,0	5490,84
	11:55	4520	20	7760	306,0	5746,37
	12:55	4521	21	7820	308,0	5999,98

	13:55	4522	22	8250	316,0	6251,67
	14:55	4523	23	8500	321,0	6501,47
	15:55	4524	24	8690	329,0	6749,39
	16:55	4525	25	9350	336,0	6995,44
	17:55	4526	26	9880	346,0	7239,64
	18:55	4527	27	9910	346,0	7481,99
	19:55	4528	28	10500	356,0	7722,52
	20:55	4529	29	10500	356,0	7961,24
	21:55	4530	30	10800	361,0	8198,17
	22:55	4531	31	11200	368,0	8433,30
	23:55	4532	32	11600	375,0	8666,67
	00:55	4533	33	11400	372,0	8898,28
	01:55	4534	34	11900	380,0	9128,14
	02:55	4535	35	12100	383,0	9356,28
	03:55	4536	36	12500	389,0	9582,69
	04:55	4537	37	12700	392,0	9807,40
	05:55	4538	38	13200	400,0	10030,42
	06:55	4539	39	13200	406,0	10251,76
	07:55	4540	40	13700	407,0	10471,43
	08:55	4541	41	14000	412,0	10689,44
	09:55	4542	42	14300	418,0	10905,81
	10:55	4543	43	13900	411,0	11120,56
	11:55	4544	44	14300	414,0	11333,68
	12:55	4545	45	14600	422,0	11545,21
	13:55	4546	46	14800	424,0	11755,13
	14:55	4547	47	15000	427,0	11963,48
	15:55	4548	48	15300	431,0	12170,26
	16:55	4549	49	15300	433,0	12375,48
	17:55	4550	50	15700	437,0	12579,15
	18:55	4551	51	16000	441,0	12781,29
	19:55	4552	52	16000	442,0	12981,91
	20:55	4553	53	16200	445,0	13181,02
	21:55	4554	54	16400	447,0	13378,62
	22:55	4555	55	16700	451,0	13574,74
	23:55	4556	56	16700	451,0	13769,38
	00:55	4557	57	17300	459,0	13962,56
	01:55	4558	58	17600	464,0	14154,28
	02:55	4559	59	17500	462,0	14344,55
	03:55	4560	60	17400	462,0	14533,40
	04:55	4561	61	17500	462,0	14720,82
	05:55	4562	62	17700	466,0	14906,83
	06:55	4563	63	17700	467,0	15091,43
	07:55	4564	64	18400	475,0	15274,65
	08:55	4565	65	18000	470,0	15456,49

	09:55	4566	66	18400	474,0	15636,96
	10:55	4567	67	18600	477,0	15816,07
	11:55	4568	68	19200	485,0	15993,83
	12:55	4569	69	18700	478,0	16170,25
	13:55	4570	70	19100	484,0	16345,34
	14:55	4571	71	19300	486,0	16519,11
	15:55	4572	72	19300	480,0	16691,58
	16:55	4573	73	19900	499,0	16862,74
	17:55	4574	74	19600	490,0	17032,62
	18:55	4575	75	19900	494,0	17201,21
	19:55	4576	76	20200	497,0	17368,54
	20:55	4577	77	20300	500,0	17534,61
	21:55	4578	78	20400	501,0	17699,42
	22:55	4579	79	20000	495,0	17863,00
	23:55	4580	80	20600	504,0	18025,34
	00:55	4581	81	21100	509,0	18186,46
	01:55	4582	82	21000	508,0	18346,36
	02:55	4583	83	21300	511,0	18505,07
	03:55	4584	84	21100	509,0	18662,57
	04:55	4585	85	21000	508,0	18818,89
	05:55	4586	86	21100	510,0	18974,03
	06:55	4587	87	22200	523,0	19128,01
	07:55	4588	88	21400	514,0	19280,82
	08:55	4589	89	21700	517,0	19432,49
	09:55	4590	90	21900	519,0	19583,01
	10:55	4591	91	21600	516,0	19732,39
	11:55	4592	92	22200	524,0	19880,66
	12:55	4593	93	21600	516,0	20027,80
	13:55	4594	94	22200	523,0	20173,84
	14:55	4595	95	21700	517,0	20318,77
	15:55	4596	96	22500	526,0	20462,62
	16:55	4597	97	22700	529,0	20605,38
	17:55	4598	98	22800	530,0	20747,07
	18:55	4599	99	22300	525,0	20887,69
	19:55	4600	100	22900	532,0	21027,25
	20:55	4601	101	22900	532,0	21165,76
	21:55	4602	102	23600	540,0	21303,22
	22:55	4603	103	23000	533,0	21439,65
	23:55	4604	104	23400	538,0	21575,06
	00:55	4605	105	23800	543,0	21709,44
	01:55	4606	106	23000	539,0	21842,81
	02:55	4607	107	23600	541,0	21975,18
	03:55	4608	108	23500	539,0	22106,54
	04:55	4609	109	23900	533,0	22236,92

	05:55	4610	110	23600	541,0	22366,32
	06:55	4611	111	23900	543,0	22494,75
	07:55	4612	112	24200	547,0	22622,20
	08:55	4613	113	24400	549,0	22748,70
	09:55	4614	114	24600	552,0	22874,24
	10:55	4615	115	24200	547,0	22998,84
	11:55	4616	116	24600	552,0	23122,50
	12:55	4617	117	24600	551,0	23245,22
	13:55	4618	118	24700	553,0	23367,03
	14:55	4619	119	24700	553,0	23487,91
	15:55	4620	120	24500	551,0	23607,89
	16:55	4621	121	24700	553,0	23726,96
	17:55	4622	122	25000	556,0	23845,14
	18:55	4623	123	25300	560,0	23962,42
	19:55	4624	124	24900	555,0	24078,82
	20:55	4625	125	25400	562,0	24194,35
	21:55	4626	126	25500	562,0	24309,00
	22:55	4627	127	25100	558,0	24422,79
	23:55	4628	128	25400	561,0	24535,73
	00:55	4629	129	25500	563,0	24647,81
	01:55	4630	130	25600	563,0	24759,05
	02:55	4631	131	25600	563,0	24869,45
	03:55	4632	132	25700	563,0	24979,02
	04:55	4633	133	25700	563,0	25087,76
	05:55	4634	134	25500	574,0	25195,69
	06:55	4635	135	26100	567,0	25302,80
	07:55	4636	136	26100	570,0	25409,11
	08:55	4637	137	25800	566,0	25514,61
	09:55	4638	138	25900	567,0	25619,32
	10:55	4639	139	26000	568,0	25723,24
	11:55	4640	140	26900	579,0	25826,38
	12:55	4641	141	26300	572,0	25928,74
	13:55	4642	142	26300	572,0	26030,33
	14:55	4643	143	25900	568,0	26131,16
	15:55	4644	144	25900	567,0	26231,23
	16:55	4645	145	26400	573,0	26330,54
	17:55	4646	146	26600	575,0	26429,10
	18:55	4647	147	26500	574,0	26526,93
	19:55	4648	148	26500	575,0	26624,01
	20:55	4649	149	26600	575,0	26720,37
	21:55	4650	150	26900	579,0	26815,99
	22:55	4651	151	27000	579,0	26910,90
	23:55	4652	152	27500	585,0	27005,10
	00:55	4653	153	27800	588,0	27098,58

	01:55	4654	154	27400	584,0	27191,36
	02:55	4655	155	26700	576,0	27283,44
	03:55	4656	156	27200	582,0	27374,83
	04:55	4657	157	27200	582,0	27465,53
	05:55	4658	158	27400	585,0	27555,54
	06:55	4659	159	27100	581,0	27644,88
	07:55	4660	160	27500	585,0	27733,55
	08:55	4661	161	27300	583,0	27821,54
	09:55	4662	162	27700	585,0	27908,88
	10:55	4663	163	27700	585,0	27995,55
	11:55	4664	164	27500	584,0	28081,58

APPENDIX C: Background Radiation of Aardorn

Table 11: RAD7 measurement of Background Radiation of Aardorn as shown on Figure 5.18 (Masia 2010)

Name of Product	Run/cycle	Duration Hour	Reading	Error
Blikkraal Background radiation	11:08	1	200	81,3
Date	12:08	2	288	94,9
n/a	13:08	3	282	94,1
Mass	14:08	4	279	62,7
n/a	15:08	5	405	74,1
Starting Time	16:08	6	410	74,3
10:08	17:08	7	334	67,9
	18:08	8	328	67,1
	19:08	9	222	56,4
	20:08	10	182	51,7
	21:08	11	277	62,1
	22:08	12	308	65,2
	23:08	13	356	69,7
	00:08	14	430	76
	01:08	15	528	83,5
	02:08	16	636	91,1
	03:08	17	659	92,6
	04:08	18	654	91,7
	05:08	19	776	100
	06:08	20	379	71,8
	07:08	21	200	53,7
	08:08	22	191	52,7
	09:08	23	242	58,6
	10:08	24	322	66,6

**APPENDIX D:
Radon concentrations of Granite Countertops.**

Table 12: RAD7 measurement of the granite Golden Beach (Figure 5.19)

Name of Product	RAD 7	Time (Actual)	Time	Reading	Error
Golden Beach	3601	15:31	1	142,0	47,2
Date	3602	16:31	2	190,0	53,5
15-Jan-15	3603	17:31	3	159,0	49,6
Starting Time	3604	18:31	4	185,0	34,8
16:48	3605	19:31	5	186,0	34,5
	3606	20:31	6	165,0	32,7
	3607	21:31	7	162,0	32,5
	3608	22:31	8	173,0	33,5
	3609	23:31	9	143,0	31
	3610	00:31	10	142,0	30,5
	3611	01:31	11	132,0	29,6
	3612	02:31	12	128,0	29,8
	3613	03:31	13	149,0	31,2
	3614	04:31	14	155,0	31,9
	3615	05:31	15	154,0	31,7
	3616	06:31	16	158,0	32
	3617	07:31	17	167,0	33,1
	3618	08:31	18	127,0	29
	3619	09:31	19	139,0	30
	3620	10:31	20	154,0	31,8
	3621	11:31	21	128,0	29
	3622	12:31	22	131,0	29,6
	3623	13:31	23	140,0	30,4
	3624	14:31	24	145,0	30,8
	3625	15:31	25	144,0	31
	3626	16:31	26	143,0	30
	3627	17:31	27	153,0	31,5
	3628	18:31	28	128,0	29,2
	3629	19:31	29	151,0	31,4
	3630	20:31	30	136,0	30,1
	3631	21:31	31	136,0	30
	3632	22:31	32	149,0	27,9
	3633	23:31	33	126,0	29
	3634	00:31	34	84,6	32
	3635	01:31	35	120,0	30
	3636	02:31	36	134,0	31,2
	3637	03:31	37	112,0	28,9
	3638	04:31	38	130,0	24,6
	3639	05:31	39	143,0	28

	3640	06:31	40	147,0	29,8
	3641	07:31	41	134,0	21,5
	3642	08:31	42	161,0	29,6
	3643	09:31	43	132,0	32,6
	3644	10:31	44	111,0	31
	3645	11:31	45	138,0	36
	3646	12:31	46	120,0	32,4
	3647	13:31	47	120,0	29,9
	3648	14:31	48	124,0	27,3
	3649	15:31	49	134,0	30,4
	3650	16:31	50	126,0	28,3
	3651	17:31	51	128,0	28,3
	3652	18:31	52	135,0	28,9
	3653	19:31	53	109,0	24,7
	3654	20:31	54	116,0	28,9
	3655	21:31	55	131,0	29,3
	3656	22:31	56	104,0	29,8
	3657	23:31	57	120,0	27,1
	3658	00:31	58	135,0	27,9
	3659	01:31	59	139,0	29,4
	3660	02:31	60	135,0	30,1
	3661	03:31	61	97,2	25,8
	3662	04:31	62	124,0	28,7
	3663	05:31	63	116,0	28,3
	3664	06:31	64	124,0	28,9
	3665	07:31	65	122,0	28,5
	3666	08:31	66	112,0	27,4

Table 13: RAD7 measurement of the granite Indiana Dakota (Figure 5.21)

Name of Product	RAD 7	Time	Time (Hours)	Reading	Error
Indiana Dakota	1801	17:48	1	93,9	16,3
Date	1802	18:48	2	54,1	11,2
20-Jun-15	1803	19:48	3	74	17,5
Starting Time	1804	20:48	4	88,2	20,1
16:48	1805	21:48	5	85,3	16,7
	1806	22:48	6	56,9	15,1
	1807	23:48	7	42,7	17,5
	1808	00:48	8	111	27,5
	1809	01:48	9	25	17,9
	1810	02:48	10	79,7	25
	1811	03:48	11	48,4	25,3
	1812	04:48	12	42,7	22,3
	1813	05:48	13	111	27,5

	1814	06:48	14	25	17,9
	1815	07:48	15	79,7	25
	1816	08:48	16	48,4	25,3
	1817	09:48	17	56,9	26
	1818	10:48	18	71,2	27,9
	1819	11:48	19	11,4	21,9
	1820	12:48	20	62,6	27,3
	1821	13:48	21	48,4	26,3
	1822	14:48	22	45,5	26,6
	1823	15:48	23	43,2	39,5
	1824	16:48	24	51,3	25,7
	1825	17:48	25	74,1	28,2
	1826	18:48	26	71,2	26,6
	1827	19:48	27	82,6	30,6
	1828	20:48	28	74,1	28,2
	1829	21:48	29	71,2	26,6
	1830	22:48	30	82,6	30,6
	1831	23:48	31	74,1	29,4
	1832	00:48	32	42,7	26,8
	1833	01:48	33	96,8	32,9
	1834	02:48	34	68,4	29,4
	1835	03:48	35	45,6	30
	1836	04:48	36	54,1	28,2
	1837	05:48	37	74,1	32,1
	1838	06:48	38	79,7	32,6
	1839	07:48	39	45,6	32,9
	1840	08:48	40	74	31,5
	1841	09:48	41	62,6	30,3
	1842	10:48	42	51,3	30,3
	1843	11:48	43	92,1	38,4
	1844	12:48	44	71,2	29,4
	1845	13:48	45	48,4	28,2
	1846	14:48	46	79,8	35,2
	1847	15:48	47	51,3	32,1
	1848	16:48	48	68,4	34,9
	1849	17:48	49	88,3	36,3
	1850	18:48	50	59,8	30,9
	1851	19:48	51	65,5	34,1
	1852	20:48	52	39,9	33,2
	1853	21:48	53	57	30
	1854	22:48	54	45,6	30,3
	1855	23:48	55	59,8	32,7
	1856	00:48	56	99,7	38,1
	1857	01:48	57	71,2	34,9

	1858	02:48	58	74	29,7
	1859	03:48	59	62,7	33,8
	1860	04:48	60	79,7	36
	1861	05:48	61	68,4	34,3
	1862	06:48	62	51,3	32,4
	1863	07:48	63	76,9	34,3
	1864	08:48	64	59,8	34,1
	1865	09:48	65	74,1	34,9
	1866	10:48	66	42,7	35,2
	1867	11:48	67	42,7	30
	1868	12:48	68	74,1	34,1
	1869	13:48	69	59,8	35,2
	1870	14:48	70	59,8	34,3
	1871	15:48	71	82,7	40,5
	1872	16:48	72	42,7	31,2
	1873	17:48	73	59,8	34,1
	1874	18:48	74	74,1	34,9
	1875	19:48	75	42,7	35,2
	1876	20:48	76	42,7	30
	1877	21:48	77	74,1	34,1
	1878	22:48	78	59,8	35,2
	1879	23:48	79	59,8	34,3
	1880	00:48	80	82,7	40,5
	1881	01:48	81	42,7	31,2
	1882	02:48	82	59,8	34,3
	1883	03:48	83	54,1	31,2
	1884	04:48	84	59,8	34,3
	1885	05:48	85	71,2	32,1
	1886	06:48	86	57	32,4
	1887	07:48	87	68,4	36
	1888	08:48	88	62,7	30
	1889	09:48	89	62,7	33
	1890	10:48	90	51,3	30
	1891	11:48	91	42,7	34
	1892	12:48	92	65,5	34,9

Table 14: RAD7 measurement of the granite Santa Cecilia (Figure 5.23)

Name of Product	RAD 7	Time (Actual)	Time(Hours)	Reading	Error
Santa Cecilia	4301	20:35	1	142	47,4
Date	4302	21:35	2	190	53,5
10-Feb-15	4303	22:35	3	159	49,6
Starting Time	4304	23:35	4	185	34,5
19:35	4305	00:35	5	186	34,5
	4306	01:35	6	165	32,7
	4307	02:35	7	162	32,5
	4308	03:35	8	173	33,5
	4309	04:35	9	143	31
	4310	05:35	10	142	30,5
	4311	06:35	11	132	29,6
	4312	07:35	12	128	29,8
	4313	08:35	13	149	31,2
	4314	09:35	14	155	31,9
	4315	10:35	15	154	31,7
	4316	11:35	16	158	32
	4317	12:35	17	107	33,1
	4318	13:35	18	127	29
	4319	14:35	19	139	30
	4320	15:35	20	154	31,8
	4321	16:35	21	128	29
	4322	17:35	22	131	29,6
	4323	18:35	23	140	30,4
	4324	19:35	24	145	30,8
	4325	20:35	25	144	31
	4326	21:35	26	143	30
	4327	22:35	27	153	31,5
	4328	23:35	28	128	29,2
	4329	00:35	29	151	31,4
	4330	01:35	30	136	30,1
	4331	02:35	31	136	30
	4332	03:35	32	116	27,9
	4333	04:35	33	127	29
	4334	05:35	34	158	32
	4335	06:35	35	136	30
	4336	07:35	36	149	31,2
	4337	08:35	37	126	28,9
	4338	09:35	38	84,6	24,6
	4339	10:35	39	120	28
	4340	11:35	40	134	29,8

	4341	12:35	41	112	21,5
	4342	13:35	42	130	29,4
	4343	14:35	43	143	32,6
	4344	15:35	44	147	31
	4345	16:35	45	134	36
	4346	17:35	46	161	32,4
	4347	18:35	47	132	29,9
	4348	19:35	48	111	27,3
	4349	20:35	49	138	30,4
	4350	21:35	50	120	28,3
	4351	22:35	51	120	28,3
	4352	23:35	52	124	28,9
	4353	00:35	53	134	24,7
	4354	01:35	54	126	28,9
	4355	02:35	55	128	29,3
	4356	03:35	56	135	29,8
	4357	04:35	57	109	27
	4358	05:35	58	116	27,9
	4359	06:35	59	131	29,4
	4360	07:35	60	104	26,9
	4361	08:35	61	120	28,3
	4362	09:35	62	135	29,8
	4363	10:35	63	139	30,2
	4364	11:35	64	135	30,1
	4365	12:35	65	97,2	25,8
	4366	13:35	66	124	28,7
	4367	14:35	67	116	28,3
	4368	15:35	68	124	28,9
	4369	16:35	69	122	28,5
	4370	17:35	70	112	27,4

Table 15: RAD7 measurement of the granite Namib Green (Figure 5.25)

Name of Product	RAD 7	RAD 7	Reading	Time	Error	model
Namib Green	4001	1	25,4	17:18	23,5	25,30
Date	4002	2	31	18:18	25,1	30,57
30-Jan-15	4003	3	47,8	19:18	29,5	35,79
Mass	4004	4	50,8	20:18	19,4	40,98
1770 gram	4005	5	54,9	21:18	20,0	46,12
Starting Time	4006	6	50,8	22:18	19,4	51,23
16:18	4007	7	62,9	23:18	21,2	56,30
	4008	8	85,6	00:18	24,3	61,33
	4009	9	96,3	01:18	25,5	66,32

	4010	10	102	02:18	26,2	71,28
	4011	11	114	03:18	27,6	76,19
	4012	12	108	04:18	26,5	81,07
	4013	13	112	05:18	26,9	85,92
	4014	14	147	06:18	27,4	90,72
	4015	15	133	07:18	30,9	95,50
	4016	16	123	08:18	29,4	100,23
	4017	17	125	09:18	28,5	104,93
	4018	18	133	10:18	28,6	109,59
	4019	19	162	11:18	29,7	114,22
	4020	20	166	12:18	32,2	118,82
	4021	21	150	13:18	32,6	123,38
	4022	22	150	14:18	31,3	127,90
	4023	23	185	15:18	34,4	132,39
	4024	24	167	16:18	32,7	136,85
	4025	25	179	17:18	33,8	141,27
	4026	26	155	18:18	31,6	145,66
	4027	27	170	19:18	33,0	150,02
	4028	28	170	20:18	33,0	154,35
	4029	29	195	21:18	35,1	158,64
	4030	30	183	22:18	34,1	162,90
	4031	31	191	23:18	34,8	167,13
	4032	32	230	00:18	37,9	171,32
	4033	33	249	01:18	39,3	175,49
	4034	34	224	02:18	37,4	179,62
	4035	35	244	03:18	39,0	183,72
	4036	36	225	04:18	37,5	187,79
	4037	37	241	05:18	38,7	191,83
	4038	38	217	06:18	36,9	195,84
	4039	39	252	07:18	39,5	199,82
	4040	40	229	08:18	38,1	203,77
	4041	41	257	09:18	40,0	207,69
	4042	42	244	10:18	39,1	211,58
	4043	43	245	11:18	39,2	215,44
	4044	44	273	12:18	41,0	219,27
	4045	45	279	13:18	41,4	223,07
	4046	46	253	14:18	39,7	226,85
	4047	47	271	15:18	40,8	230,59
	4048	48	262	16:18	40,3	234,31
	4049	49	246	17:18	39,1	238,00
	4050	50	279	18:18	41,5	241,66
	4051	51	246	19:18	39,1	245,30
	4052	52	277	20:18	41,3	248,90

	4053	53	293	21:18	42,4	252,48
	4054	54	280	22:18	41,5	256,04
	4055	55	303	23:18	46,3	259,56
	4056	56	264	00:18	43,1	263,06
	4057	57	283	01:18	40,6	266,53
	4058	58	323	02:18	41,7	269,98
	4059	59	304	03:18	44,3	273,40
	4060	60	311	04:18	43,1	276,80
	4061	61	315	05:18	43,6	280,17
	4062	62	285	06:18	43,8	283,51
	4063	63	301	07:18	41,9	286,83
	4064	64	354	08:18	42,9	290,12
	4065	65	328	09:18	44,6	293,39
	4066	66	325	10:18	44,6	296,64
	4067	67	324	11:18	44,4	299,86
	4068	68	339	12:18	45,4	303,05
	4069	69	348	13:18	46,2	306,23
	4070	70	344	14:18	45,8	309,37
	4071	71	313	15:18	43,7	312,50
	4072	72	329	16:18	44,9	315,60
	4073	73	337	17:18	45,4	318,68
	4074	74	346	18:18	46,0	321,73
	4075	75	347	19:18	45,9	324,76
	4076	76	344	20:18	45,9	327,77
	4077	77	335	21:18	45,1	330,76
	4078	78	341	22:18	45,6	333,72
	4079	79	325	23:18	44,5	336,66
	4080	80	341	00:18	45,5	339,58
	4081	81	331	01:18	44,5	342,47
	4082	82	324	02:18	44,4	345,35
	4083	83	347	03:18	45,9	348,20
	4084	84	354	04:18	43,6	351,03
	4085	85	328	05:18	43,8	353,84
	4086	86	325	06:18	41,9	356,63
	4087	87	324	07:18	42,9	359,40
	4088	88	339	08:18	44,6	362,15
	4089	89	348	09:18	44,6	364,88
	4090	90	344	10:18	44,4	367,58
	4091	91	360	11:18	45,4	370,27
	4092	92	350	12:18	46,2	372,93
	4093	93	337	13:18	45,8	375,58
	4094	94	346	14:18	43,7	378,21
	4095	95	347	15:18	44,9	380,81

	4096	96	344	16:18	45,4	383,40
	4097	97	335	17:18	46,0	385,96
	4098	98	341	18:18	45,9	388,51
	4099	99	347	19:18	45,9	391,04

Table 16: RAD7 measurement of the granite African Red (Figure 5.27)

Name of Product	RAD 7	Time	Hours	Reading	Error	model
African Red 1	4101	12:27	1,00	153	48,2	117,53
Date	4102	13:27	2,00	90,8	38,8	125,01
07-Feb-15	4103	14:27	3,00	159	48,2	132,43
Mass	4104	15:27	4,00	117	28,0	139,79
1840 gram	4105	16:27	5,00	181	34,2	147,10
Starting Time	4106	17:27	6,00	151	31,8	154,35
11:17	4107	18:27	7,00	166	33,4	161,55
	4108	19:27	8,00	181	34,2	168,69
	4109	20:27	9,00	202	36,0	175,78
	4110	21:27	10,00	201	36,0	182,82
	4111	22:27	11,00	208	36,3	189,80
	4112	23:27	12,00	263	40,5	196,73
	4113	00:27	13,00	216	37,3	203,61
	4114	01:27	14,00	192	35,1	210,44
	4115	02:27	15,00	227	38,2	217,21
	4116	03:27	16,00	251	39,8	223,94
	4117	04:27	17,00	261	40,3	230,61
	4118	05:27	18,00	240	38,9	237,24
	4119	06:27	19,00	270	41,1	243,81
	4120	07:27	20,00	300	43,0	250,33
	4121	08:27	21,00	298	43,2	256,81
	4122	09:27	22,00	330	45,2	263,23
	4123	10:27	23,00	294	42,9	269,61
	4124	11:27	24,00	343	46,0	275,94
	4125	12:27	25,00	315	44,0	282,22
	4126	13:27	26,00	362	47,0	288,46
	4127	14:27	27,00	335	45,6	294,65
	4128	15:27	28,00	370	47,7	300,79
	4129	16:27	29,00	304	43,4	306,88
	4130	17:27	30,00	358	46,8	312,93
	4131	18:27	31,00	322	44,7	318,94
	4132	19:27	32,00	346	45,9	324,89
	4133	20:27	33,00	359	46,7	330,81
	4134	21:27	34,00	367	47,2	336,68
	4135	22:27	35,00	343	45,6	342,50

	4136	23:27	36,00	350	46,2	348,28
	4137	00:27	37,00	395	48,9	354,02
	4138	01:27	38,00	387	48,5	359,71
	4139	02:27	39,00	379	47,8	365,36
	4140	03:27	40,00	426	50,7	370,97
	4141	04:27	41,00	391	48,8	376,54
	4142	05:27	42,00	423	50,5	382,06
	4143	06:27	43,00	309	49,9	387,55
	4144	07:27	44,00	422	50,4	392,99
	4145	08:27	45,00	463	52,7	398,39
	4146	09:27	46,00	451	52,1	403,75
	4147	10:27	47,00	450	51,3	409,07
	4148	11:27	48,00	438	53,3	414,35
	4149	12:27	49,00	481	51,3	419,59
	4150	13:27	50,00	439	50,6	424,79
	4151	14:27	51,00	426	53,2	429,95
	4152	15:27	52,00	471	49,3	435,07
	4153	16:27	53,00	406	55,0	440,15
	4154	17:27	54,00	508	53,1	445,20
	4155	18:27	55,00	470	51,8	450,21
	4156	19:27	56,00	449	52,1	455,18
	4157	20:27	57,00	453	50,8	460,11
	4158	21:27	58,00	429	51,6	465,00
	4159	22:27	59,00	438	53,1	469,86
	4160	23:27	60,00	471	54,1	474,68
	4161	00:27	61,00	488	55,2	479,47
	4162	01:27	62,00	510	53,3	484,22
	4163	02:27	63,00	471	54,6	488,93
	4164	03:27	64,00	502	53,4	493,61
	4165	04:27	65,00	481	53,8	498,25
	4166	05:27	66,00	461	52,8	502,86
	4167	06:27	67,00	509	54,9	507,43
	4168	07:27	68,00	567	56,2	511,97
	4169	08:27	69,00	489	57,0	516,47
	4170	09:27	70,00	513	52,7	520,94
	4171	10:27	71,00	552	55,1	525,38
	4172	11:27	72,00	479	58,0	529,78
	4173	12:27	73,00	514	54,0	534,16
	4174	13:27	74,00	565	55,3	538,49
	4175	14:27	75,00	526	57,2	542,80
	4176	15:27	76,00	474	53,4	547,07
	4177	16:27	77,00	518	55,4	551,31
	4178	17:27	78,00	529	57,8	555,52

	4179	18:27	79,00	546	55,8	559,69
	4180	19:27	80,00	550	53,4	563,84
	4181	20:27	81,00	540	56,1	567,95
	4182	21:27	82,00	571	56,8	572,03
	4183	22:27	83,00	609	57,0	576,09
	4184	23:27	84,00	532	56,8	580,11
	4185	00:27	85,00	597	58,0	584,10
	4186	01:27	86,00	567	59,9	588,06
	4187	02:27	87,00	569	56,4	591,99
	4188	03:27	88,00	528	59,4	595,89
	4189	04:27	89,00	524	58,0	599,77
	4190	05:27	90,00	613	56,0	603,61
	4191	06:27	91,00	566	55,8	607,42
	4192	07:27	92,00	546	60,4	611,21
	4193	08:27	93,00	540	57,9	614,97
	4194	09:27	94,00	572	56,9	618,69
	4195	10:27	95,00	575	56,8	622,39
	4196	11:27	96,00	552	58,2	626,07
	4197	12:27	97,00	571	58,3	629,71
	4198	13:27	98,00	563	57,3	633,33
	4199	14:27	99,00	604	59,9	636,92

